Journal of
Instrumentation

Cryogenics and purification systems of the ICARUS T600 detector installation at Fermilab

To cite this article: F. Abd Alrahman *et al* 2026 *JINST* **21** P04012

Published by IOP Publishing for Sissa Medialab

Received: *December 11, 2025*
Revised: *February 26, 2026*
Accepted: *March 18, 2026*
Published: *April 15, 2026*

Cryogenics and purification systems of the ICARUS T600 detector installation at Fermilab

The ICARUS collaboration

F. Abd Alrahman et al.

Full author list at the end of the paper

E-mail: hope@fnal.gov, cmontana@fnal.gov

Abstract: This paper describes the cryogenic and purification systems of the ICARUS T600 detector in its present implementation at the Fermi National Laboratory, Illinois, U.S.A. The ICARUS T600 detector is made of four large Time Projection Chambers, installed in two separate containers of about 275 m^3 each. The detector uses liquid argon both as target and as active medium. For the correct operation of the detector, the liquid argon must be kept in very stable thermal conditions and the contamination of electronegative impurities must be consistently kept at the level of small fractions of parts per billion. The detector was previously operated in Italy, at the INFN Gran Sasso Underground Laboratory (LNGS), in a three-year run on the CERN to LNGS Long Baseline Neutrino Beam. For its operation on the Booster and NuMI neutrino beams at Fermilab, for the search of sterile neutrinos and measurements of neutrino-argon cross sections, the detector was moved from Gran Sasso to CERN for the upgrades required for operation at shallow depth with high intensity neutrino beams. The liquid argon containers, the thermal insulation and all the cryogenic equipment have been completely re-designed and rebuilt, following the schemes of the previous installation in Gran Sasso. The detector and all the equipment have been transported to Fermilab, where they have been installed, tested and recently put into operation. The work described in this paper has been conducted as a joint responsibility of CERN and Fermilab with the supervision provided by the ICARUS Collaboration. Design, installation, testing, commissioning and operation are the result of a common effort of CERN, Fermilab and INFN groups.

Keywords: Cryogenic detectors; Noble liquid detectors (scintillation, ionization, double-phase); Neutrino detectors; Time projection chambers

ArXiv ePrint: 2509.18392

https://doi.org/10.1088/1748-0221/21/04/P04012

2026 JINST 21 P04012

Contents

1 Introduction

1.1 The ICARUS T600 detector and the Gran Sasso run

Argon, naturally present in the atmosphere at the 1% level, has by long been recognized as an excellent radiation detection medium. In the liquid form (Liquid Argon -> LAr) is characterized by high electron mobility and dielectric strength and a relative density of 1.4, making it an ideal candidate as active target for rare events searches such as proton decays, neutrino and dark matter interactions,

2026 JINST 21 P04012

etc., which require the deployment of detectors with large sensitive mass (hundreds or thousands of tons). Electron-ion pairs are abundantly produced by the passage of charged particles in LAr: about 90,000 electron-ion pairs per centimeter are generated along the trajectory of a minimum ionizing single charged particle (m.i.p.). By means of an appropriate electric field, electrons that survive the initial recombination with their parent ions[1] can be efficiently transported toward a set of electrodes (wires or “pixels”) placed at the boundary of the field region where their passage or arrival can be recorded in the form of an electrical signal. If the electric field is reasonably uniform and the effects of LAr turbulence or non-uniformity are negligible during the time required for the electrons to reach the sensing electrodes, the geometry of the ionization tracks is preserved during transport in LAr. If wires are used, multiple planes with different wires orientation can be employed to obtain different “views” of the same ionizing event, each view corresponding to a 2-dimensional projection of the event with one coordinate orthogonal to the wires direction and the second one being the drift time (common to all the views). Multiple views can be then combined to provide a 3-dimensional representation of the event. From measurement of the amplitude of the signals, additional important information about the event can be derived, such as energy deposition (for calorimetry), local ionization density (used e.g. for particle identification), etc. Liquid argon is also an excellent inorganic scintillator. Scintillation light is produced with about the same abundance as ionization charge, at a wavelength of 128 nm, in the Vacuum UltraViolet (VUV) region. Detection of scintillation light provides, among others, the absolute time of the ionizing event, allowing for the correct positioning of the ionization tracks along the drift coordinate and a convenient prompt trigger signal.

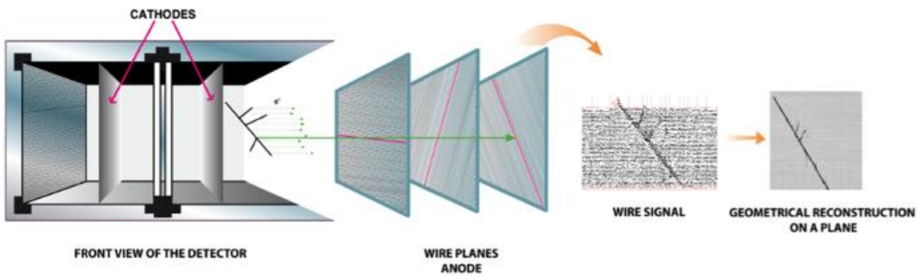

Figure 1. Sketch of the detector layout showing the LAr-TPC working mechanism.

In summary, the Liquid Argon Time Projection Chamber (LAr-TPC) is a continuously sensitive and self-triggering detector that can provide an excellent 3D imaging and calorimetric reconstruction of ionizing events occurring inside the sensitive volume. First proposed by C. Rubbia in 1977 [1], this detection technique allows for a detailed study of the neutrino interactions, spanning a wide energy spectrum (from few keV to several hundred GeV).

The ICARUS T600, with a total active mass of 476 ton, is the first large-scale operating LAr-TPC detector [2]: it consists of a large cryostat split into two identical, adjacent modules. Each module houses two LAr-TPCs separated by a common cathode and the maximum drift distance is 1.5 m, equivalent to ~ 1 ms drift time for the nominal 500 V/cm electric drift field. The anode is made of three parallel wire planes (wire chambers). The other sides of the sensitive volume are covered by a set of parallel electrodes (field cage), each one forming a rectangular ring, that are kept at a uniformly decreasing voltage and ensure a uniform field between the cathode and the anodes. Behind the wire

[1] Approximately 50% of the electrons produced by a m.i.p. survive recombination if a field of 500 V/cm is used.

2026 JINST 21 P04012

chambers there are sets of photomultipliers (PMTs) to collect the scintillation light produced by the charged particles in LAr and used for the trigger of the detector [3]. ICARUS concluded in 2013 a very successful 3 years long run in the Gran Sasso underground laboratory (LNGS).

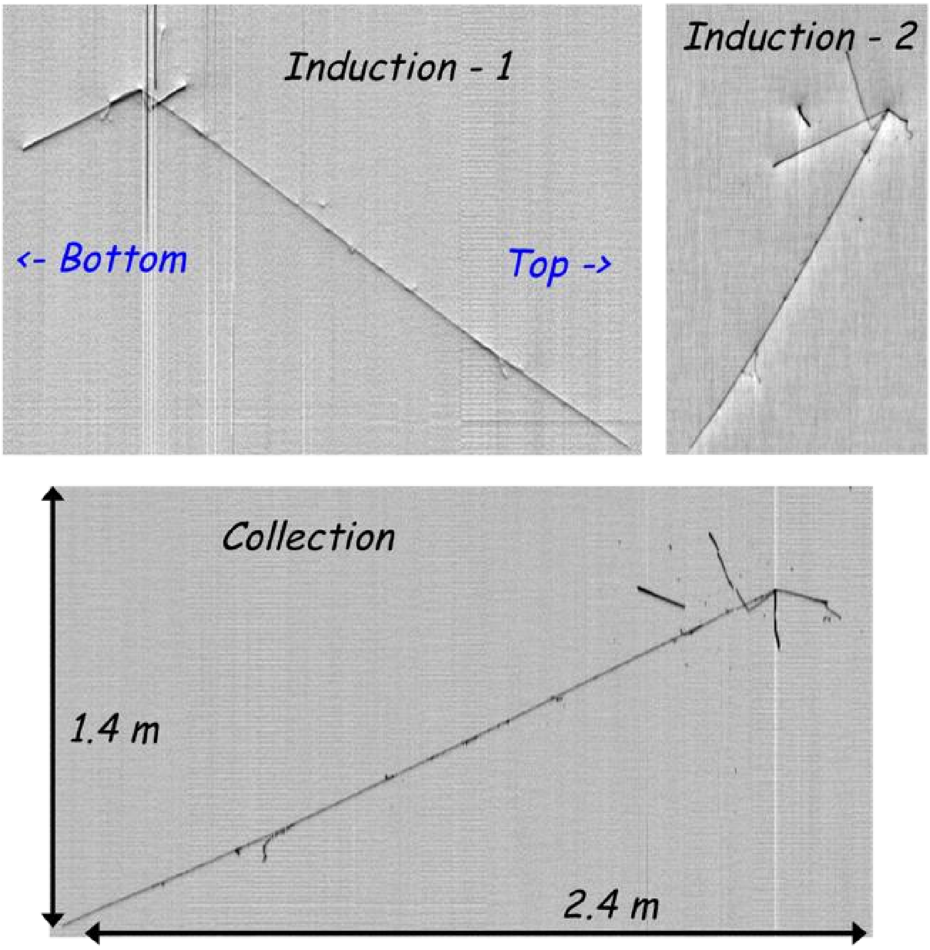

Figure 2. An atmospheric muon neutrino event ($E_{\mathrm{DEP}} \sim 1.7$ GeV) collected by ICARUS-T600 at LNGS as measured in the three — Induction-1, Induction-2 and Collection — views is shown.

During the data taking the liquid argon was kept at an exceptionally high purity level (< 50 ppt of O_2 equivalent contaminants) reaching in 2013 a 16 ms lifetime corresponding to 20 ppt O_2 equivalent LAr contamination [4], paving the way to the construction of larger LAr-TPC detectors with drift distances up to 5 m. The detector has been exposed to the CERN to LNGS neutrino beam and to cosmic rays and the recorded events demonstrate the high-level performances and the physical potentialities of this detection technique: the detector showed a remarkable e/γ separation and particle identification exploiting the measurement of dE/dx versus range [5]. Furthermore, the momentum of escaping muons has been measured studying the multiple Coulomb scattering with $\sim$ 15% average resolution in the 0.4–4 GeV/c energy range, which is relevant to the next generation neutrino experiments [6]. The events related to cosmic rays have been studied to identify also the atmospheric ν interactions: 6 ν_μCC and 8 ν_eCC events in a 0.43 kton y exposure have been identified and reconstructed, demonstrating that the automatic search for the ν_eCC in the sub-GeV range of interest for the future short and long baseline neutrino experiments is feasible [7].

1.2 The sterile neutrino puzzle and the SBN program

Some experiments, in particular LSND [8], and MiniBooNE [9] have reported anomalous signals that may imply the presence of an additional mass-squared difference $\Delta m^2_{\text{new}} \sim 1.0\,\text{eV}^2$ driving oscillations at small distances and pointing toward the possible existence of non-standard heavier sterile neutrino(s). A sensitive search for a possible ν_e excess related to the LSND anomaly in the CNGS ν_μ beam has been performed using the neutrino events collected in the T600 detector during the Gran Sasso run. 2650 CNGS neutrino interactions, identified in 7.9×10^{19} pot exposure, have been studied in details to identify the ν_e interactions. Globally, 7 electron-like events have been observed to be compared with the 8.5 ± 1.1 expected from the intrinsic beam contamination and standard 3-flavor oscillations: this study constrained the LSND signal to a narrow parameter region at $\sin^2 2\theta \sim 0.005$, $\Delta m^2 < 1\,\text{eV}^2$ that should be definitely investigated [10]. The MicroBooNE experiment, which took data between 2015 and 2021, did not observe any significant excess of events, further constraining the allowed parameter space [11].

The SBN Short-Baseline Neutrino program at Fermilab can provide the required clarification of the LSND anomaly. It is based on three LAr-TPC detectors (ICARUS-T600, MicroBooNE with 89 t active mass and SBND with 82 t active mass) exposed at shallow depth to the ~ 0.8 GeV Booster neutrino beam at different distances from the target (600 m, 470 m and 110 m respectively) [12]. The used detection technique will provide an unambiguous identification of the neutrino interactions, the measurement of their energy and a strong mitigation of the possible sources of background. In addition, the study with almost identical detectors at different distances from the source will allow to identify any variation on the spectra, that will be a clear signature of neutrino oscillations. For these reasons, this experiment will allow for a very sensitive search for $\nu_\mu \to \nu_e$ appearance signals, covering the LSND 99% C.L. allowed region at $\sim 5\sigma$ C.L. The high correlations between the event samples of the three LAr-TPC's and the huge event statistics at the near detector will also allow for a simultaneous sensitive search in the ν_μ disappearance and in the ν_e appearance channels.

During the data taking at Fermilab, the T600 detector will be also exposed to the off-axis neutrinos from the NuMI beam, in the 0–3 GeV energy range, with an enriched component of electron neutrinos (few %). The analysis of these events will provide useful information related to the detection efficiencies and to the neutrino cross-sections at energies relevant to the future long baseline experiment with the multi-kt DUNE LAr-TPC detector.

1.3 The T600 in the SBN program

The ICARUS-T600 detector at Fermilab takes data at shallow depth, protected by a 3 m concrete overburden: O(10^6) ν interactions should be recognized amongst the ~ 11 cosmic muons that are expected to cross the detector randomly in the 1 ms drift time corresponding to each triggered event. In addition, the associated photons produced by cosmic rays can become a serious background source for the ν_e search since the electrons produced via Compton scattering and pair production can mimic ν_eCC events. To prepare the detector for this new SBN data taking, the T600 underwent an intensive overhauling at CERN in the Neutrino Platform framework before being shipped to US in 2017, introducing several technology developments while maintaining the already achieved performance.

2026 JINST 21 P04012

The T600 is now equipped with an upgraded inner light detection system with 360 new 8” photo-multipliers, installed behind the TPC wire planes (90 PMTs in each TPC) [13, 14]. The PMTs gain equalization, and timing will be performed by 405 nm laser pulses flashing the PMTs via a fiber system. This new light detection system will provide a sensitivity below 100 MeV of deposited energy, a ∼ 1 ns time resolution with a high granularity: all these features are fundamental to effectively identify the events associated to the neutrino beam and to measure the time of occurrence of each cosmic interaction crossing the detector.

The overhauling of the T600 also gave the opportunity to design an upgraded “warm” TPC read-out electronics, finalized to a better event reconstruction quality. This includes a front-end based on analog low noise-charge sensitive pre-amplifier, serial 12-bit ADCs, one per channel, with 400 ns synchronous sampling [15]. A ∼ 1.5 µs faster shaping time allows to match the electron transit time in the wire plane spacing, providing a better physical signals position separation, a drastic reduction of the undershoot in the preamp response as well as the low frequency noise while maintaining a S/N ≥ 10 ratio as demonstrated with a 50-liter LAr-TPC prototype exposed to cosmic rays at CERN. Finally, a new compact design allows to host both the analogue and digital electronics in a new A2795 CAEN board, directly mounted on ad-hoc signal feed-through flanges and on each flange a custom mini-crate hosts nine boards, corresponding to 576 channels.

To reject the cosmic background, during the new data taking the T600 will be surrounded also by an external ∼ 4π segmented Cosmic Ray Tagging (CRT) system, composed by 3 subsystems each one with two layers of plastic scintillators (∼ 1100 m^2). This additional system, in conjunction with the T600 internal PMT system, will allow to unambiguously identify cosmic rays entering the detector: the few ns time resolution provided by this system, combined with the activity in the LAr volume will allow measuring the direction of the particle propagation via time of flight and discriminate the incoming/outcoming particles.

After the placement in the pit of the two ICARUS modules in August 2018, all the feedthrough flanges for the TPCs and PMTs signals and for the injection of the laser flashes used to calibrate the PMTs have been installed (December 2018). The gain and the dark rate for all the 360 PMTs have been measured as a function of the applied voltage at room temperature. All the new TPC readout electronics in the 96 mini-crates and the low noise power supplies have been installed and verified: the full readout chain has been tested injecting test pulses at far end of the chamber wires and reading out the signals by the A2795 boards on the other end, to check the full system for noise monitoring purposes. In parallel all the cryogenic equipment has been installed, welded and the complete system has been tested at 350 mbar overpressure. Then the cold vessels have been successfully evacuated at 10^{-5} mbar residual pressure.

The detector installation has been completed at the beginning of 2020 and between February and April the detector has been filled with Liquid Argon, and the liquid and gas recirculation systems that are needed to purify the Argon have been activated. The LAr TPC and the LAr light detection system have been fully activated in August 2020, starting to take cosmic rays data. Activation of the side CRT followed immediately. First neutrino data have been recorded early 2021 and the first uninterrupted neutrino run (RUN 0) has been conducted between May and June 2021. After verification that no interventions requiring the use of the overhead cranes were needed, the experimental setup has been completed with the installation of the top CRT (Dec 2021–Jan 2022) and of 3-meter-thick concrete overburden (Jun 2022). Since its activation, in August 2020, the detector has been practically continuously active, operating at the nominal field, and at nominal conditions of all sub-components. No interruptions of data taking due to failures or instabilities have occurred. The target LAr purity (concentration of electronegative impurities < 0.1 ppb of Oxygen equivalent molecules, corresponding to a free electrons lifetime of 3 ms) was reached in the spring of 2021, and then stabilized at about two times the nominal value in the following months. The stability of the cryogenics and argon purification systems has been remarkable, with fluctuations in the absolute pressure within few mbar and temperature uniformity across the entire sensitive volume within 0.1 K.

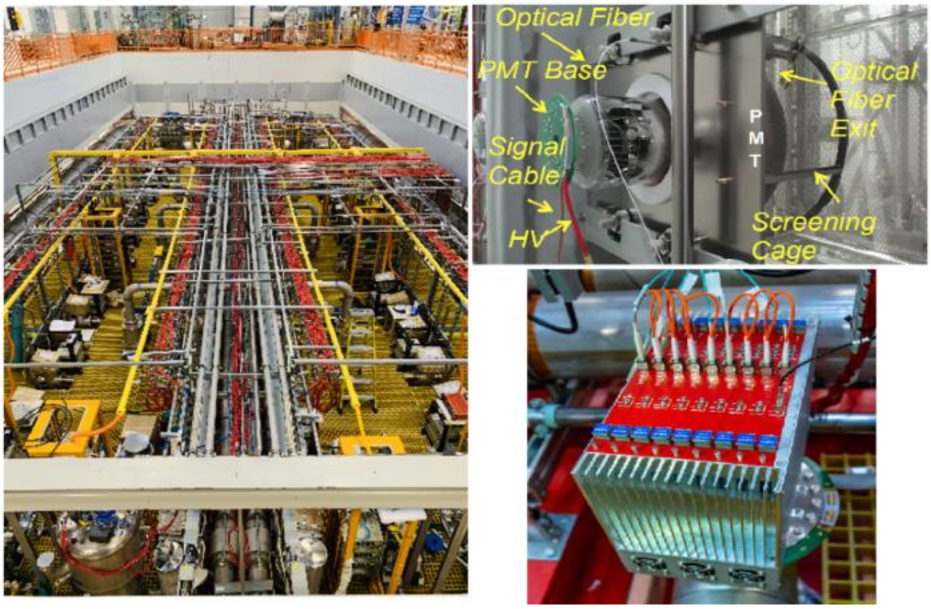

Figure 3. Left: ICARUS installation at SBN. Top right: one of the PMT installed inside the detector. Bottom right: one of the new mini crates containing 9 CAEN A2795 boards used to collect the TPC wire signals.

1.4 Specifications of the cryogenics and purification systems

The goals of the cryogenic and purification systems are to maintain the LAr volume in stable thermal conditions and to achieve and maintain purity levels, in terms of concentration of electronegative impurities at the level of ≤ 0.1 ppb (O_2 equiv.), to allow for the transport of the ionization electrons over the distance between the cathode and the anode with the smallest possible attenuation. For reference, at 0.1 ppb (O_2 equiv.) of e-negative impurities concentration, the corresponding free electrons lifetime is ≈ 3 ms and the ionization electrons attenuation, after 1 ms drift time (corresponding to 1.5 m drift, at 500 V/cm) is about 28.5%; for an impurities concentration of 0.05 ppb (O_2 equiv.) the attenuation is ≈ 15%. The typical O_2 and H_2O concentration in standard commercial LAr is ≤ 1 ppm.

Non-electronegative impurities present at small concentrations (ppm level) are, in general, not a concern for the operation of a LAr TPC. A notable case is nitrogen, which is typically present in commercial LAr at concentrations of the order of one to a few ppm. While nitrogen at these levels does not affect the transport of ionization electrons in liquid argon, it has been shown to suppress the slow component of the scintillation light. The suppression of the slow component is approximately 20% for nitrogen contaminations around 3 ppm [16].

2026 JINST 21 P04012

The implementation of a dedicated commercial system for nitrogen removal is, however, both costly and impractical for the large argon volumes involved in modern LAr TPC detectors, as it requires heating the carrier fluid (argon, in this case) to temperatures of the order of 400 °C. Operational experience has demonstrated that the purity specifications guaranteed by the vendor for commercial LAr (see table 1), combined with stringent leak-tightness requirements and established purification procedures for electronegative contaminants, are sufficient to ensure adequately low nitrogen concentrations over extended periods of operation (years).

Some polar molecules such as H_2O or CO_2, typically present at the ppm level in commercial LAr or desorbed from material surfaces, are effectively removed by molecular sieves. In contrast, the removal of O_2 and other electronegative contaminants requires chemical filters. Pure copper has been demonstrated to be an effective alternative to the original ICARUS choice (Oxysorb™), whose use is not permitted in the United States.

During operation, the LAr purity is determined from the charge attenuation measured along cosmic muon tracks crossing the full drift volume and recorded by the TPCs. This method provides the highest sensitivity to electron attenuation over the maximum drift distance. For a drift length of 1.5 m (the maximum in ICARUS) and a drift field of 500 V/cm, distortions of the electric field due to space charge effects are small, and the corresponding corrections to the extracted electron lifetime are negligible for lifetime values up to several milliseconds.

During the filling phase, the argon purity is monitored at several locations, including the outlet of the storage dewar, points along the filling lines, and a few positions on the chimneys at the top of the detector, by means of gas analyzers (see table 2). These analyzers are connected to the sampling points through stainless steel piping.

We note that radioactive contaminants naturally present in atmospheric argon, such as ^{39}Ar and ^{85}Kr, as well as radioactive decays from members of the ^{238}U and ^{232}Th chains present in detector and cryostat materials (primarily aluminum and stainless steel), are not a limiting factor for the present physics program.

Another relevant requirement of the cryogenic and purification system is that it must not interfere with the operation of the TPC. The signals recorded by the TPC readout electronics are very small.[2] Therefore we must make sure that any potential source of electromagnetic interference is appropriately shielded and grounded. The experimental setup is provided with two separate grounding systems:

- a detector ground, used as a reference for the detector components and the associated electronics. Also the main aluminum containers (section 3) and the cold shields (section 5) are connected to the detector ground, acting as a Faraday cage for the internal detector components;

- a building ground, used as a reference for all other equipment. The cryogenic equipment (pumps, actuators, cryogenic sensors, transfer lines, auxiliary cryostats, cryogenic controls, etc.) must all be referenced to the building ground and remain electrically isolated from the detector ground under normal operating conditions. A safety bonding device automatically connects the two grounds if the potential difference exceeds a predefined threshold.

To minimize electromagnetic interference the cryogenic controls must be on building ground hosted in shielding cabinets positioned outside the area occupied by the detector assembly (outside the warm

[2] The typical signal produced by a minimum ionizing particle on a single wire is of the order of 15,000 electrons

vessel, see section 4). This includes the sources of auxiliary power (UPS). Finally, all auxiliary equipment must be tested for potential electromagnetic interference before approval.

The ICARUS detector at the SBN facility is primarily devoted to the study of neutrino interactions in the $\gtrsim 100$ MeV energy range, including appearance and disappearance searches in accelerator neutrino beams, as well as detailed reconstruction of neutrino-induced final states. These analyses rely on the reconstruction of extended ionization tracks rather than on isolated low-energy deposits.

Two considerations make radioactive contaminants negligible for the present application:

1. The energies associated with the dominant decays of ^{39}Ar and ^{85}Kr ($\lesssim 600$ keV), as well as those from the ^{238}U and ^{232}Th chains ($\lesssim 3.5$ MeV), are well below the typical energy scale of neutrino-induced events of interest. Furthermore, these decays produce localized energy deposits that are readily distinguishable from the multi-track topologies characteristic of neutrino interactions.

2. The detector operates at shallow depth (under approximately 3 m of concrete overburden), and the overall background rate is dominated by cosmic radiation, primarily cosmic muons. The energy deposition rate in the liquid argon due to cosmic rays exceeds that from ^{39}Ar decays by approximately a factor of 50, making the latter a subdominant contribution to the total background budget.

For these reasons, while radioactive contaminants are of primary concern in low-background experiments searching for rare processes at the keV–MeV scale, they do not impose additional purity constraints for the ICARUS physics program. The required purity levels are therefore driven by the need to ensure adequate electron lifetime for long-drift charge collection rather than by radiological considerations.

As the drift velocity depends on the LAr temperature, a temperature uniformity to within 1 K is required within the LAr volume. As a reference, the reduction in drift velocity corresponding to a temperature variation from 88 K to 89 K, is about 2%.

To prevent electrical discharges inside the detector (the voltage on the cathodes is −75 kV, in nominal operating conditions), the risk of bubbles formation inside the LAr volume must be kept to as low as possible. This translates into a requirement on the diffuse and localized heat loads on the LAr volume. On the other side, to achieve an effective and uniform purification of the LAr volume, a reasonable amount of convection is also required.

Another requirement arises from the mechanical stability of the wire chambers frames. The frames, entirely constructed from Stainless Steel AISI 304L, were designed to achieve a precision in the relative positioning of the wires to < 0.1 mm and the overall structure is aligned to < 0.3 mm. In addition, and most important, breaking of a single wire would potentially compromise the operation of a large fraction of a wire chamber (see Reference [17] for a detailed description of the detectors and its interfaces with the aluminum containers). Therefore, the mechanical stress on the wire chambers during the cooldown and during operation must be minimized. The wire chambers were specifically designed to minimize the stress with the introduction of elastically compensating (spring loaded) rocking frames for the wire holders. The specification for the maximum allowable thermal gradient on the wire chambers is 50 K. This has driven the design of the cooling system and procedures.

1.5 Functional description of the cryogenic and purification systems

The reference layout of the T600 cryogenics and purification systems was developed after several years of intense R&D and first implemented and tested on prototypes during the nineties ([15] and references therein). The first full scale implementation was performed in the T600 detector [17, 18]. All large LAr-TPCs use the same layout for the LAr purification and recirculation. In the T600, the process of initial removal of air from the LAr containers is achieved by vacuum pumping. In other detectors, the same goal is obtained by argon purging at room temperature; this requires a specific design of the internal mechanical components, to achieve an effective removal of air at the level required for the argon purity (typically at the level of < 1 ppm, before starting the cooling and filling process).

As the initial air removal is achieved by vacuum pumping, the main LAr volumes are required to be vacuum tight (the specification is for localized Helium leak tightness $< 10^{-8}$ mbar lt/s and for a global leak rate $< 10^{-3}$ mbar liter/s) and mechanically capable to withstand the atmospheric pressure. To achieve an initial LAr purity ≈ 1 ppb (O_2 equiv.), the residual pressure, before the initial cooling, has to be $< 10^{-4}$ mbar with a corresponding global leak rate $< 10^{-1}$ mbar lt/s (typically dominated by H_2O outgassing of cables and other plastic detector components).

To minimize the contamination of the argon from outgassing, the cooldown must be as fast as possible, compatibly with the requirement of maximum gradients on the wire chambers and on the LAr containers (cold vessels).[3] The cooling is performed by flowing LN_2 through heat exchangers (cold shields) placed inside the thermal insulation and surrounding the two LAr containers. The function of the cold shields is twofold:

1. Cool down the LAr containers and the internal materials to LAr temperature, before the start of filling with LAr;

2. Prevent the heat, coming through the thermal insulation, from reaching the LAr volumes (shielding function), thus preventing large thermal gradients in the liquid and the risk of bubbles formation.

The thermal insulation must take the heat load on the cold shields to a level which is low enough that it can be handled by standard commercial equipment (cryogenic pumps, valves, piping, etc.). In our case the average design thermal load was set at 10 W/m^2. Such a target value can be obtained using standard commercial solutions based on pure passive, non-evacuated, insulating materials (foams, powders, . . .). Passive thermal insulation is also attractive for practical, economical and safety reasons and it has been the reference choice also for the previous installation at LNGS.

During operation, most impurities are coming to the argon gas phase from outgassing of materials (mostly cables) and from micro-leaks possibly developed in some of the many feedthroughs located at room temperature on top of the detector. To prevent these impurities to diffuse in the main LAr volumes, the T600 is provided with units dedicated to the purification of the argon gas phase: these are called gas recirculation units. These units are also used to stabilize the pressure of the LAr containers, that must be kept at a safe level above the atmospheric pressure to prevent air back streaming from leaks.

While the role of the gas recirculation system is to minimize the amount of impurities entering the liquid from the gas phase, the purification of the bulk liquid is achieved in two steps:

1. during the filling, commercial LAr is flown through dedicated filters (a combination of O_2 and H_2O filters) before being injected in the cold vessels; this removes the contaminants initially present, typically at the ppm level, in commercial LAr;

[3] The outgassing rate, for any given substance, is, in first approximation, an exponential function of the temperature. In our case, outgassing is typically dominated by water and it is reduced by several orders of magnitude when the temperature decreases from ambient to LAr temperature.

2. during operation, LAr in the cold vessels is continuously recirculated, by means of cryogenic pumps, and passed through filters; this removes the impurities continuously migrating in the liquid from the gas phase or originating from other possible internal sources not removed during the vacuum phase (this second source is purely hypothetical).

In the following sections, a detailed description of the cryogenic and purification systems is provided, including the thermal insulation and the cold vessels (sections 2 to 5). Section 6 is dedicated to the architecture and implementation of the control process. The commissioning process and the results after one year of operation are reported in section 7. Safety protocols and adopted standards are covered in appendix A.

2 Description of Icarus cryogenic plant

The Icarus cryogenic plant is designed, built and installed at Fermilab by a scientific collaboration of three international institutions, CERN, INFN and Fermilab, to support operations of the ICARUS liquid argon time projection chamber (LAr-TPC). The original Icarus T600 LAr-TPC was installed at the INFN Gran Sasso Underground Laboratory (LNGS), where it was operated from May 2010 to June 2013 taking data on the CERN to Gran Sasso neutrino beam with extremely high argon purity, stability and detector lifetime [2, 17]. One of the most important key elements of the LAr TPC is the liquid argon purity: residual compounds with high electron affinity have to be kept as low as 0.1 parts per billion (ppb) all over the argon volume during the whole detector run, thus allowing the ionization tracks created by interacting particles inside LAr to be transported practically undistorted in a uniform electric field up to a multi-wire anodic structure placed at the end of the drift path. The cryogenic plant installed and operated at LNGS supported all aspects of operations of the Icarus LAr-TPC, including cool down, fill and purification of the approximately 760 tons of liquid argon divided over two identical vessels. These vessels with internal dimensions of 3.6 (width) $\times$ 3.9 (height) $\times$ 19.6 (length) m^3 are together enveloped by a thermal shield cooled by a vaporizing liquid nitrogen flow [18, 19]. The cryostat and the cryogenic plant were dismantled in 2014. The detectors were moved to CERN for modifications to match the design requirements for installation at Fermilab Short-Based Neutrino (SBN) experiment at the SBN far detector building (SBN-FD). After these modifications, the detectors were installed in two new cold vessels, and this installation has been delivered from CERN to Fermilab in 2017, installed in 2018, cooled down and filled with purified liquid argon in 2019–2020, and tuned to stability by May of 2021.

To achieve the physics goals of the ICARUS experiment at Fermilab, the Icarus cryogenic plant had to fulfill the design and operational parameters as given in table 1.

The components of the Icarus cryostat, warm support structure and cryogenic plant were delivered by three institutions included in Icarus collaboration, Fermilab, CERN and INFN. By institutional delivery responsibilities, the overall cryogenic plant was initially divided into three cryogenic systems, External, Proximity and Internal as shown schematically in figure 4 and figure 5.

- The *External system* delivered by Fermilab is responsible for storage and supply of cryogens, venting of gases, gas analysis, regeneration of filtration media, electrical power, process and safety controls systems.

Table 1. Design and operating parameters

Parameter	Value
Cryostat module type and size	Two aluminum vessels with common LN_2 shields within a warm self-standing steel structure with passive insulation; cold vessel internal dimensions: 3.6 m $\times$ 19.6 m $\times$ 3.9 m, $\sim$ 380 tons each ($\sim$ 2% ullage). Gas purge for insulation space.
Contamination for LAr delivery	$O_2 < 1$ ppm, $H_2O < 1$ ppm, $N_2 < 2$ ppm
LAr purity	$<$ 100 ppt O_2 equivalent, $N_2 < 2$ ppm (corresponding to 3 ms free electron lifetime)
Cold vessels design pressure	320 mbarg (also designed for high vacuum)
Operating gas pressure	1.070 bara with ±5%
Initial purification technique (warm)	Pump cold vessels to full vacuum at warm conditions
Cooldown technique	Initial with LN_2 shield enveloping the cold vessels (−2 K/hr), final with LAr fill
TPCs cool-down rate restriction	$<$ 70 K/hr
Liquid argon recirculation rate (normal operation)	up to 2.5 m^3/hr per cold vessel
Total heat load intercepted by nitrogen	15 kW
Number of side/bottom penetrations (in LAr)	1 side and 1 bottom penetration per module (with use of external safety valves to prevent accidental spillage of LAr)
Included sub-systems	LAr and LN_2 storage and transport, O_2-N_2-H_2O monitoring, LAr and GAr recirculation and filtration, GAr condensing and recovery, safety and process controls
Grounding for noise requirement	Complete electrical isolation of the two cold vessels from external systems

- The *Proximity system* delivered by CERN is responsible for all transport and distribution of liquid argon and nitrogen at the temperatures and pressures demanded by the internal cryogenic system, for removal of impurities from argon, recirculation and filtration of boil-off argon gas.

- The *Internal cryogenic system* delivered by INFN and Fermilab is responsible for interfacing internal volume of the modules with cryogenic plant, LN_2 shields, measurement of argon temperatures and levels.

All three systems have been installed, connected at mechanical interfaces and integrated into Icarus cryogenic plant with common electrical and controls systems in 2018–2019.

2026 JINST 21 P04012

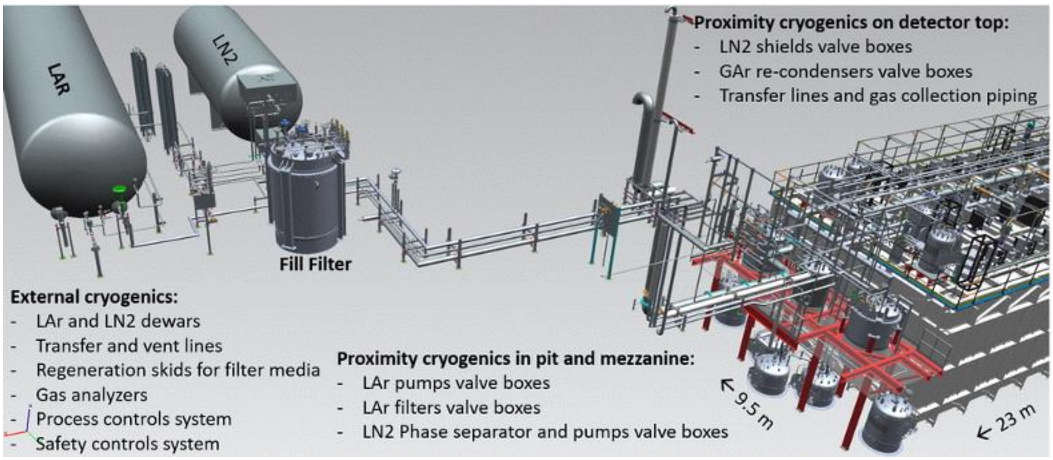

Figure 4. ICARUS cryogenic plant physical layout.

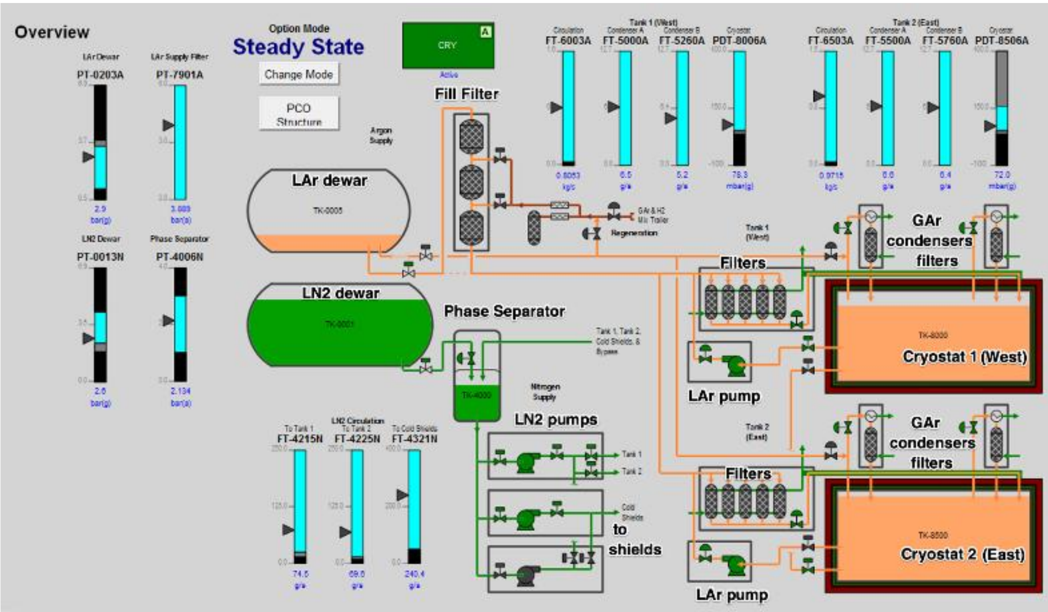

Figure 5. ICARUS cryogenic plant schematical layout.

The ICARUS cryogenic plant at SBN-FD at Fermilab was fully designed, delivered, and installed by July 2019, with the commissioning phase started by January 2020. The equipment included into the ICARUS cryogenic plant is schematically divided into the external components supplied by Fermilab, the proximity components supplied by Demaco Holland B.V. under contract with CERN and components internal to the cryostat supplied by INFN. Figure 4 and figure 5 show the physical and schematic layouts.

The main schematical description of the Icarus cryogenic plant is represented in its Process and Instrumentation Diagram (P&ID). While this 6-sheet drawing is not included in this paper, it is stored in Fermilab Teamcenter F10041251 and in Fermilab DocDB SBN-doc-783.

The main components of the Icarus cryogenic plant included:

2026 JINST 21 P04012

Figure 6. Cryogenic dewars and fill filter.

- *Liquid nitrogen storage dewar* with ~ 75 m^3 capacity (figure 6). This vacuum jacketed and perlite insulated tank rated and protected at 4.5 barg was built by Process Engineering in 1988, operated at Fermilab and then moved to SBN-FD where it was completely refurbished with new piping, reliefs and instrumentation in 2019. The dewar has been in operations since 2019. It is currently on 24/7 fill delivery by Matheson Gas to support LN_2 consumption by the Icarus cryogenic system of approximately 360 liter/hr at 3.6 bara to compensate for a thermal load of approximately 14.6 kW. The dewar is equipped with an external vaporizer that generates gaseous nitrogen used for purge of the Icarus warm vessel.

- *Liquid argon storage dewar* with ~ 30 m^3 capacity (figure 6). This vacuum jacketed and perlite insulated tank rated at 17 bara and protected at 4 barg was built by CRYOVAT in 2007, operated as part of the Icarus cryogenic system at LNGS, and then moved to Fermilab via CERN. It was refurbished with new piping, reliefs and instrumentation in 2019. The dewar has been in operations since October 2019. The dewar is equipped with a vaporizer that generates gaseous argon used for regeneration of the copper and molecular sieve media stored inside the liquid and gas filters. Additionally, the gaseous argon could be used for any make-up gas needed by the Icarus system. While not being in continuous active operations since completion of the fill of the modules, the dewar is maintained clean at positive argon pressure. It is being re-cooled and partially refilled on demand when/if it is necessary to refill the modules to compensate for vented argon.

- A *vacuum insulated liquid argon purification vessel* (figures 6, 7) containing two filters filled with Cu 0226 to remove oxygen and one vessel filled with molecular sieve to remove water from liquid argon coming from the storage vessel. All the liquid argon transferred from the storage tank to the ICARUS detector passes through this purifier system. The purity level of the liquid having passed this purifier is in the high ppt level.

- *Regeneration system* (figure 8), consisting of several piping skids incorporating valves and instrumentation required for delivering, metering, mixing and heating pure argon gas from LAr dewar and a 97.5% Ar/2.5% H_2 mix from a high-pressure tube trailer parked outside. The gaseous mix is delivered to external fill filter vessels or filter cartridges to remove water from molecular sieve and to activate or regenerate copper filter media (Cu 0226) using the hydrogen gas mixture to reduce the copper oxide. The system uses Brooks SLA5850 mass flow controllers and includes

2026 JINST 21 P04012

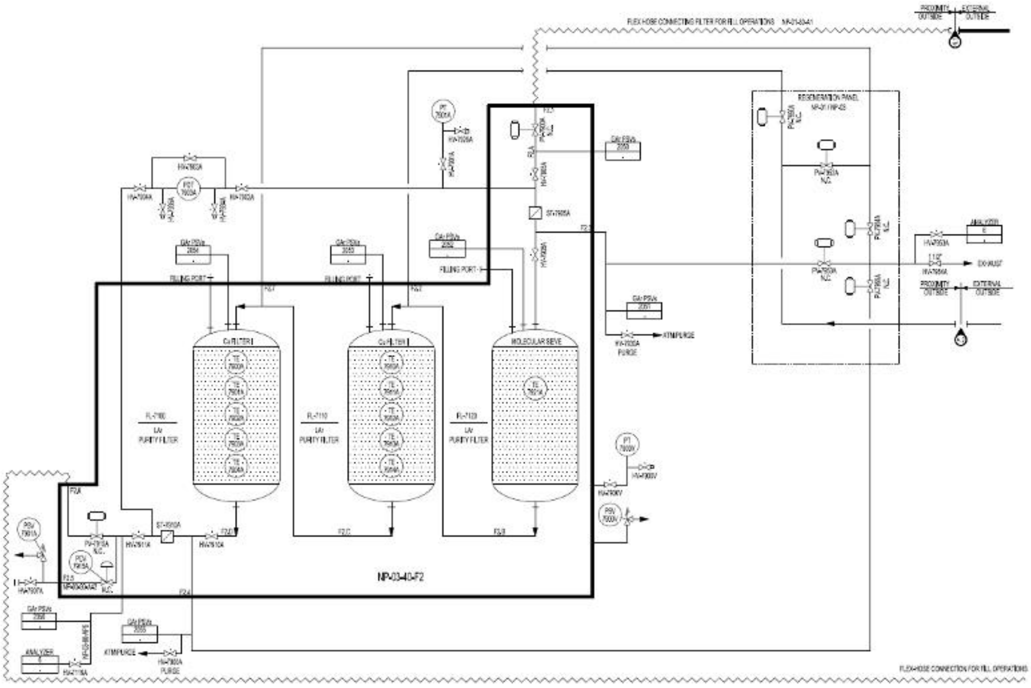

Figure 7. Fill filter P&ID.

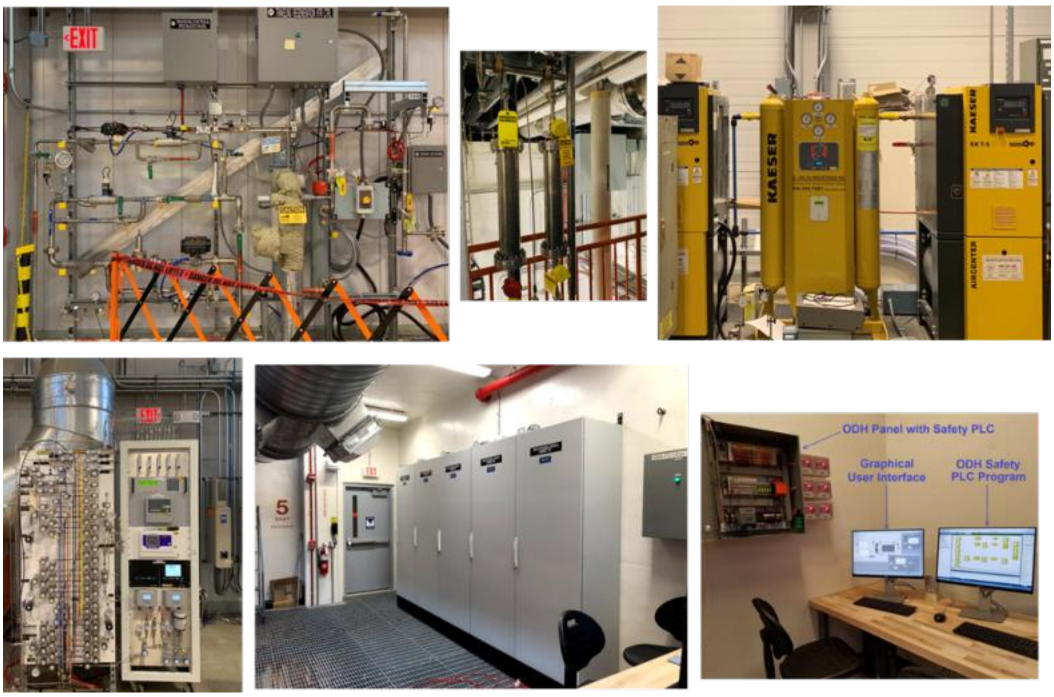

Figure 8. Top row — left to right: regeneration panel, gas make-up filters, air skid; bottom row — left to right: analyzers panel, S7 process controls, Beckhoff ODH controls with access controls station.

2026 JINST 21 P04012

a 12 kW heater to preheat the purifier medium to at least 160°C. Once the correct temperature is reached, the hydrogen gas mixture is introduced. The system was commissioned in late 2019.

- The *gas analyzer system* (figure 8) consists of six analyzers installed in a common switch panel, plumbed to 14 different sample ports in the cryogenic system. The most prominent purpose is to sample argon quality in the Air Products delivery tanks before accepting it to the liquid argon dewar.

Table 2. Gas analyzers

Gas	*Manufacturer*	*Model*	*Set range*
Oxygen	Servomex	310E-H05000	0–100 ppm O_2
Oxygen	Servomex	560E	0–5 ppm O_2
Nitrogen	Servomex	Plasma	0–100 ppm N_2
Water	Viasala	DMT348	−70–80°C H_2O
Water	Viasala	DMT348	−70–80°C H_2O
Water	Tiger Optics	HALO3-H_2O	0–9 ppm H_2O

- A vacuum insulated *liquid nitrogen 1000-liter phase separator* (figures 9, 10) is placed inside the building. It receives LN_2 from the storage tank, separates liquid from gas phase, and supplies liquid nitrogen to the pumps located below. At the same time, two-phase LN_2 returning from the cooling circuits (cryostat shields, gaseous argon condensers, liquid argon purifiers, and protected transfer lines) is returned to this separator. The saturated nitrogen pressure in the separator is the lowest in the nitrogen circuit and is regulated at 2.1 bar absolute, ensuring all temperatures in the cooling circuits remain above the argon triple point.

- Three vacuum insulated *LN_2 pump boxes* (figures 11, 12) are situated below the separator, receiving gravity-driven LN_2. One pump supplies LN_2 to the cryostat thermal shields; a second pump supplies the liquid nitrogen to each of the four condenser boxes, to the shield of the LAr purification boxes and to the transfer line between these purification boxes and the cryostat inlet. The third pump box is backup pump, which can be used for any of the two systems discussed in case one of the two has problems or is in maintenance. All pumps are Barber Nichols BNCP-68-M1. Mass flow and outlet pressure are regulated using bypass valves downstream of each pump to ensure that load variations in one circuit do not affect the others.

- The cold shields enveloping the two detector cold vessels (described in more detail in section 5) have been equipped with a total of 10 nitrogen cooling circuits. The distribution of the cooling circuits over the shields is given in figure 11. The vacuum-insulated shield inlet box distributes the liquid coming from the dedicated LN_2 pump over the 10 different heat exchangers. The amount of flow going through each heat exchanger is regulated by a valve placed in each of the ten individual circuits. The outlet of the ten different cold-shield circuits is collected in the vacuum insulated heat exchanger outlet box. The pressure in, and thus the temperature of, each circuit can be regulated by a valve placed in each of the ten circuits. The liquid/gaseous mixture coming from the heat exchangers is returned to the nitrogen phase separator via the shield outlet box.

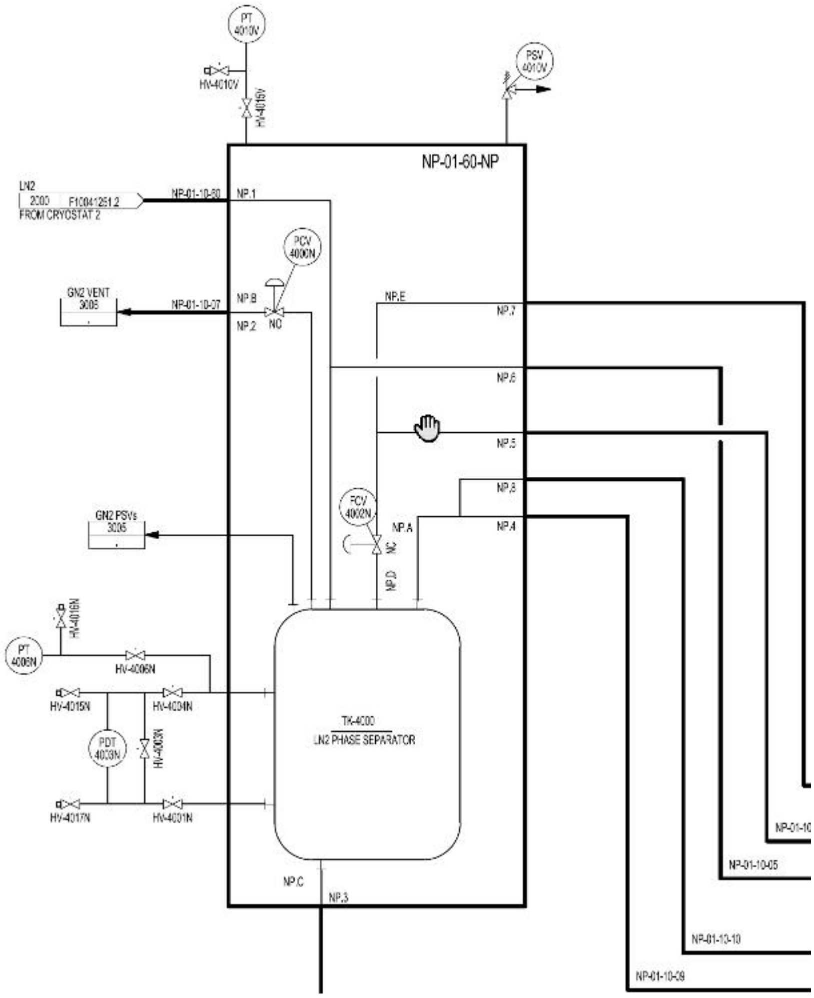

Figure 9. LN_2 phase separator box.

Figure 10. LN_2 phase separator and LAr filter boxes.

2026 JINST 21 P04012

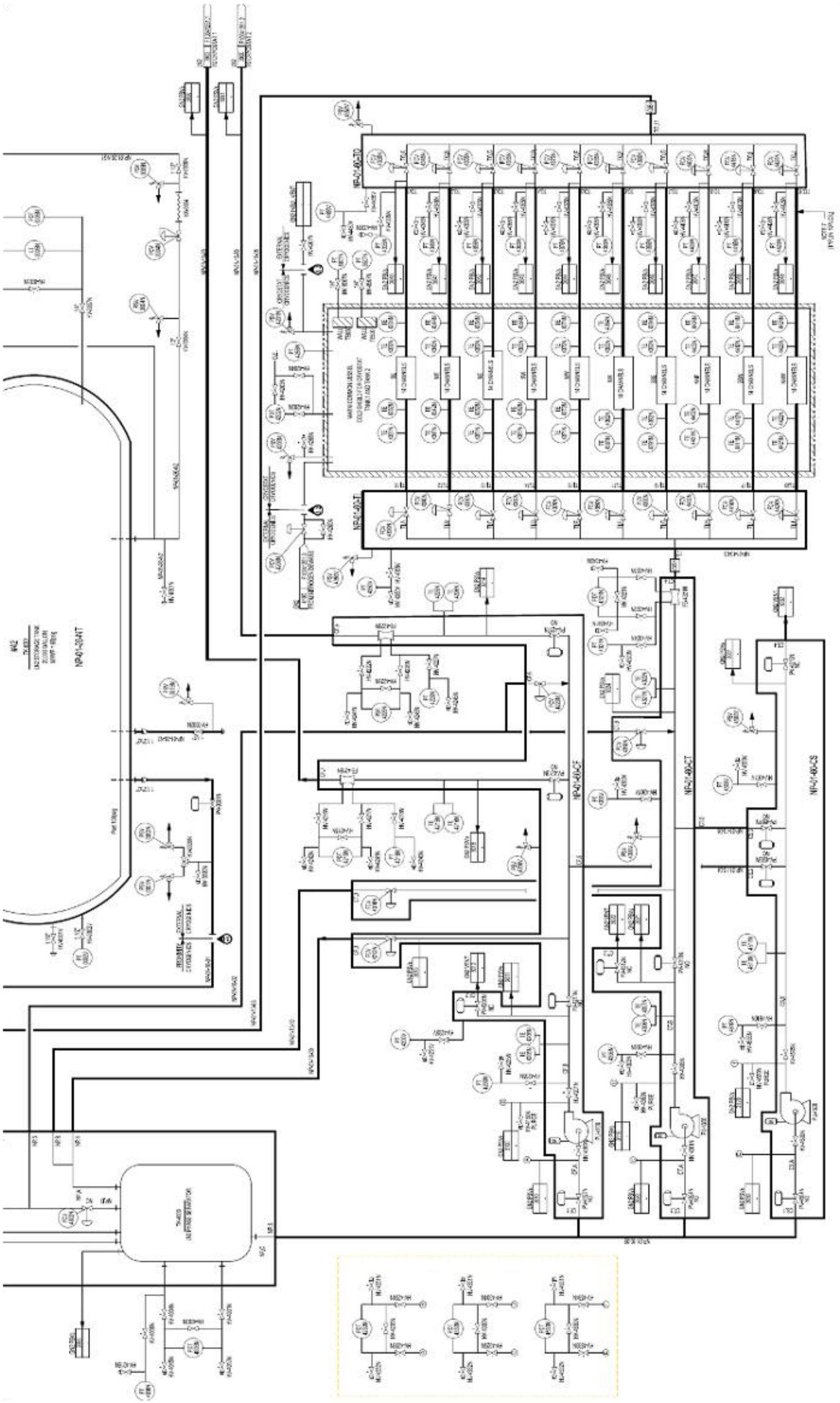

Figure 11. Phase separator, LN_2 pump boxes and cold shields.

2026 JINST 21 P04012

Figure 12. Three LN_2 pump boxes (left) and West LAr pump box (right).

- Each of the modules is connected to a vacuum insulated liquid argon pump box (see figure 12, figure 13 and figure 14), placed at the bottom level of the module. These pumps circulate a liquid argon flow from each module to a dedicated vacuum insulated argon purification valve box. The West module is configured to take LAr from the top penetration, while the East module takes LAr from the bottom penetration. This choice is due to the differences in piping from the top or bottom penetrations inside the warm-vessel space. The piping incorporates goosenecks to create a positive gas lock in case of interruption of flow, thus creating various degrees of difficulty in starting the cold flow from the cold vessels to the pumps.
  - *West 40-CP PU-6000 pump (BNCP-32C).* The pump is set to run at 41.8 Hz, 1.4 bara discharge while maintaining ~ 0.81 kg/s flow to the West modules via the 40FC filter box. The operating point is set by adjusting the flow with a discharge valve at ~ 37%.
  - *East 50-CP PU-6500 pump (BNCP-32E).* The pump is set to run at 49.6 Hz, 2.0 bara discharge while maintaining ~ 0.96 kg/s flow to the East modules via the 50FC filter box. The operating point is set by adjusting the flow with a discharge valve at ~ 44%.
- Each of the LAr purification boxes (figure 15) is equipped with five parallel active copper-filled purifiers enclosed by nitrogen-cooled thermal shields. The inlets to the purification boxes are from either the transfer line from the LAr dewar (during cooldown and fill) or from the LAr circulation pump. The outlets of these argon purification valve boxes are connected to the modules via a thermally shielded liquid argon transfer line. The shield in this line is also cooled using evaporating liquid nitrogen.

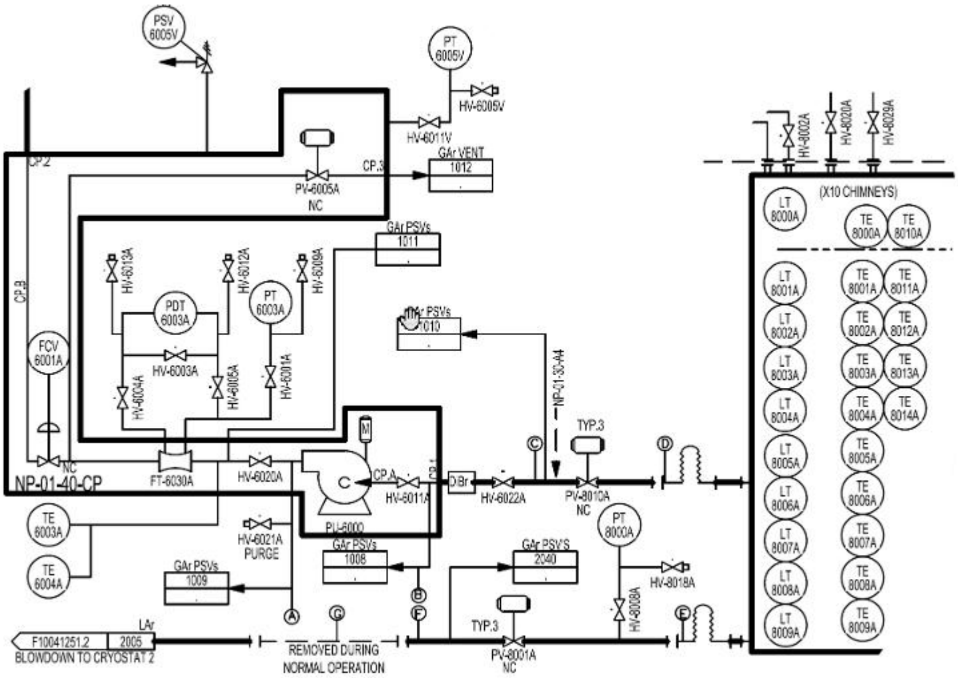

Figure 13. West module's LAr recirculation pump box (40-CP PU-6000) schematics. The inlet of the pump is connected to the top side penetration, about 1.5 m above the bottom of the module (right side of the image). The outlet of the pump goes to the inlet of the cold filter box shown in figure 15. The diagram shows the pump, the various valves to control the flow and for the startup of the pump, and the associated instrumentation. The diagram also shows the bottom side penetration of the west module (right side of the image).

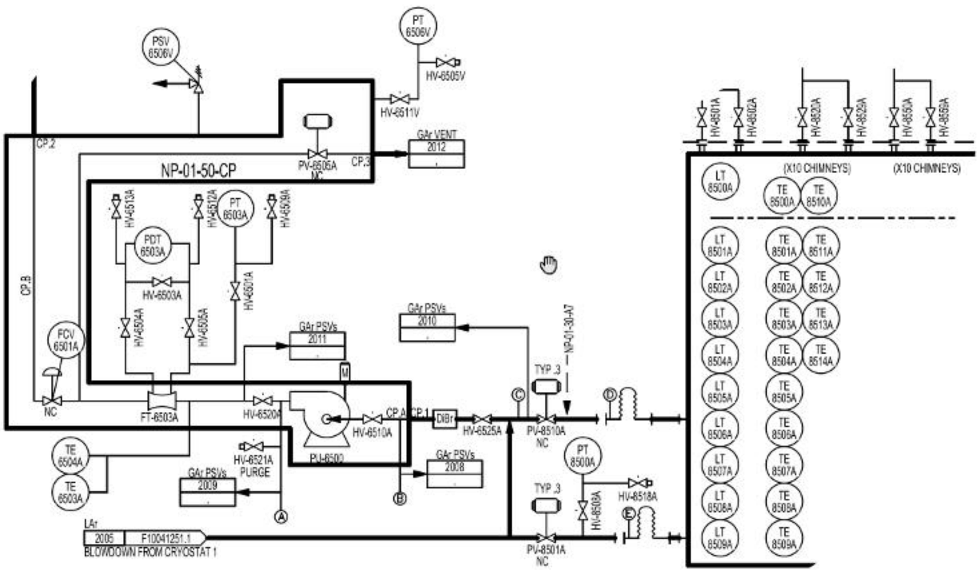

Figure 14. East module's LAr recirculation pump box (50-CP PU-6500) schematics. The layout is identical to the one of the west module (figure 13) with one relevant exception: the bottom and the top side penetrations are interconnected after the intercept valves. This allows for recirculation from either level (or both, in principle). LAr recirculation in the east module is performed using the bottom side penetration as inlet (see section 7); note that during operation the line marked as "BLOWDOWN FROM CRYOSTAT 1" is closed with a flange.

2026 JINST 21 P04012

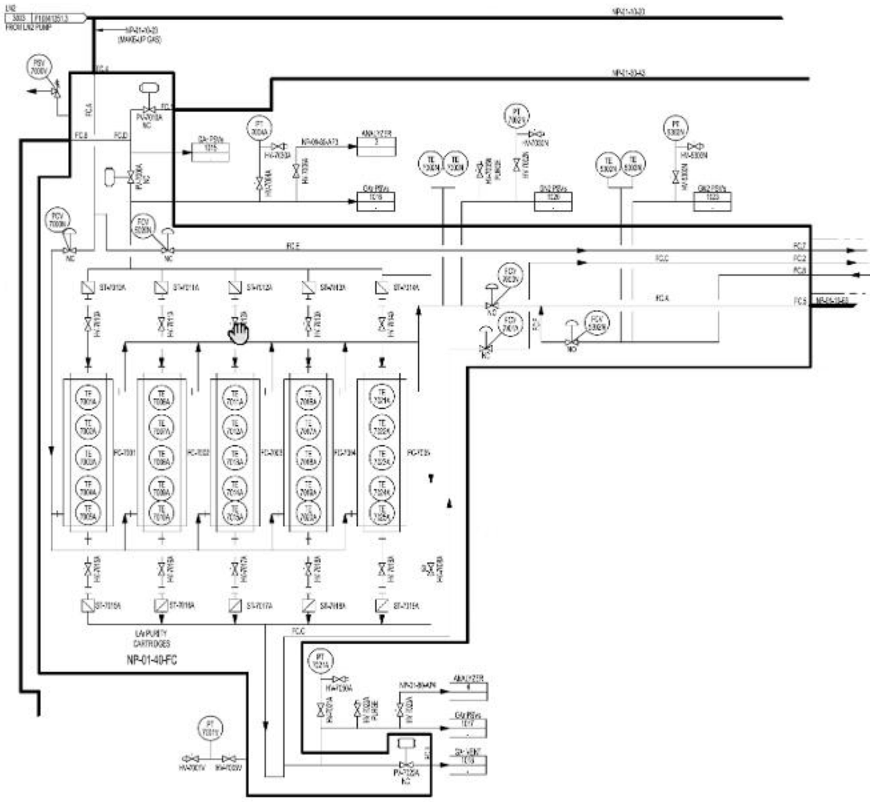

Figure 15. LAr purification box (West 40-FC, identical to East 50-FC). The diagram shows both the LAr and the LN2 circuits. LN2 is flown around the filter cartridges and then around the LAr output line (labels FC.7 and FC.8 for the LN2 line in and return, and FC.2 for LAr) to prevent gas formation in the LAr circuit. In the physical circuit, LAr is flown from the bottom of the cartridges to the top. Mechanical filters (labels ST-70XXA) are also shown at the inlet and outlet of each cartridge.

- A boiloff gas collection system forwards the argon boiloff gas from 40 × DN15 chimneys (per module) to argon gas condensers via a Vortex flow meter and control valves. To ensure that the gaseous argon in contact with the cables and other warm surfaces at the top of the cold vessels is continuously purified, an argon flow is drawn via the signal feed-throughs mounted on the cold vessels to the liquid argon condenser boxes (see figure 16). Each cold vessel has been equipped with two identical condenser boxes (40-CA and 40-CB for West; 50-CA and 50-CB for East). The room temperature gas flow from the cold vessels is first condensed in these boxes using liquid nitrogen- powered heat exchangers. After this re-liquefication, the liquid argon is passed through an active copper purifier before being returned to the module volume. These condenser boxes serve as both condensers and argon gas purifiers.

- A *gas venting system* (figure 17) consists of three separate piping networks: low- and high-pressure argon, and high-pressure nitrogen, to vent argon from modules, as well as argon and nitrogen from the proximity valve boxes, to outside the Icarus detector building. This is required to mitigate oxygen deficiency hazards inside the building. The piping ranges from DN50 to DN350 and is constructed using flexible joints and support systems to accommodate 3D movement of the vessels during cooldown as well as thermal contraction during release of cold gases. To minimize

2026 JINST 21 P04012

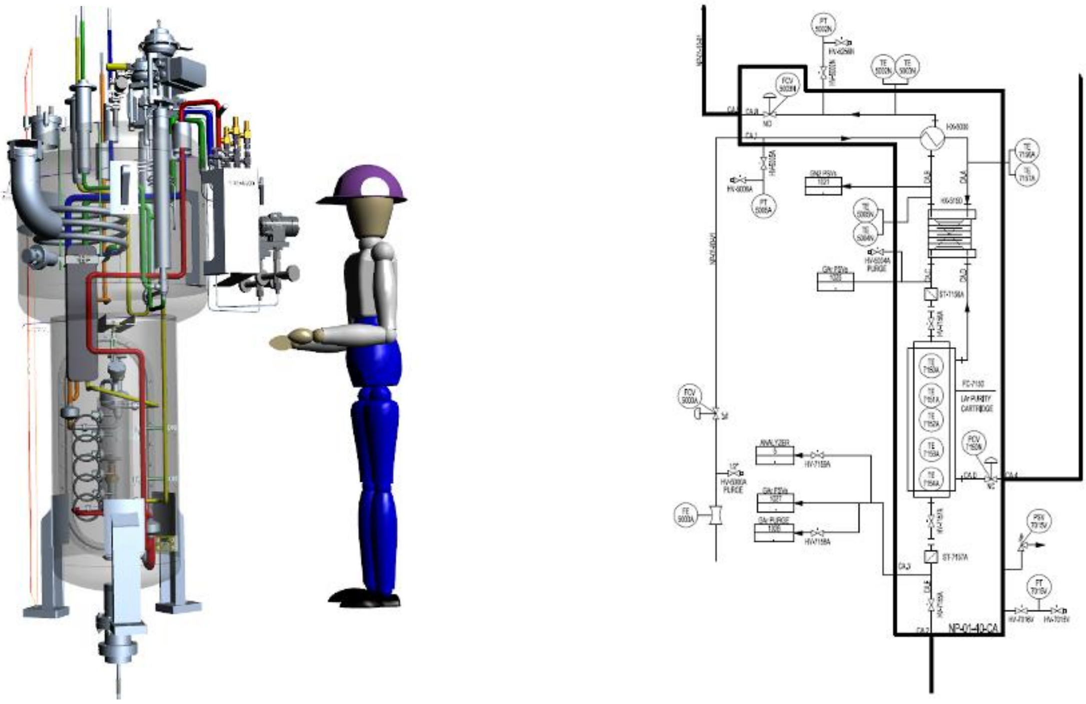

Figure 16. Gas recondensing unit. Two identical units are installed at the two ends of each module, for a total of four units. Each unit cools, recondenses, and purifies gaseous argon collected from half of the chimneys of a module. The rendered view shows the liquid nitrogen (LN_2) piping in red. The opening at the rear is used for installation and removal of the filter cartridge.

electrical noise in the electronics, all piping directly connecting to the modules incorporates dielectric joints to separate the module electrical ground from the building electrical ground.

The *instrument air system* is based on a dual Kaeser rotary screw air compressor skid (figure 8), with integrated refrigerated air dryer and adsorption swing desiccant dryer to supply all pneumatically actuated valves with air dried below −40°C dew point.

The *control and safety instrumented systems* (figure 8) are described in detail in section 6.

The *internal cryogenic system* is comprised mostly of instrumentation located inside the Icarus cold vessels (figure 18). The instrumentation includes temperature resistors and diodes to measure accurately the temperature on the TPC frames and level of the modules within (−6) cm to (+1.5) cm of the design level.

Additional information related to the Icarus cryogenic system at Fermilab is given in references [20] through [26].

3 LAr main containers (cold vessels)

As part of SBN Program at Fermilab and Neutrino Platform at CERN, two identical Icarus Cold Vessels T300, each holding TPC, are installed in one common warm vessel T600 at the SBN-FD building (references [26] to [30]). In this paper we refer to them as West and East modules.

The T300 internal dimensions of each vessel are 3.62 m × 3.92 m × 19.65 m (see figure 20) with volume 279 m^3 filled with ∼ 380 tons of liquid argon at maximum 350 mbarg gas pressure in the

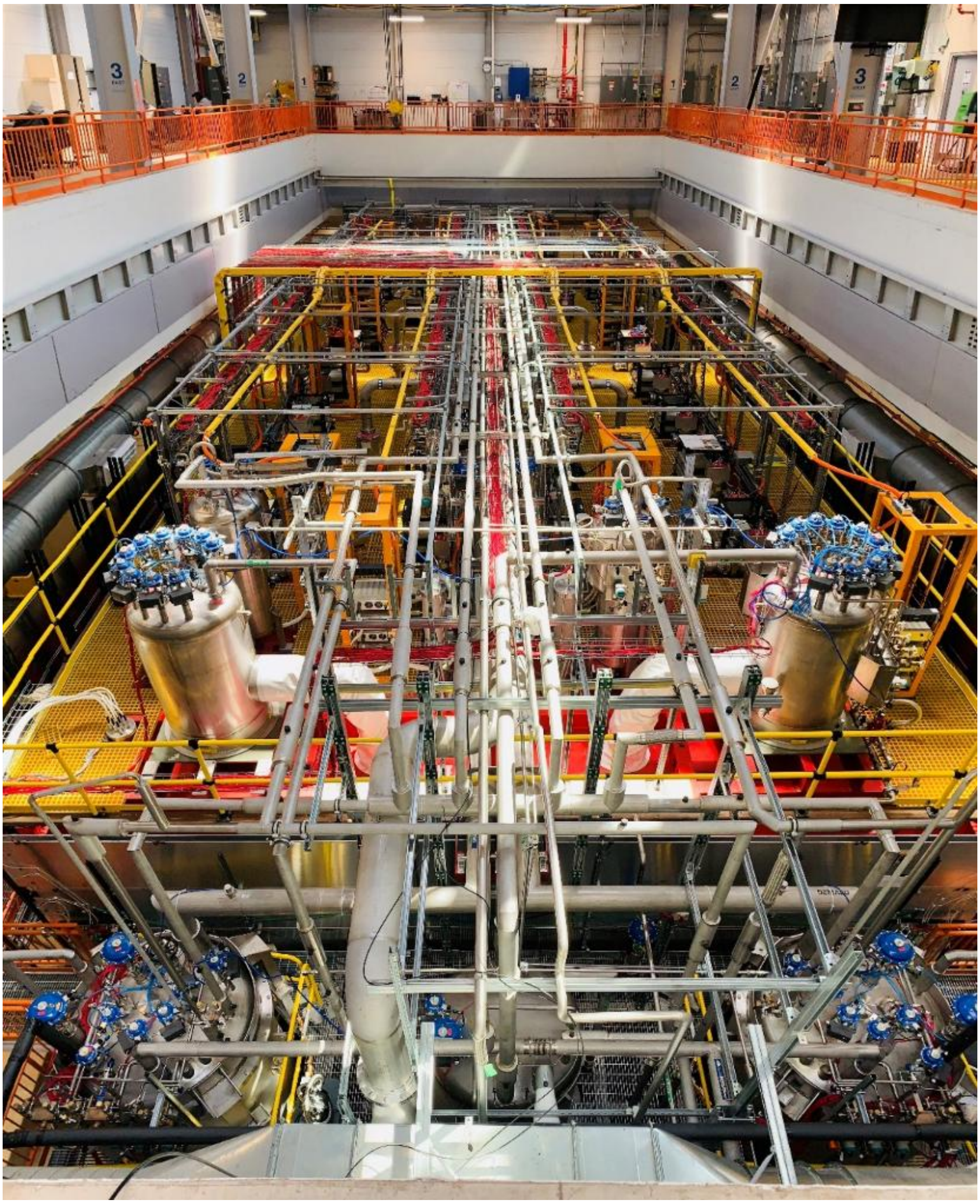

Figure 17. Top of Icarus detector with cryogenic components. Visible: LAr purification boxes 50-FC (left) and 40-FC (right); LN_2 phase separator (center, North mezzanine); inlet 60-TI (left) and outlet 60-TO (right) LN_2 boxes for the shields (North end detector); 50CA (left) and 40CA (right) condenser boxes; transfer lines and vent lines (center).

2026 JINST 21 P04012

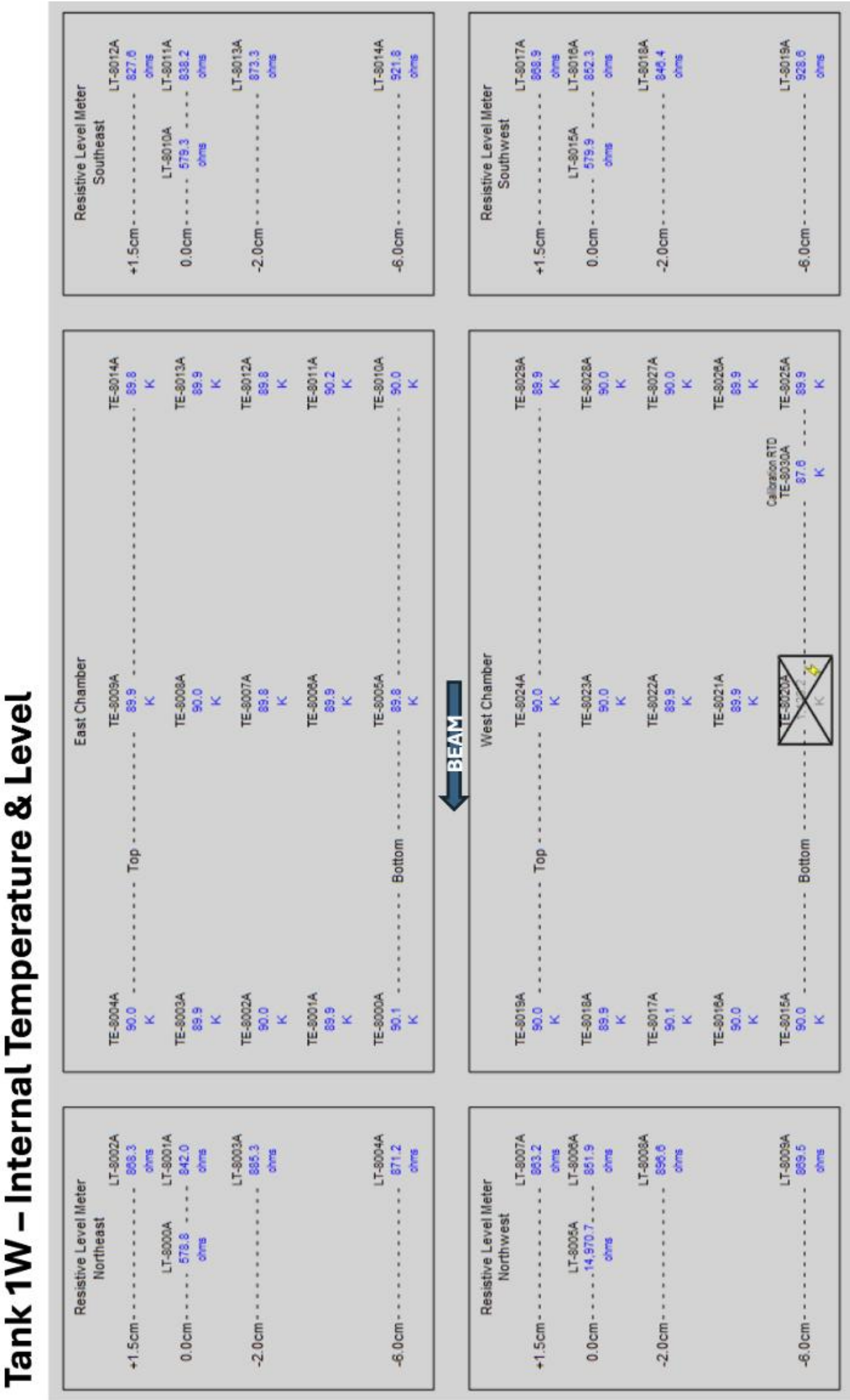

Figure 18. Internal cryogenic instrumentation for West modules (identical to East).

ullage (based on relief set pressure). The vessels are pressurized during "normal" operations, but they were also pumped down to full vacuum for leak checking and cleanup before commissioning into "normal" operations.

The vessels were originally designed by Finzi Associati, Milano, Italy for design pressure of 350 mbarg at the ullage. The design used EN-AW 6082 T6 aluminum as material for all structural elements. The choice of AW 6082 T6 was justified based on the maximum capabilities of the best available extrusion presses so to maximize size of the extruded panels and minimize number of welds. The original design by Finzi was based on Eurocode EN 1999 "Design of aluminium structures".

The rectangular shell of the vessels is closed on each side with the doors. The doors are attached with studs and nuts. This bolted connection is responsible for the structural integrity under internal pressure. The roof of the vessels has multiple flanged penetrations, including 40 chimneys (per vessel), plus 2 flanged penetrations for re-condensed argon, 1 flanged connection for liquid argon return from pumps, and 3 flanged connections for magnetic safety devices. Each vessel has $2 \times 800\,\text{mm} \times 420\,\text{mm}$ manholes blanked with flanges and secured with clamps. Each vessel also has 2 flanged side penetrations to extract liquid argon to the argon circulation pumps. The safety impact from having penetration below the liquid argon level is considered in design of the cryogenic piping system and in the ODH analysis; double safety-interlocked isolation valves leading to the pumps are installed to mitigate probability of liquid spill into the building space.

The fabrication and welding of the extruded panels comprising the vessels were performed by ST Extruded Products Group — STEP-G, Germany GmbH. ST Extruded Products Group — STEP-G supplied CERN with material certificates listing destructive test data for extruded profiles. That data confirms material properties for EN-AW 6082 T6 with strength and ductility to be better than listed properties. The final welding and assembly have been performed at CERN by CERN personnel. The final closure weld between the vessel and the doors on both sides, as well as closure welds for the manhole covers, are performed by Fermilab weld shop.

CERN did the final assessment of the design and construction. CERN presented a methodology [27] to demonstrate compliance with harmonized European standards. Though the design pressure of 350 mbarg places the cold vessels outside the scope of US and EU pressure vessels standards, CERN chose EN 13445 "Unfired Pressure Vessels" as the design code for both, internal pressure case and vacuum case. Specifically, CERN chose Finite Element Analysis (FEA) as the calculation method used for the design of the vessel per methodology of EN 13445-3 Annex B — Design-by-Analysis "direct route". CERN issued documents to validate methodology [27], FEA calculation results [28], buckling analysis results [29] and door bolts calculations [30]. The safety assessment of the cold vessels was done per Fermilab ESH Manual and described in EN02601 and EN02615 [31]. That included verification of design calculations, manufacturing data and installation QA/QC.

It is important to mention that both, Finzi and CERN listed two loading cases for the T300 vessels: operational case at internal pressure of 350 mbarg and vacuum test case at external pressure of 1 bar. CERN further tested the T300 vessels at full vacuum (EDMS Doc. No: 1761013 and 1769691) and verified that results of FEA calculations agreed with measured stresses and strains.

The vessels were further tested and accepted for vacuum operations at Fermilab in summer of 2018 per Engineering Notes EN02613 and EN02614. The vessels were then equipped with sets of strain gauges (like those used at CERN for vacuum tests) and then installed in the T600 warm vessel (figure 19). The vessels were pneumatically pressure tested at 350 mbarg in April 2019, and then

2026 JINST 21 P04012

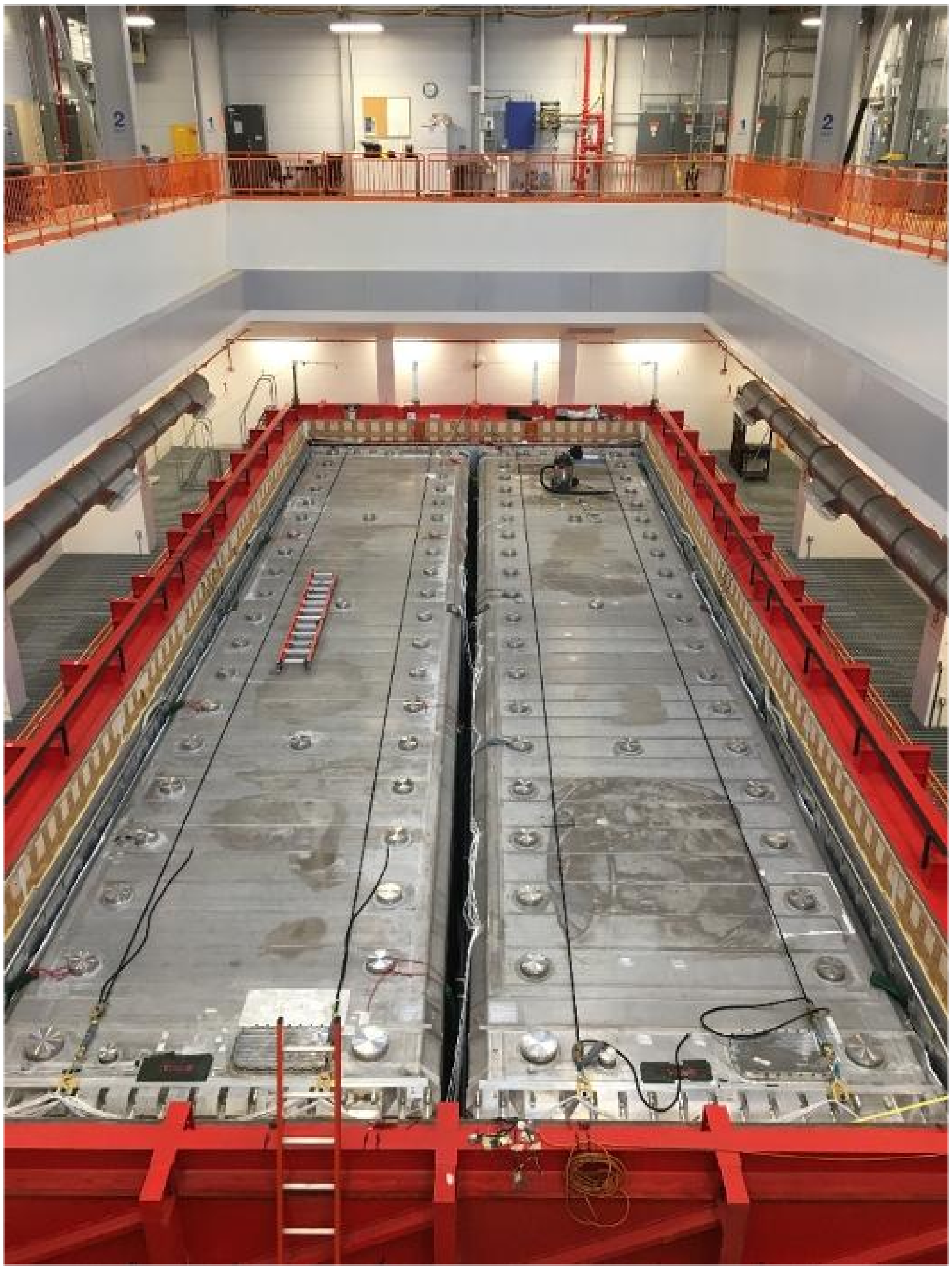

Figure 19. T300 cold vessels installed (Aug. 2018).

successfully filled with liquid argon during commissioning in February–April 2020. The pressure control for the cold vessels is implemented with gas re-condensers at $\sim$ 1.050 bara. Additionally, two vent valves per cryostat are set to control the pressure at 1.150 bara. Additionally, a single control valve with Cv = 70 is set to control the pressure at 175 mbarg with full opening at 250 mbarg based on analogue pressure readout or pressure limit switch status. Finally, the pressure safety for each of the T300 cold vessels is implemented with three (3) magnetic safety devices by VELAN (France),

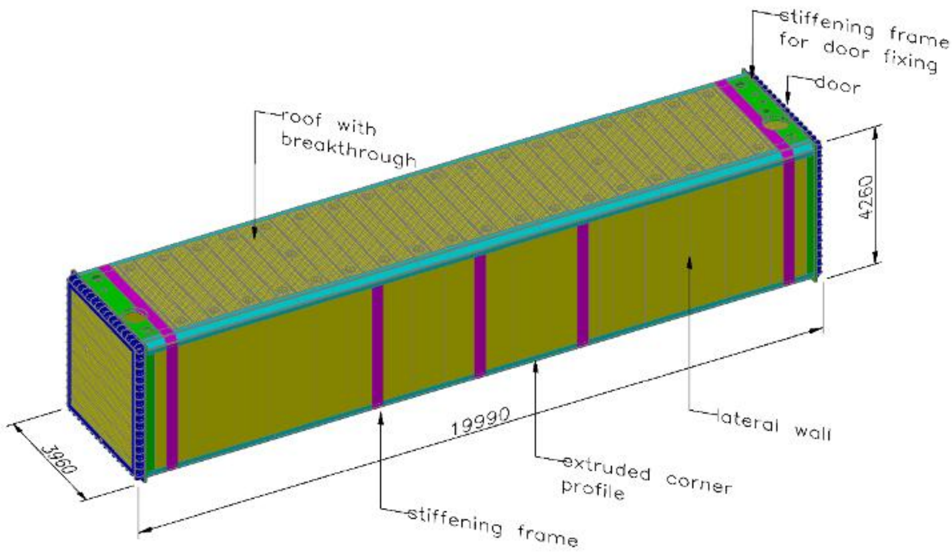

Figure 20. Modules external dimensions.

model 2N2573 with orifice 168.3 mm (22156 mm^2 flow area) and discharge coefficient 0.68. They are calculated to protect the vessels from at least these four main over-pressurization scenarios:

1. Loss of LN_2,
2. Overfill from LAr dewar,
3. Runaway makeup gas,
4. External fire engulfing warm vessel.

4 Passive insulation and supporting structure

CERN designed the WA104 warm vessel [32–34]. The structure (figure 22, figure 23) is classified as execution class 2 (EXC2) in accordance with EN 1090. It provides the mechanical support of the inner insulation and containment of low-pressure nitrogen purge gas.

The structure consists of vertical beams alternated with horizontal beams and extra stiffeners to support and stiffen the structural steel plate. Inside the steel structure, a skin of structural steel plate is welded. On top of the plates a layer of insulation is installed. The insulation is glued on the side walls, which means that the weight of it concerning the side walls as well as the weight of the plate are directly taken by them, and no extra load is transferred to the floor of the steel structure.

The dimensions of the warm vessel structure are shown in table 3.

CERN subcontracted the manufacturing (including welding) and delivery of 84 modules + 93 connecting elements, following the specification drawings provided by CERN. The total weight of the structure is around 87 T. Each subassembly is constructed of IPE beams welded together. The subassemblies are delivered equipped with pre-welded steel plates.

Acceptance tests (witnessed by CERN) per EXC2 requirements as per EN 1090, plus multiple additional tests per EU regulations were conducted prior to delivery.

2026 JINST 21 P04012

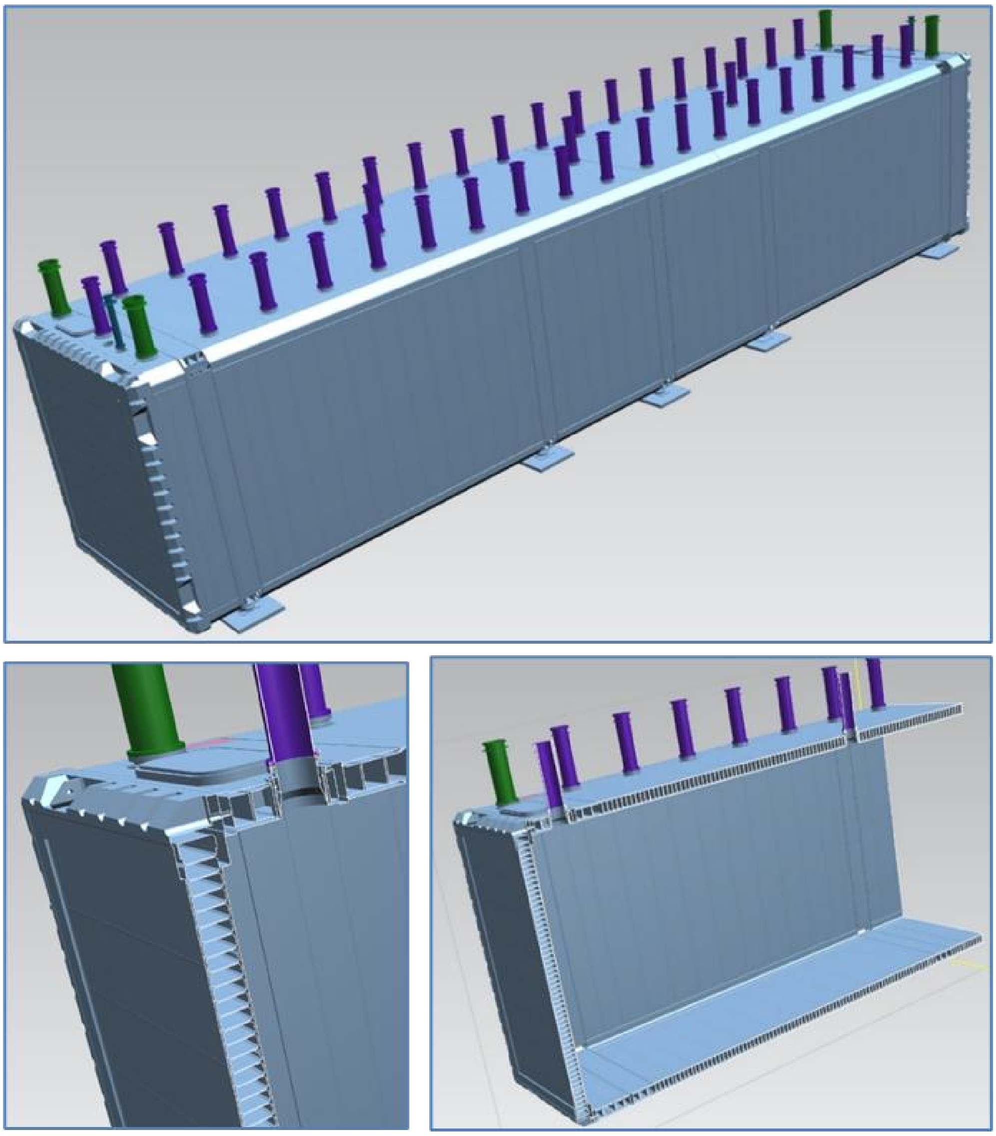

Figure 21. Details of construction of T300 cold vessels

The structure was erected in the SBN-FD building in 2017 (with the exception of the roof) by a joint CERN/INFN/Fermilab team. The prefabricated components were assembled by bolting the structural elements together, followed by TIG welding of the external skin to the beams and of the individual skin panels to form a continuous, leak-tight surface.

In addition to standard weld quality assurance procedures — including welder certification, visual inspection, and liquid penetrant testing — the leak tightness of the welds between skin panels was verified using dedicated vacuum test fixtures. These tools enabled the application of vacuum to sections of weld approximately 40 cm in length, allowing localized leak detection. All weld qualification and leak tests were completed prior to installation of the insulation panels. The insulation panels were then installed on the floor and walls (see figure 24, figure 25).

Two cold vessel tanks (see section 3) were installed inside the warm vessel in July–August 2018, after the installation of the lower and vertical side elements of the cold shields (section 5). Each tank sits

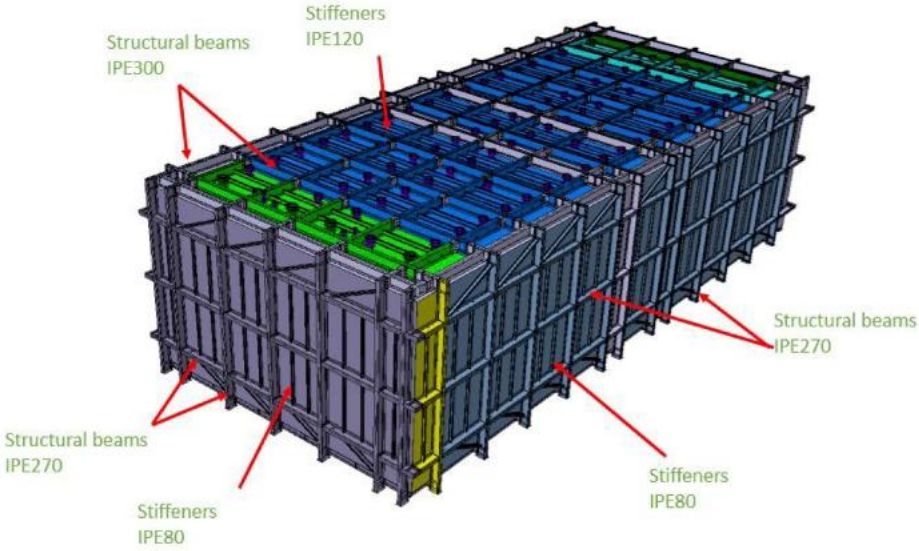

Figure 22. Support structure layout (top view).

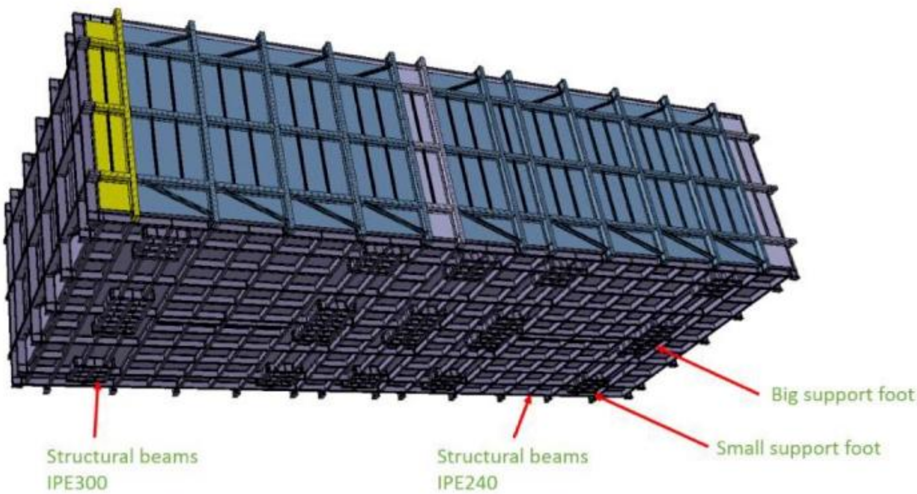

Figure 23. Support structure layout (bottom view).

Table 3. Warm vessel structure geometrical parameters.

Dimensions	Width (mm)	Length (mm)	Height (mm)
External	10268	22638	6218
Inner (structural steel plate to structural steel plate)	9720	22090	5664
Inner (from insulation to insulation)	8520	20890	4664
Middle axis of beam to middle axis of beam	9998	22368	5948

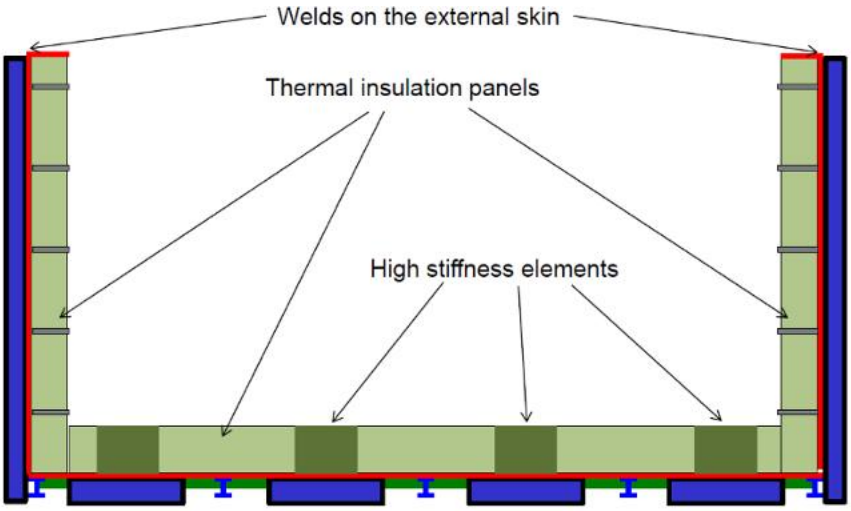

Figure 24. Warm vessel assembly schematics.

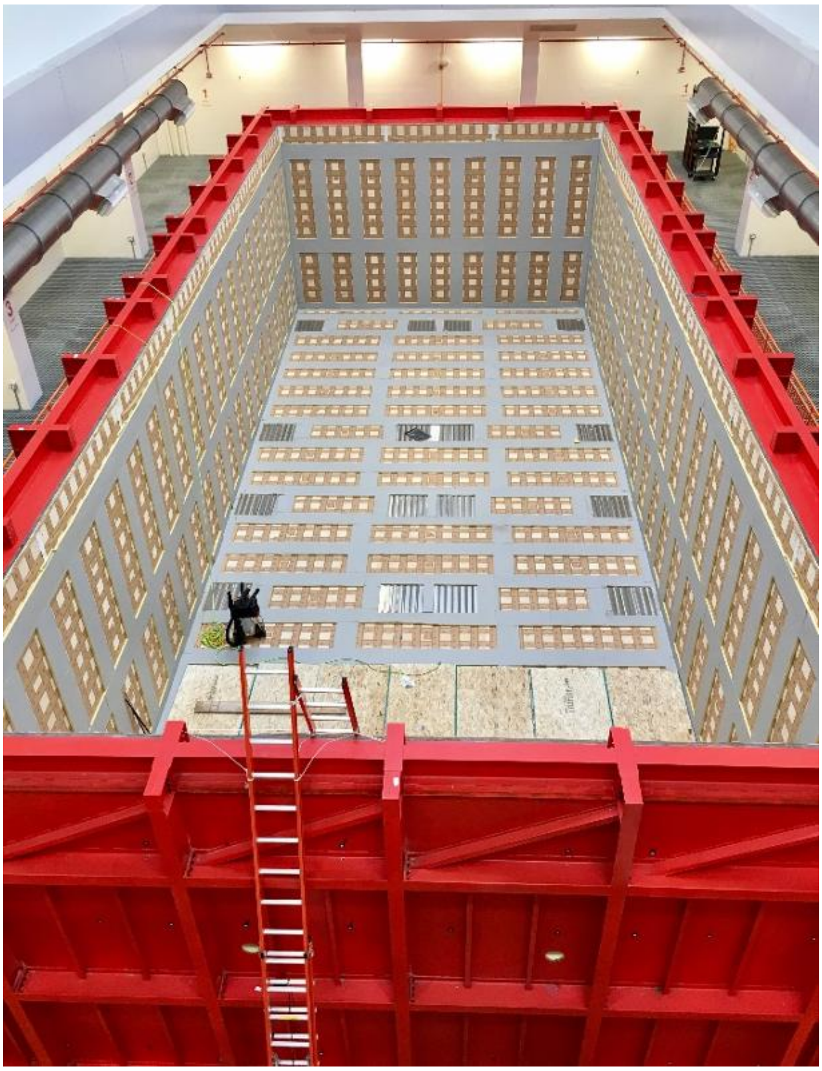

Figure 25. Warm vessel assembly (2018).

on ten feet. The insulation below those feet is a denser one so that it is suitable to withstand the total load. For that reason, on the floor of the support steel structure special metallic feet were designed to support the total weight coming from the tanks. The rest of the area of the floor only supports the insulation.

The top of the steel structure was accessible for installation of nitrogen shields and cold vessels and was closed later, after the T300 vessels were installed. The feedthroughs are only supported on the roof of the inner tanks and not on the roof beams or the roof steel plates of the steel structure. The insulation thickness is 600 mm on the bottom and side walls, and 400 mm on the roof. The structural steel skin thickness is 4 mm on the side walls and roof, and 10 mm on the bottom wall. See figure 26 for an illustration of cold vessels installation inside the structure.

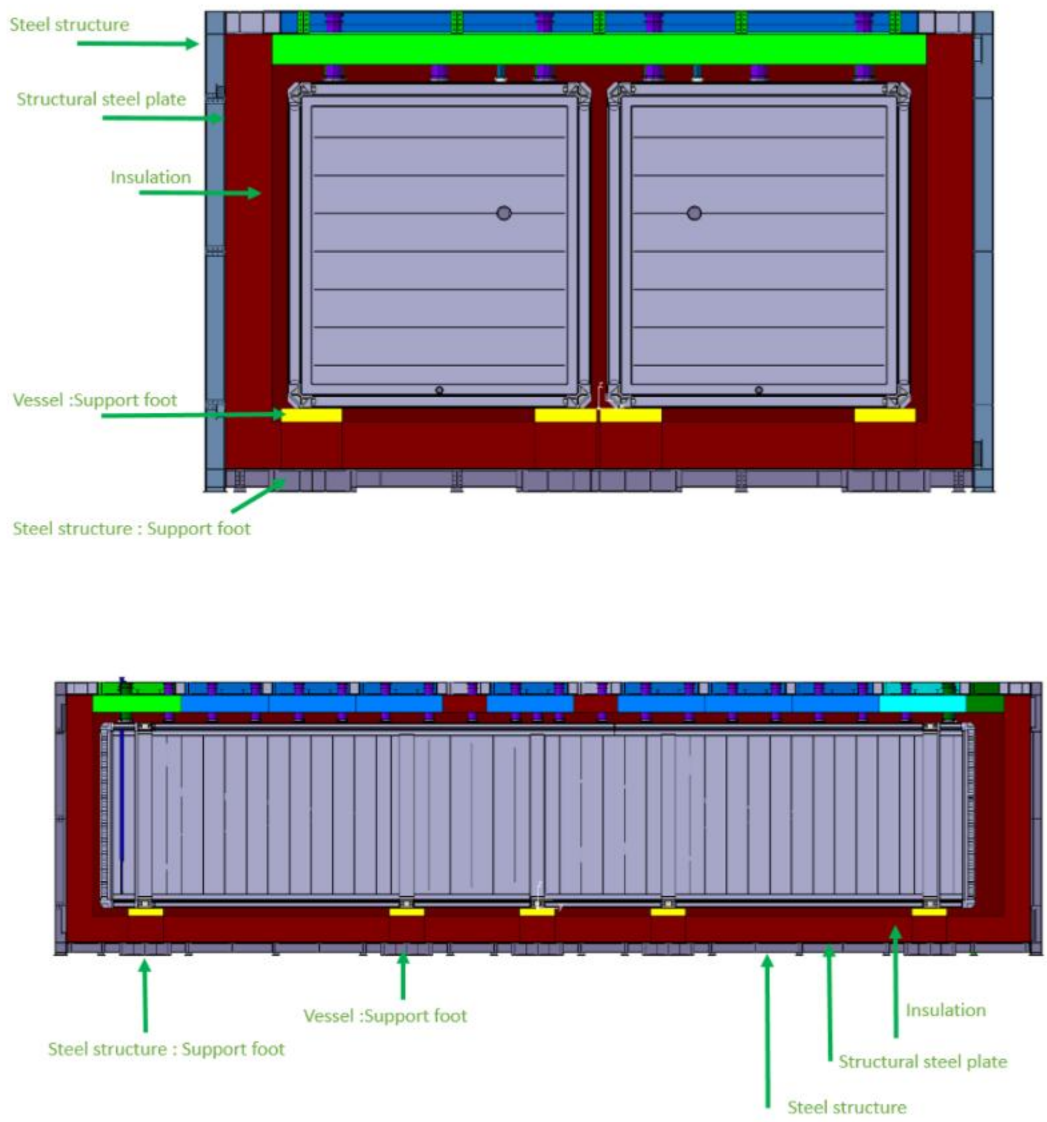

Figure 26. Inner tanks & Support feet

The cold nitrogen shields (see section 5 assembled inside the warm structure (see figure 27) and positioned between the cold vessels and the foam insulation, thus effectively intercepting the heat

2026 JINST 21 P04012

leak from atmosphere through the passive insulation. The weight load from the nitrogen shields is accounted for in the design of the structure, while a possible rupture and subsequent leak of nitrogen into the warm-structure space is accounted for in the venting calculations.

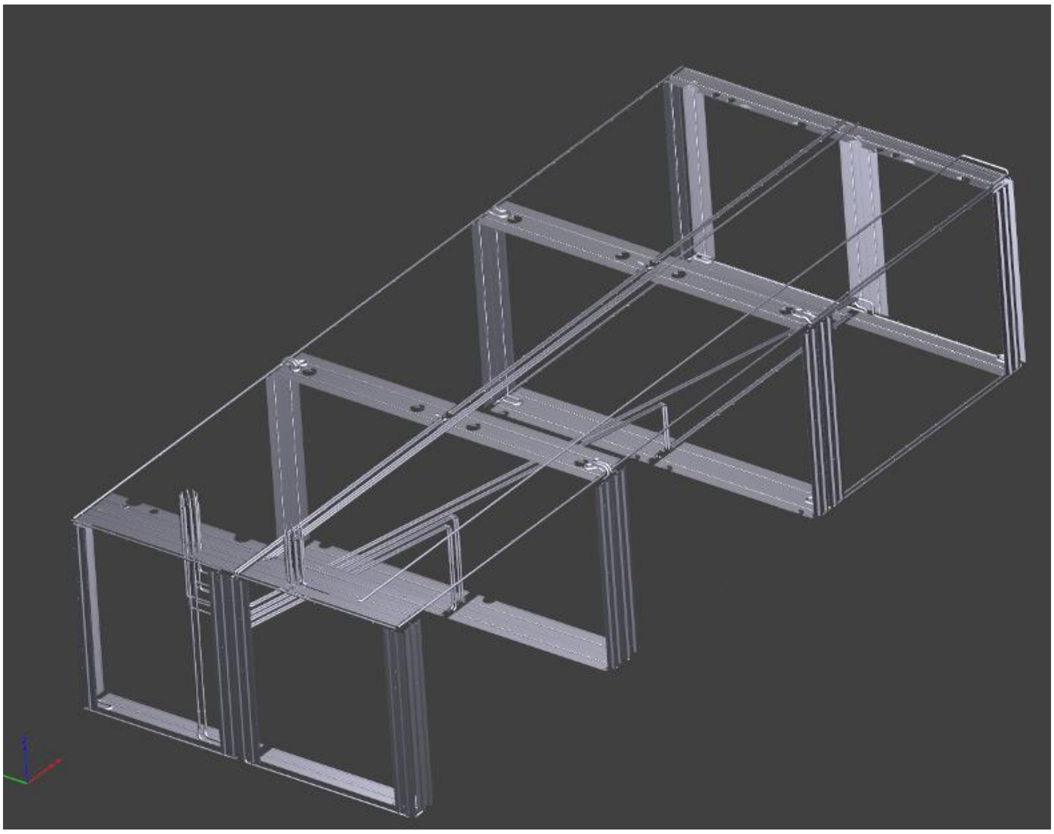

Figure 27. Cold nitrogen shields assembly.

The support structure therefore serves a dual purpose: it houses the modules inside the common insulated space and maintains the inert nitrogen environment inside the structure to prevent any moisture content plating on the cold surfaces. The penetrations on the roof (chimneys, transfer lines, etc.) are sealed with plastic covers to minimize leakage of purging gas to atmosphere.

The safety assessment of the warm structure was done per Fermilab ESH Manual and described in EN02602. That included verification of design calculations, manufacturing data and installation QA/QC.

The pressure safety included the following over-pressurization scenarios:

1. Internal failure of GN_2 purge supply and release of max available $10\,m^3$/hr,
2. Failure of LN_2 shield supply pipe and release of full LN_2 pump discharge flow into the warm vessel,
3. Failure of a module or its component and release of LAr into the volume of the warm vessel.

The warm structure (with nitrogen shields inside it) is schematically shown in figure 28. It shows that the volume is purged with gaseous nitrogen at $\sim$ 7 mbarg and is protected from overpressure with two pressure reliefs set at 10 mbarg. The reliefs are Construzioni Meccaniche Lupi S.r.l., Model 493 — 10″ (DN250). It is set at 100 mm H_2O (10 mbar) and has a rated flow of ~ 3813 Nm^3/hr at 11 mbar.

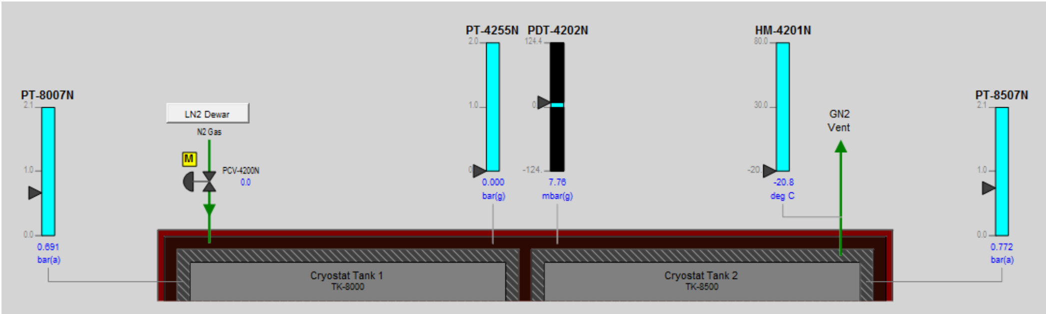

Figure 28. Warm structure volume process diagram

The warm structure was pneumatically pressure tested at ~ 33 mbarg in November 2019.

5 Cold shields

5.1 Functional description of the cold shields

The cold shields are a set of heat exchangers placed in the space between the internal surface of the thermal insulation and the external surface of the two cold vessels. They surround the ensemble of the two cold vessels: there is no cold shield in between the two cold vessels. The heat exchangers are made of St. Steel pipes (AISI 316L), flown with liquid and gas nitrogen, mechanically attached to aluminum (AL 6101B) extruded profiles.

The cold shields serve three main purposes:

1. During the initial phases of the cryogenic commissioning: cool down the cold vessels and the internal detector components in less than 10 days, while maintaining the thermal gradients on the St. Steel detector structures to within the specifications ($\Delta T_{\mathrm{Max}} = 50$ K). During this phase, the temperature profiles across the thermal insulation are also established.

2. During the filling and operation: define the bulk temperature, and therefore the saturation pressure, of the liquid argon mass.

3. During operation: avoid that localized heat inleaks, coming through the thermal insulation, induce boiling or large convective motions in the liquid argon volume and establish a temperature uniformity in the liquid argon volume to within the specifications ($\Delta T_{\mathrm{LAr,Max}} = 1$ K).

Thermal exchange between the cold shields and the thermal insulation, on one side, and the cold vessels, on the opposite side, is provided mainly by thermal convection of the nitrogen gas at atmospheric pressure, that fills the volume between the thermal insulation and the cold vessels. On the top, there is also thermal contact between the cold shields' aluminum profiles and the cold vessels.

To intercept heat inleaks, the cold shield panels must cover the largest possible fraction of the internal surface of the thermal insulation, in particular on the bottom and vertical sides. The requirement on the temperature uniformity ($\Delta T_{\mathrm{LAr,Max}} = 1\,\mathrm{K}$) sets a constraint on the minimal conductance of the nitrogen circuit that must be large enough to prevent heating of the liquid nitrogen beyond the above specification.

Following the original scheme that was implemented in Gran Sasso, the cold shields are divided in ten sub-circuits according to the layout shown in figure 29. Six sub-circuits, three for each cold vessel, cover the bottom, the East, the West and the top sides. Each one of these six sub-circuits is obtained by joining in series a horizontal heat exchanger panel on the bottom with a vertical heat exchanger panel on the side (East or West) and then with a horizontal heat exchanger panel on the top to form a C-shaped circuit. The remaining four sub-circuits (two per cold vessel) cover the North and South vertical sides, each one made of a single vertical heat exchanger panel.

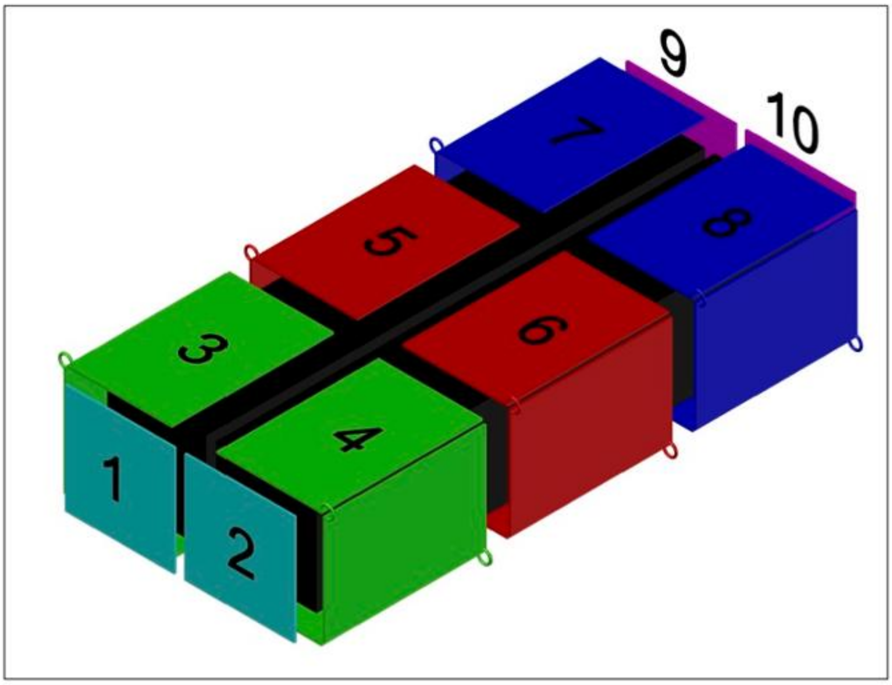

Figure 29. Layout of LN_2 shields.

Liquid nitrogen is provided to the cold shields either by pressure transfer from the external storage dewar or from the phase separator, through a Barber Nichols cryogenic liquid circulation pump. The common input is separated through the ten sub-circuits in a valve box where a set of 10 proportional valves is used to regulate the LN_2 flow in each sub-circuit. Another valve box collects the output of cold shields and another set of 10 proportional valves is used to regulate the LN_2 pressure in each sub-circuit before merging the flows and returning them to the phase separator.

At the beginning of the cool down, the input to the cold shields is coming, by pressure transfer, from the external LN_2 storage dewar. In this initial phase, all the LN_2 is gasified before reaching the output valves and it is exhausted to the atmosphere, outside the building. When the temperatures are sufficiently low, a fraction of the cooling nitrogen will return in the liquid state and will start to fill the phase separator. At this point, the LN_2 circulation pump can be started, and the cooling will proceed with forced circulation through the pump.

5.2 Cold Shields: design and construction specifications

The design of the cold shields was initially developed assuming a structure completely made of aluminum, with plates with a circular hole in the middle where LN_2 at the desired temperature (87 K) was flown (figure 30). The minimal design specifications are: < 1 K temperature gradient across the panel, with a heat load of 10 W/m^2 uniformly distributed on the panel surface (the specifications for the thermal insulation require an average heat inleak of < 10 W/m^2).

The geometry illustrated in figure 30 was simulated with the ANSYS code, taking as reference material the alloy AL 1050A (thermal conductivity = 270 W/m/K at 87 K). The results (figure 31) show that a temperature difference of < 0.5 K is achieved with a thermal load of 20 W/m^2: the chosen geometry provides a comfortable safety factor of 4 with respect to the specifications. Similarly, the pressure drop across the nitrogen circuit was calculated for two different flow conditions: single phase (liquid) and two phases with gas to liquid mass ratio 1/5.

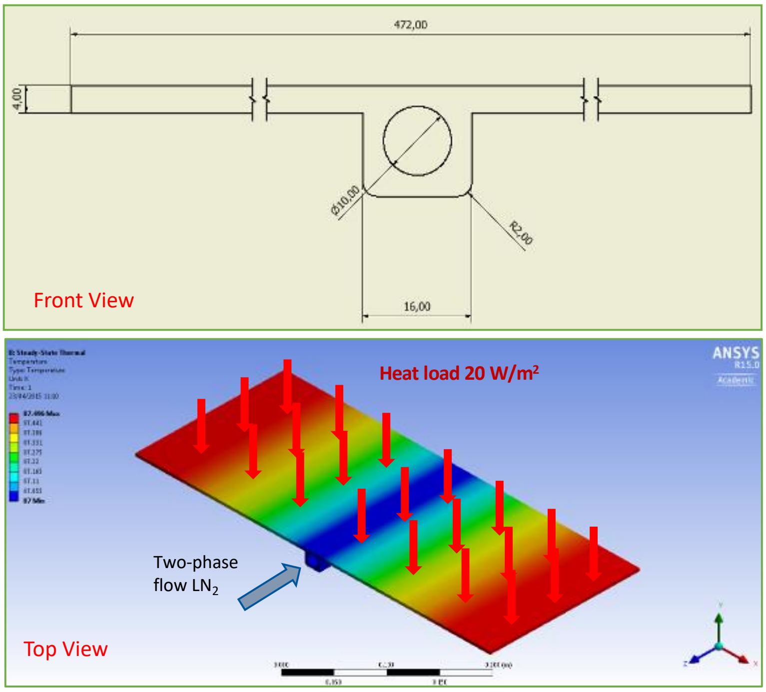

Figure 30. View of the panel geometry and thermal loads used in the thermal simulation. Dimensions are in mm.

The theoretical calculations were then validated with a test conducted at CERN on a mock-up sample of three panels arranged in a cylindrical shape (figure 32) so that they could be hosted inside a cylindrical dewar. The measurements confirm the prediction from the simulations (figure 33).

Due to the technical difficulty and cost in realizing the entire cold shields in aluminum, a hybrid design was developed, with stainless steel pipes, for LN_2 distribution, mechanically coupled (clamped) to aluminum plates as illustrated in figure 34.

All the extruded aluminum panels have the profile shown in figure 35. The groove at the top center of the profile hosts the stainless-steel pipe where LN_2 is flown. The ribs in the lower part of the panels ensure mechanical stiffness and create some distance from the adjacent surface allowing for a

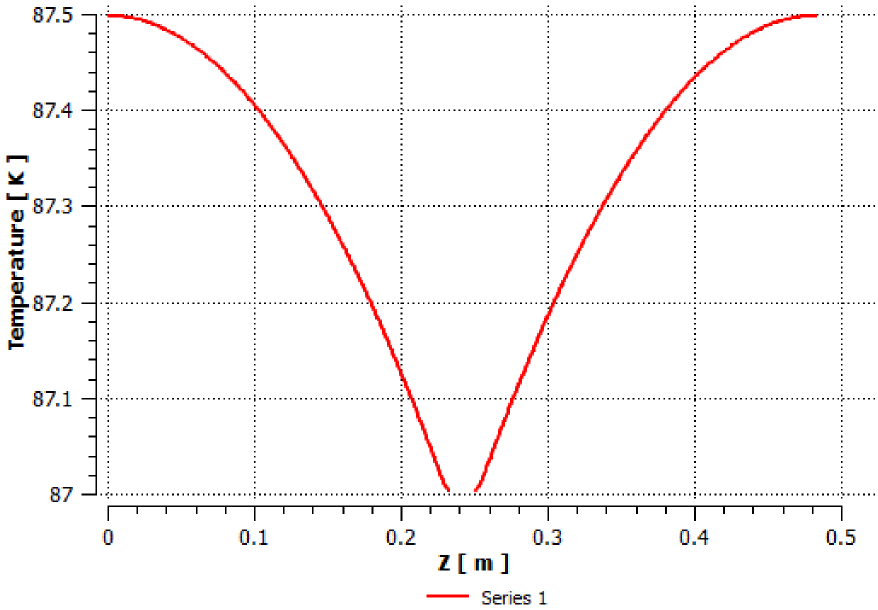

Figure 31. Calculated temperature profile across the panel for a heat load of 20 W/m^2 uniformly distributed on the panel's surface.

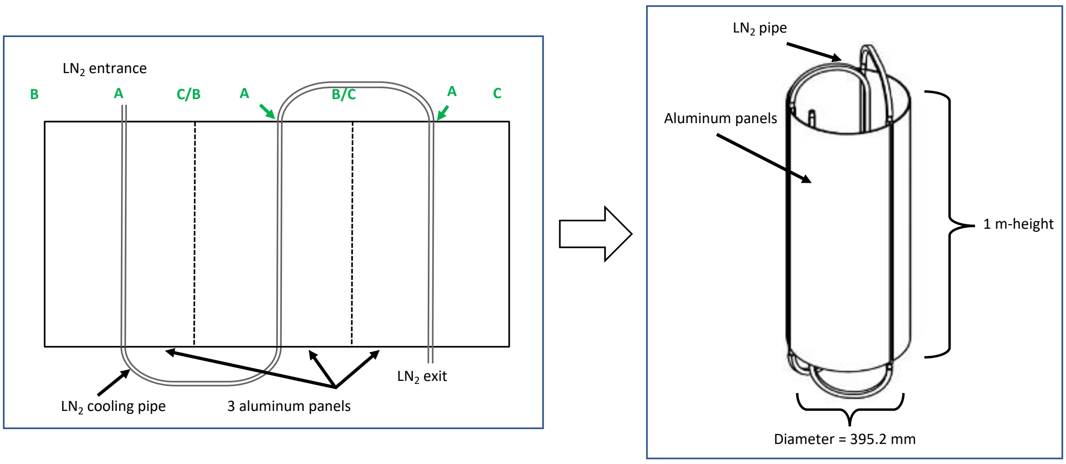

Figure 32. Schematic drawing of the panel tested at CERN. Each one of the three sections shown on the drawing on the left has the same width of the panel in figure 30. The arrangement in a cylindrical shape (right drawing) ensures that the thermal load is on the external side only. This configuration provides a thermally equivalent boundary condition to a single panel with length equal to three times the length of one section laying flat on a surface providing a heat load of 20 W/m^2.

more uniform thermal exchange. Also, the aluminum thickness was increased from 4 mm to 5 mm, to partially compensate for the thermal resistance added by the stainless-steel pipes and to increase mechanical stiffness. During installation, operators need to walk on the cold shields to perform various tasks, including welding and positioning relatively heavy equipment.

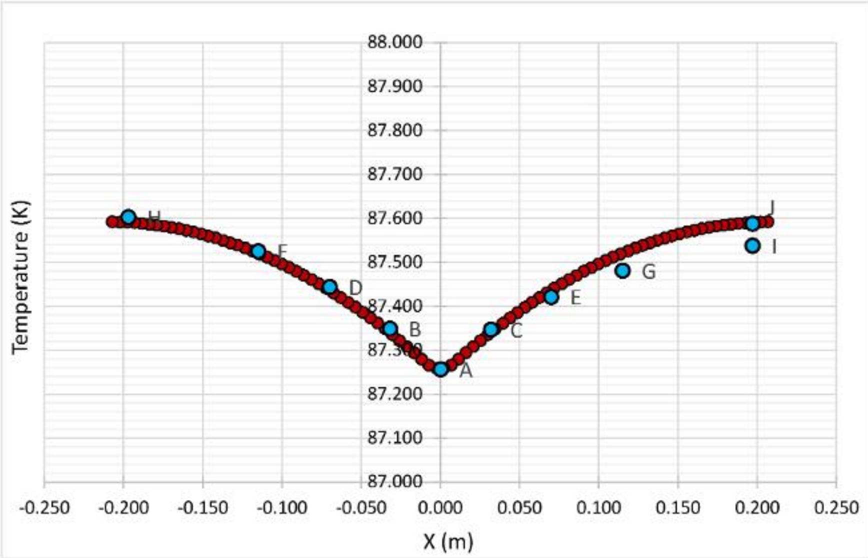

Figure 33. Results of the measurements performed on the test panel (blue circles) compared with the theoretical predictions (red circles), demonstrating the validity of the theoretical calculations. The theoretical curve differs from that reported in figure 31, as the calculation was adapted to the geometry and thermal configuration of the mock-up test setup.

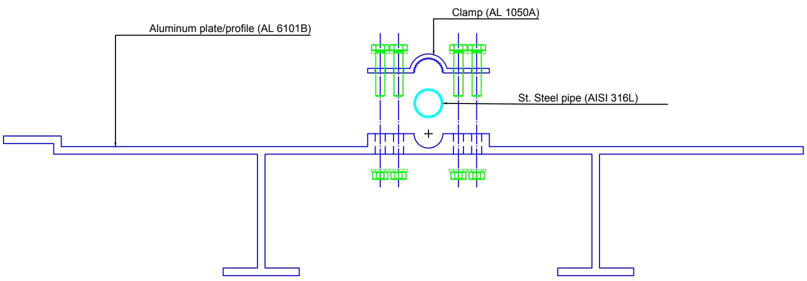

Figure 34. Coupling between an aluminum panel and the St. Steel LN_2 distribution pipe.

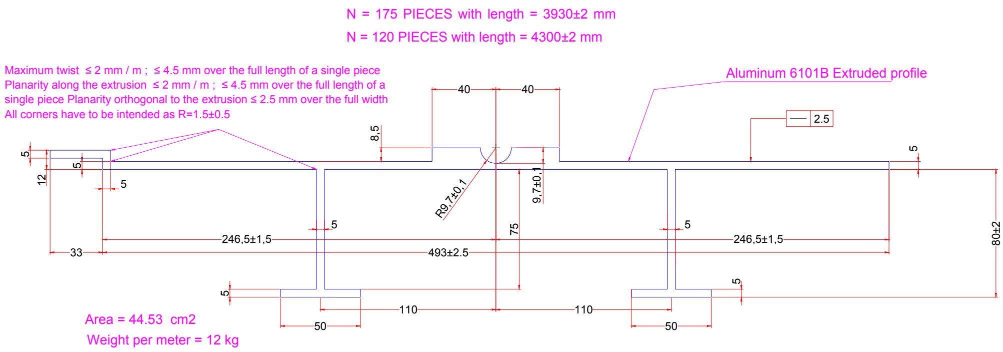

Figure 35. Technical drawing of the aluminum panels cross-section used for the extrusion.

To ensure a good thermal contact between the pipe and the aluminum panel, 100 mm wide clamps are placed every 400 mm (figure 36). The cylindrical inner surface of the clamps is grooved, to ease the relative displacement of the pipes with respect to the panels due to thermal contractions (figure 37).

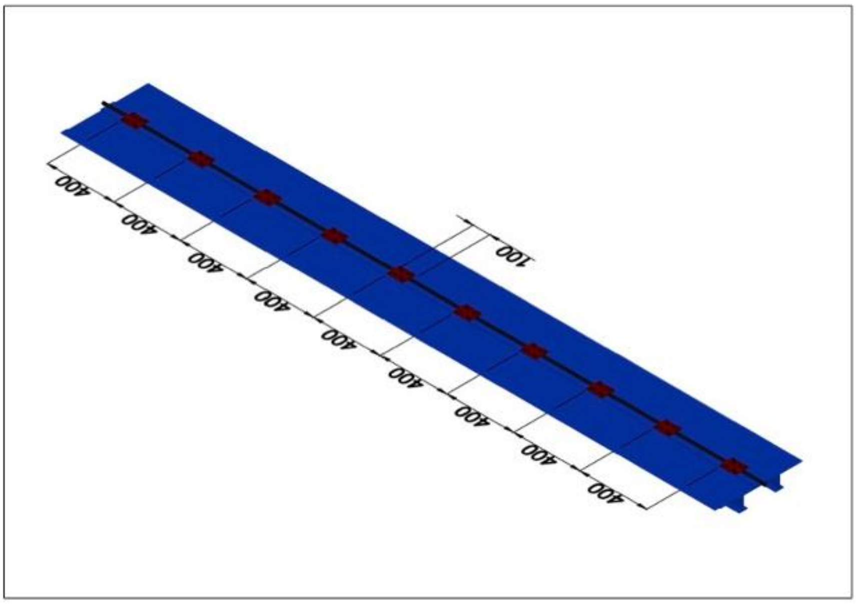

Figure 36. Illustration of the assembly of the piping on the aluminum plates.

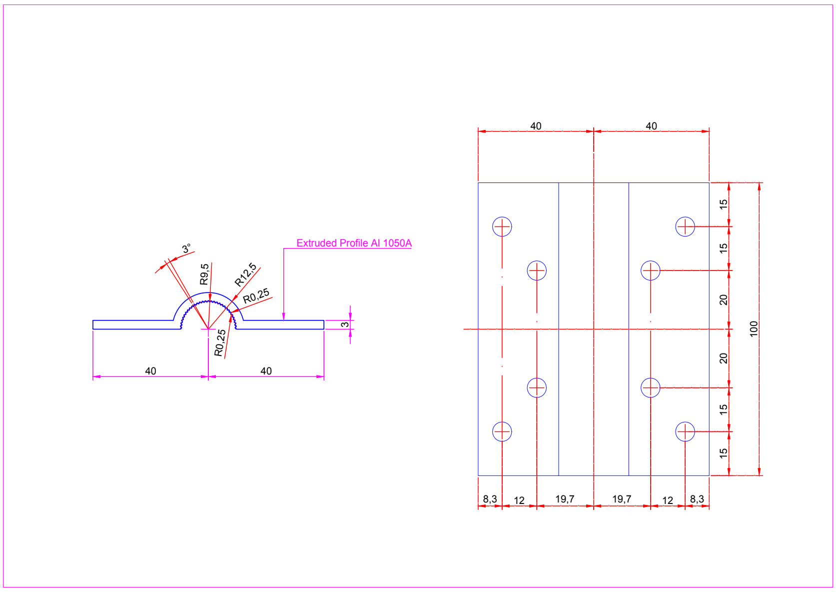

Figure 37. Technical drawings of the clamps for the cold shield panels.

The extruded plates are cut to two lengths, one of 3930 mm for the horizontal (top and bottom) sides, and one of 4300 mm for the vertical (lateral) sides. All the holes for installation of the clamps, passage of LAr pipes, cold vessel supports, chimneys for the passage of the wire cham-

2026 JINST 21 P04012

bers cables, etc., as well as the reduction in width of some panels to adapt the assembly to the required lengths, are realized by machining of the extruded plates (see figure 38 for an example of machining specification and figure 39 as an example of assembled panels of one of the circuits on the top side).

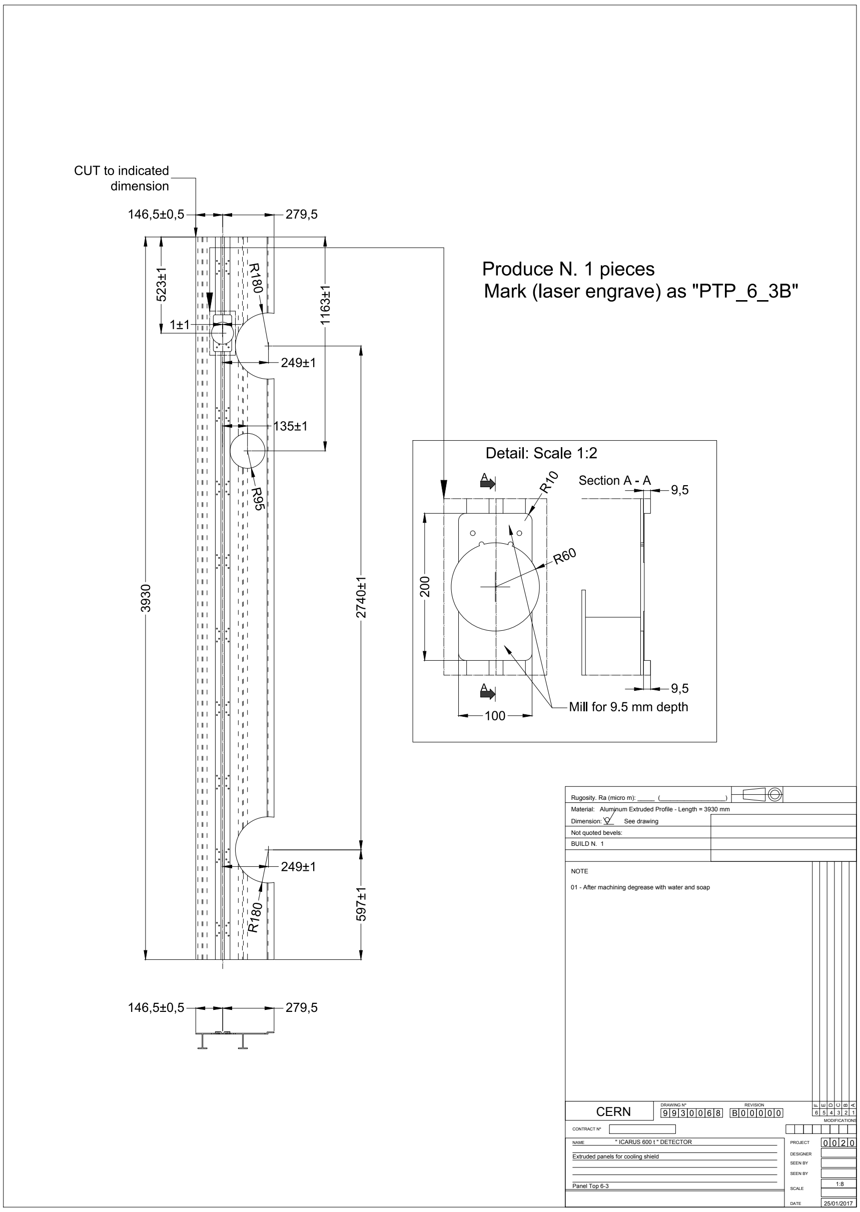

Figure 38. Machining drawing of one of the extruded panels for the top side.

The nitrogen distribution circuit is made by sets of parallel AISI 316L stainless steel pipes of 16 mm ID, 19 mm OD, connected at both ends to manifolds, also AISI 316L stainless steel, with 50 mm ID, 54 mm OD. Each set of pipes, mechanically coupled (clamped) to the appropriate set of extruded aluminum plates, realizes one of the cold shields' planar sub-elements (22 in total) illustrated in figure 29.

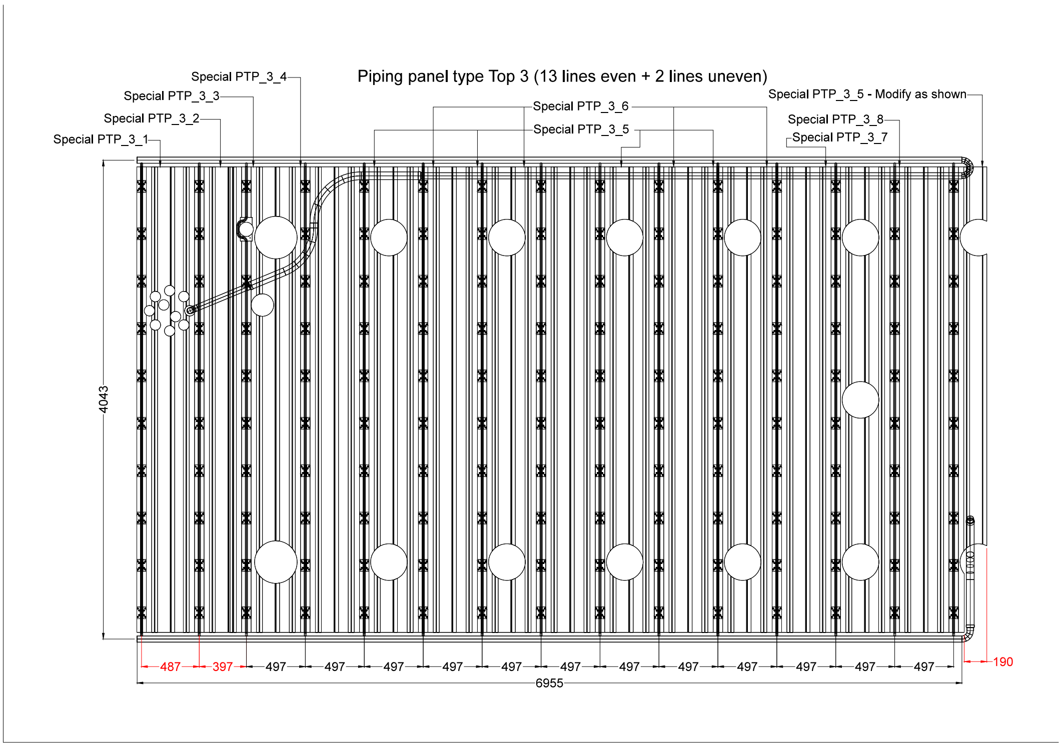

Figure 39. Assembly drawing of one of the cold shield top panels.

5.3 Cold Shields: procurement, assembly, installation and test

The aluminum plates and the clamps were ordered by CERN to two aluminum extrusion companies: one operating in Turkey for the plates, and one operating in Israel for the clamps. The two companies also provided all the required machining (cutting, drilling of holes, etc.) and QA/QC documentation. To ensure a good thermal contact between the plates and the LN_2 distribution pipes, the central groove was machined to the required dimension and tolerance starting from a smaller groove realized by extrusion. Standard CERN specifications for material conformity were applied (Certificates type 3.1, according to EN 10240). For both components, the material is aluminum type 6101b.

The 22, pre-assembled planar LN_2 circuits, made of stainless steel type AISI 316L, were also ordered by CERN to an external company. Specifications referred to applicable European codes for metallic industrial piping (EN 13480-2,3,4,5), stainless steel (EN 10088-1), stainless steel piping for pressurized circuits (EN 10216-5; EN 10217-7), welding (ISO 3834; EN ISO 15614-1; EN ISO 15609-1; EN ISO 14732; EN ISO 9606-1), cryogenic vessels (EN 13458-2), non-destructive testing (ISO 17637; ISO 17636-1; EN ISO 5817; EN ISO 9712; ISO 13585), certificates (EN 10204). In particular, the pre-assembled circuits were tested for helium leak tightness at 1×10^{-9} mbar liters/s at room temperature. All pre-assemblies were also pressure tested at 10 bar for at least 1 hour.

Additional components, such as pipes, joints, braided flex hoses, to realize input and output lines and for panels interconnections, were procured by Fermilab.

Funding for all cold shields parts was provided by INFN.

All components were delivered at Fermilab for the final assembly and installation.

2026 JINST 21 P04012

The first step has been the clamping of the aluminum plates to the pipes of the LN_2 circuit to realize the basic panels of the cold shields (figure 40). The first panel was thermal shocked in liquid nitrogen, to verify that the clamping was allowing for the reciprocal displacement between the pipes and the aluminum plates due to thermal contractions.

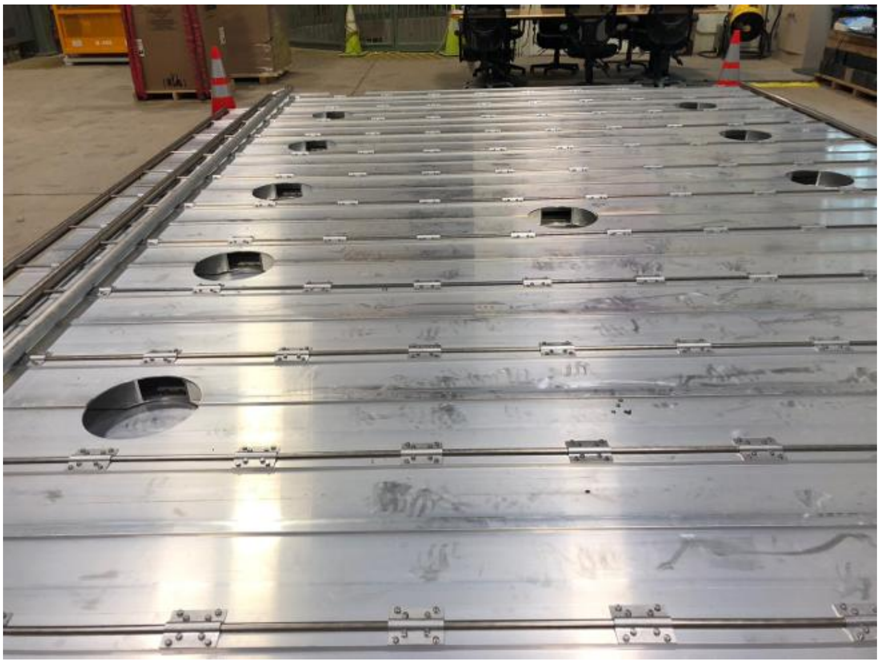

Figure 40. Photograph of one of the top cold shield panels after assembly.

The bottom and the vertical panels were then moved inside the thermal insulation. The bottom panels were connected with braided flex hoses to the lateral panels (side panels). The inlet pipes, running at the center, in the region between the two cold vessels and welded to the lower part of the cooling circuit, were installed (figure 41). Temperature gauges were glued to the aluminum panels in correspondence of the inlets and cabled. To ensure accessibility of the parts for inspection and repair, the half-completed circuits were sealed and tested for helium leak tightness before positioning of the cold vessels. They were also pressure tested at 10 bar for 1 day.

After positioning of the two cold vessels (figure 42) and installation of the chimney, the top cold shield panels were put in place and connected with braided hoses to the side panels to complete the cold shields subsections 3 to 8 of figure 29. The output lines were installed and welded to the top part of the panels (figure 43). The completed circuits were tested for helium leak tightness of the added parts. They were then pressure tested at 10 bar for 1 day. Welding of the input and output lines to the valve boxes was performed after installation of the top part of the thermal insulation and of the warm vessel (figure 44).

6 Process controls

The Icarus cryogenics control system is a fully automated system, which allows a continuous cryogenic operation through the various modes of operation as described in section 2, while allowing manual

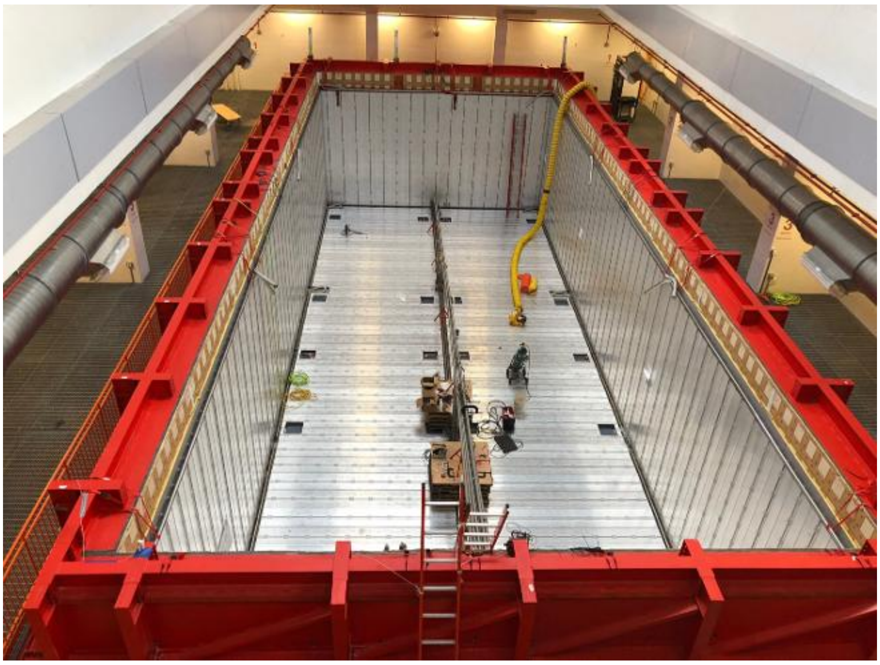

Figure 41. Photograph of ICARUS cryostat after installation of the bottom and vertical cold shields panels.

Figure 42. Picture taken after the positioning of the first cold vessel showing also the cold shields inlet pipes.

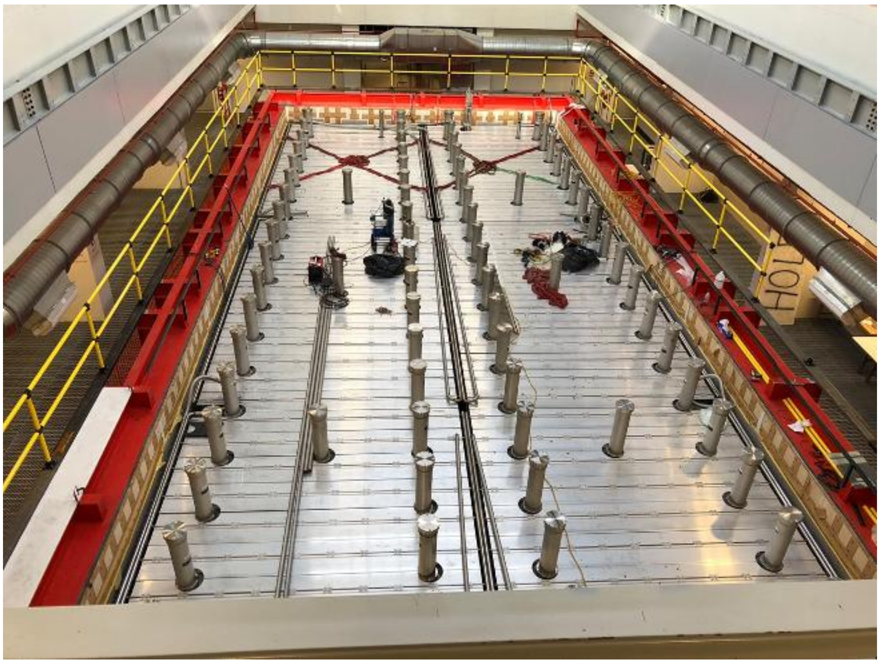

Figure 43. Photograph of the cold shields top part.

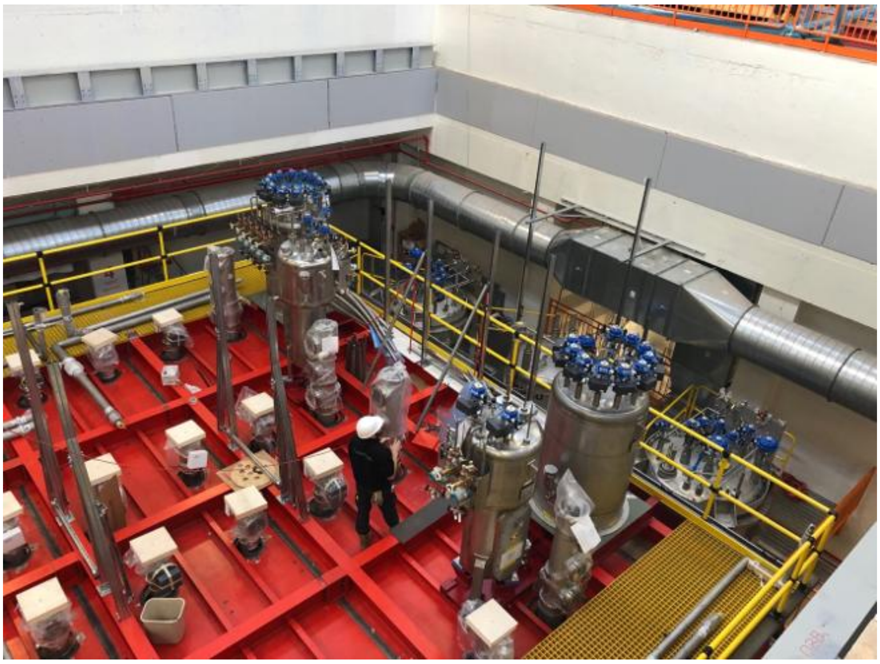

Figure 44. Photograph taken during the installation of the cold shields inlet (right) and outlet (left) valve boxes. In the picture, the visible outlet pipes are yet to be welded to the ones exiting the corresponding valve box.

actions by the operator at any moment. It unifies the control of the external, proximity and internal cryogenics into a single control system. The safety system for ODH is also within scope.

The cryogenics control system was designed, constructed and programmed by Fermilab based on logic specifications provided by CERN for the overall controls integration and proximity cryogenics, by Fermilab for the external cryogenics and ODH system and by INFN for the internal cryogenics.

Prior to full operation, the cryogenic control system and associated auxiliary equipment were activated progressively, starting from the control electronics and followed by pumps and actuators, while continuously monitoring the noise levels of the TPC readout electronics. No measurable increase in electronic noise was observed at any stage of this procedure. This operational validation ensures that power supply stability and electromagnetic compatibility of the cryogenic system are adequate for detector operation.

This section describes the selected hardware and software solutions together with the electrical and control architecture. The software architecture is then presented. Finally, the methodology and the results for the I/O tests and the functional tests are given.

6.1 Control system architecture and selected hardware and software solutions

6.1.1 System architecture and networking

The cryogenic control system utilizes iFIX by GE Digital, a SCADA software platform. The redundancy is implemented by installing iFIX on two computers with full redundancy.

The primary components of the cryogenic control system include two iFIX computers, one of which is also an engineering station (for PLC programming), and multiple PLCs (figure 45).

6.1.2 Centralized topology

The main PLCs provide control and monitoring of most cryogenic equipment. These reside in the first of a series of five control cabinets in the cryogenic controls alcove on the mezzanine level in the SBN-FD building. The remaining four cabinets house all the corresponding I/O terminals.

The cryostats' internal cryogenic sensors have the requirement of being readout by non-switching signals and thus cannot use Siemens RTD modules. A separate PLC handles readout of these sensors.

6.1.3 Networks

The regular Fermi network is available at the SBN-FD building. The iFIX / engineering station computers make use of this network for connection to the central iFIX and iHistorian virtual machines as well as remote control system development.

For security, access to the iFIX and iHistorian virtual machines, as well as historical data access through Seeq, is restricted to machines on the Fermi network (including via VPN connection).

The Cryo Network is private. The iFIX/engineering station computers make use of this network for communication with the PLCs.

6.1.4 Supervisory control and data acquisition

The control system uses Industrial Gateway Server (IGS), also from GE Digital. IGS provides an OPC DA server that both iFIX and PLCs can connect to and share data. It also provides read-only channels for the detector control system, which runs on Experimental Physics and Industrial Control System (EPICS), to collect data.

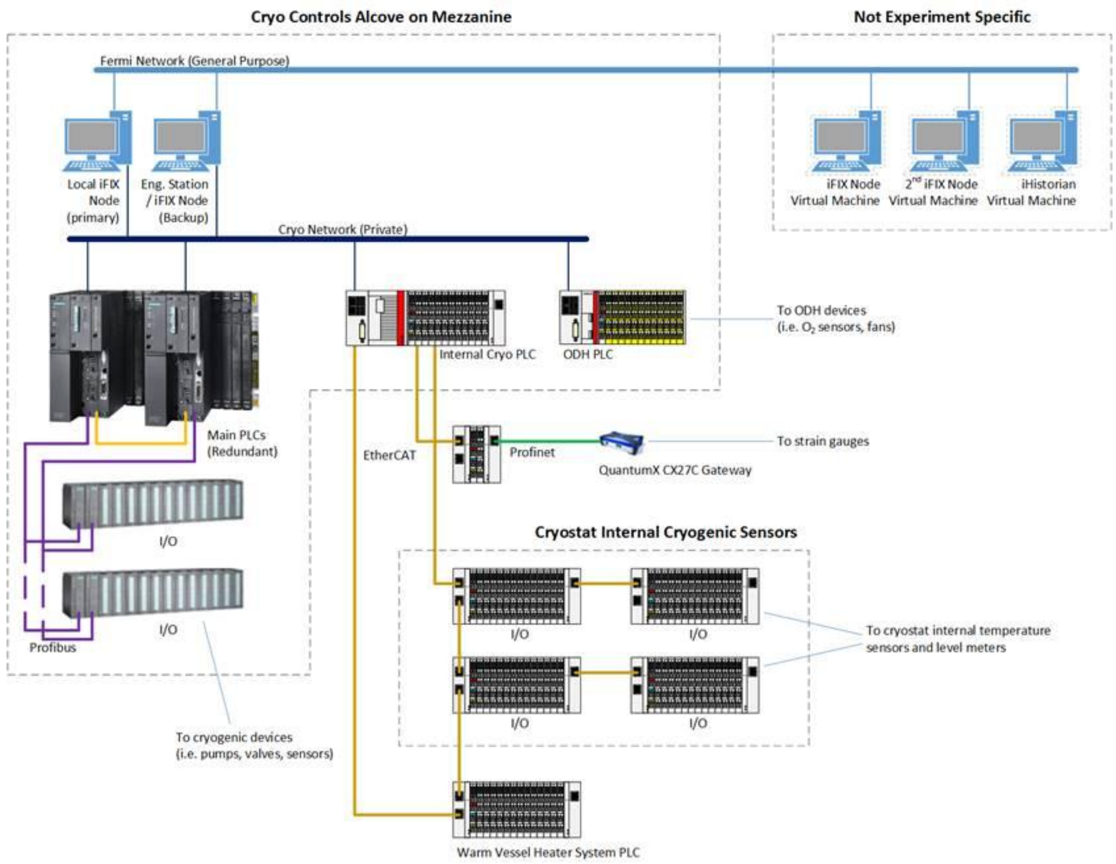

Figure 45. System architecture.

6.1.5 Human Machine Interface (HMI)

The cryogenic control system includes an HMI, using the iFIX Workspace. The HMI provides monitoring and commanding of all cryogenic equipment. However, the HMI does not contain any control logic. (PLCs are not dependent on the HMI to operate.)

The design of the HMI incorporates best practices from ANSI/ISA-101.01-2015, Human Machine Interfaces for Process Automation Systems. This includes implementation of a hierarchy of displays, as illustrated in figure 46, figure 47, figure 48, figure 49 below.

The above-mentioned hierarchy of displays follows the software architecture described in section 6.2 including the Process Control Object (PCO) break-down structure, associated modes and status information, and steppers animation.

The HMI has been developed to enable the display and the simulation of a number of variables in order to limit the actions needed in the PLC program and the need of controls expert during the commissioning and operation stages. The simulation of variables is a feature allowing to substitute the real values read from analogue field devices with a virtual value in order to force the action by the logic or control loop. These variables include the field inputs and outputs together with associated limits, ranges, thresholds, the controllers with associated set point and PID parameters, the alarms and interlocks, a selection of PLC computed variables and the user commands, while the PID parameters of the controllers remained hard coded into the PLC and the field digital inputs cannot be simulated.

2026 JINST 21 P04012

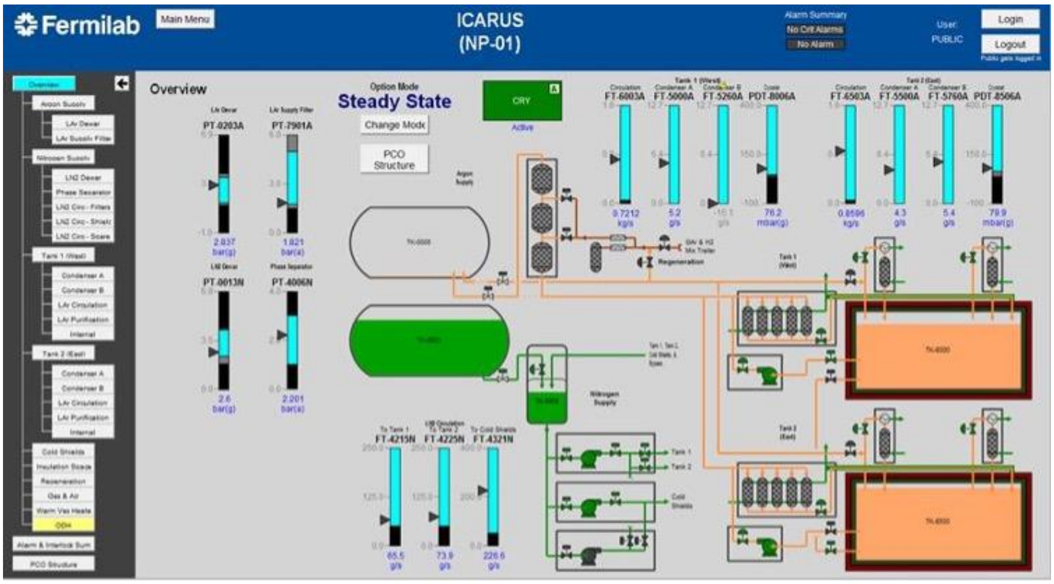

Figure 46. Level 1 display — Entire system overview.

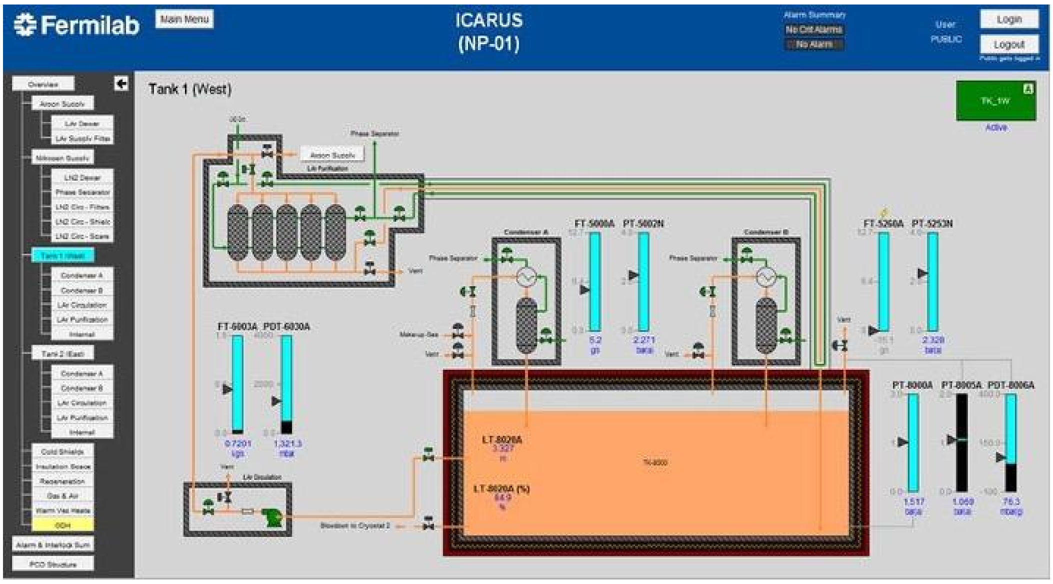

Figure 47. Level 2 display — Tank 1 (West) overview.

The HMI employs a simple security scheme. It defaults to a "public" user, which allows monitoring only. To gain access to manipulate the system, users must be granted access by the Admin and log in.

6.1.6 Alarm management

Alarm logic is in the PLC, but limits are set, and alarms are acknowledged through the HMI. Alarms incorporate best practices from ANSI/ISA-18.2-2016, Management of Alarm Systems for Process Industry. This includes such features as alarms states, dead band, delays, shelving, and auto acknowledgement (figure 50).

Alarms are designated as critical or non-critical based on their severity.

2026 JINST 21 P04012

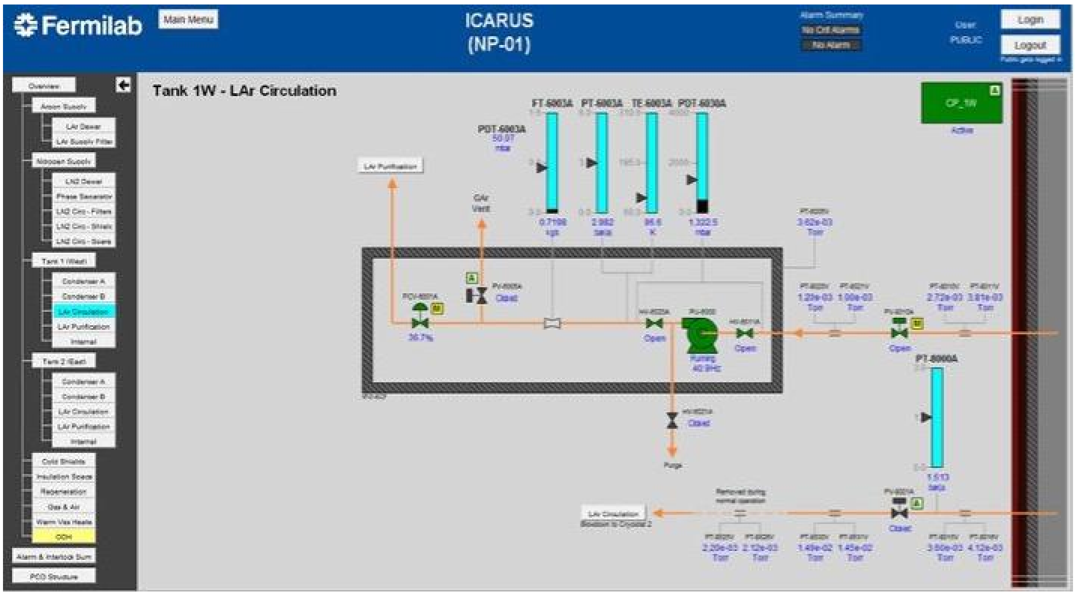

Figure 48. Level 3 display — Tank 1W LAr circulation.

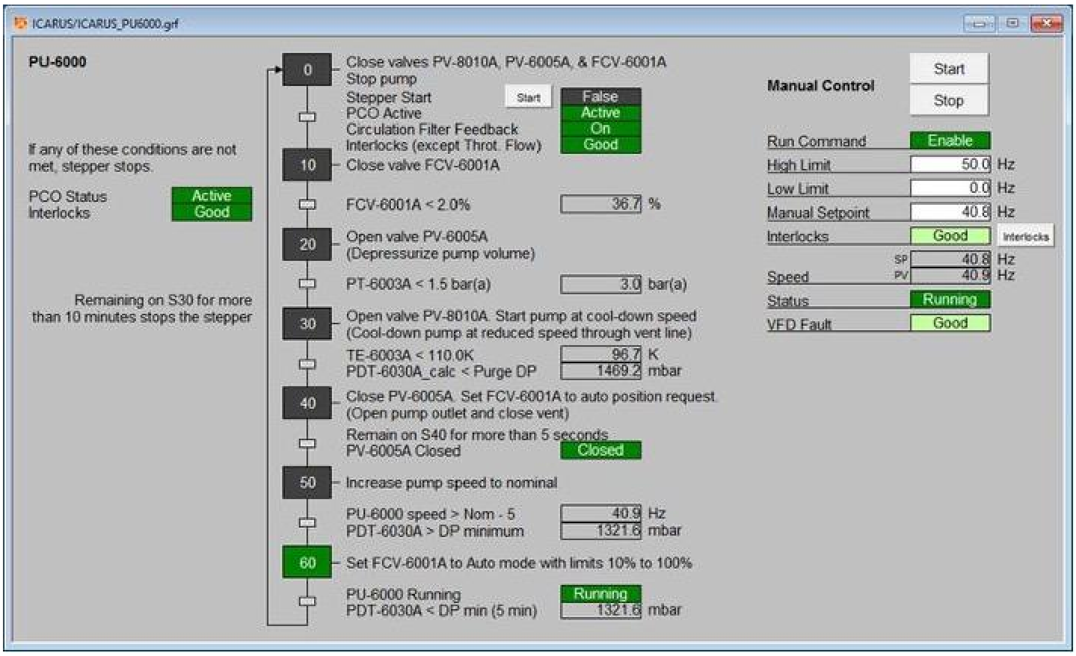

Figure 49. Level 4 display — Pump PU-6000 stepper.

Outside of the HMI, remote notification of alarms is implemented by an auto-dialer called WIN-911. Critical alarms prompt immediate notification at all times, while non-critical alarms only prompt notification during business hours. (Notifications of non-critical alarms occurring in off hours are sent when business hours begin.)

One person is designated as the cryo coordinator and holds the cryo coordinator smart phone. Alarm notifications are sent via text to the cryo coordinator phone as well as by email to a short LISTSERV list of experts.

2026 JINST 21 P04012

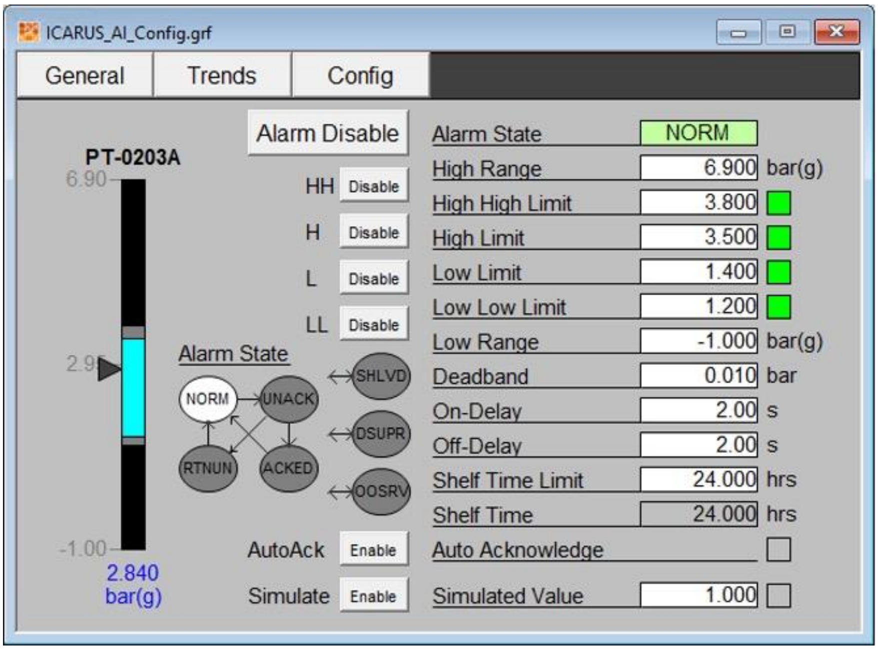

Figure 50. Example alarm configuration display.

Additionally, critical alarms trigger the SBN-FD Cryo Alarm to Fermilab Dispatch via the FACILITY INCIDENT REPORTING UTILITY SYSTEM (FIRUS) system. They have a prioritized list of system experts to call.

6.1.7 Historian (data logging and plotting)

Historical data collection is accomplished by iHistorian by GE Digital. This system stores data, typically on a one second interval, to a virtual machine managed for Fermilab Core Computing.

Recent (up to 1 day) historical data pertaining to individual devices is available in the popup window for the device in iFIX. All historical data, as well as tools for data analytics, are made available via Industrial Plotting and Analytics Workbench software by Seeq.

6.1.8 Programmable Logic Controllers

The cryogenic process control system includes Siemens and Beckhoff PLCs (ODH safety is implemented separately, see appendix A). Direct control of all cryogenic equipment is done exclusively via PLC. PLCs contain all control logic necessary to operate all connected equipment. Under normal conditions, PLCs operate the cryogenic systems autonomously (without input from SCADA).

The engineering station contains the PLC configuration and programming tools. The engineering station contains the PLC programs (control logic) for all PLCs. Note, the programs do not run on the engineering station itself.

The main PLCs for the cryogenic control system are a redundant pair Siemens S7-400 PLCs (figure 51). The internal cryogenics PLC is a Beckhoff CX590. The ODH system uses a Beckhoff CX990 for standard (non-safe) operations and an EL6910 safety PLC (figure 52).

Figure 51. Redundant Siemens S7-400 PLCs.

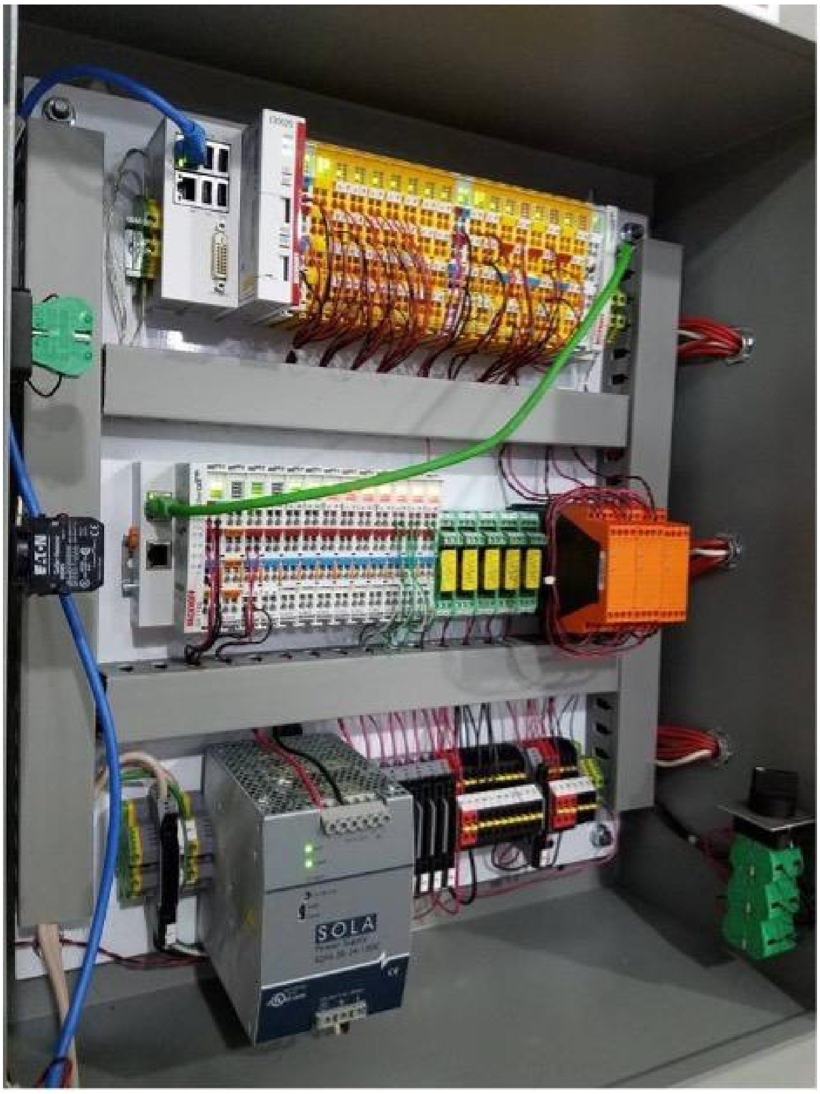

Figure 52. ODH control system enclosure.

2026 JINST 21 P04012

6.1.9 Field inputs/outputs

The cryogenic system includes numerous devices of many types. This section addresses the I/O connections to the most common devices, those with several instances throughout the system.

In general, devices are powered by 24 V DC from the corresponding I/O terminal. Discrete (on/off) signals use 24 V logic. Most analog signals are 4–20 mA.

- Pressure control valves (PCVs) and flow control valves (FCVs) are the same type of device, a valve with a pneumatic positioner. The distinction between PCV and FCV is based on the valve's role in the system under normal operation. The valve positioner is provided a single 4–20 mA analog signal from the PLC. There is no readback to the PLC.

- Pneumatic valves (PV) are on/off devices actuated by a pneumatic solenoid. The solenoid is provided a single 24 V discrete signal from the PLC. PVs are outfitted with two hall effect sensors for position readback, one for the open position and the other for closed position. These provide a 24 V discrete signal back to the PLC.

- Hand valves (HV) are on/off devices actuated manually. Certain HVs, namely those where large volumes of cryogens flow (e.g. before and after a pump), are outfitted with one or two hall effect sensors for position readback. They are the same as those for pneumatic valves and provide a 24 V discrete signal back to the PLC.

- Pressure transmitters (PTs) and pressure differential transmitters (PDTs) provide an absolute pressure reading or pressure relative to another pressure. These devices provide a single 4–20 mA analog signal to the PLC.

- Vacuum pressure transmitters measure the absolute pressure in vacuum spaces. These devices provide a 0–10V analog signal to the PLC. Additionally, the vacuum pressure transmitters on the side penetrations of the modules provide a 24 V discrete signal to the ODH safety PLC. The additional signal is for discrete indication of vacuum loss for use in the safety PLC's discrete only logic.

- Resistance temperature detectors (RTDs) are essentially resistors that change value based on temperature. The control system includes RTD terminals made specifically to read them.

- Variable frequency drives (VFD) provide power to the liquid Argon and Nitrogen pumps. The control system makes use of one analog input, one analog output, two discrete inputs, and two discrete outputs per VFD. The PLC provides a speed command via 4–20 mA analog signal to the VFD, which provides a speed readback signal back to the PLC. The PLC provides a run/stop command 24 V discrete signal to the VFD, which returns a run/stop status back to the PLC. The VFD provides an internal fault 24 V discrete signal to the PLC for which the PLC has a fault reset signal back to the VFD.

The total number of I/O for main, internal and ODH control subsystems include: 222 analog inputs, 176 RTDs, 40 potentiometers, 94 analog outputs, 184 digital inputs, 124 digital outputs. Provision is made for system evolution (figure 53).

2026 JINST 21 P04012

Figure 53. Cryogenic control cabinets.

6.1.10 Backup power

The cryogenic control system makes use of the generator and UPS (uninterruptable power supply) provided by FESS (Facilities Engineering Services Section). The PLCs, I/O, and VFDs for LN_2 pumps are included, as they are necessary for cold shield and condenser operation to maintain modules pressure and minimize loss of LAr. The VFDs for LAr pumps and heaters are not included.

6.2 The software architecture

The software architecture is based on the Functional Analysis (FA) of the cryogenic system, on the subsequent Product Break-down Structure (PBS), associated Piping and Instrumentation Diagram (P&ID) and parts-list (detailing the characteristics of the instrumentation), and on the process logic specification. The logic specification used as basis for the programming is designed with a modular structure relying on a master-child control units hierarchy, on associated option modes, sequencers and interlocks.

6.2.1 Functional breakdown structure and control units hierarchy

The functional analysis of the ICARUS cryogenic system was carried out following the ICARUS requirements described in section 1.4, in order to define a set of main service functions, technical functions and constraints. The detailed functional breakdown structure is summarized in table 4.

The software architecture relies on a "PCO" breakdown structure, which itself is derived from the Functional breakdown structure. The PCO breakdown structure consists in a master-child control units hierarchy, where the acronym PCO stands for Process Control Object and is borrowed from the CERN UNICOS CPC terminology. A PCO is a control unit with reference to IEC 61512-1 standard which represents a collection of field objects (actuators and/or other units) performing a common function or assembly of functions. For instance, a pump unit is the assembly of a pump, its inlet and outlet

Table 4. Main service and constraint functions of the ICARUS cryogenic system.

N°	Name	Description
S2	To have a stable gas phase density	To have a stable gas phase density
S3	To control LAr level	To have a liquid level and level stability according to detector needs
S4	To have a homogeneous temperature	To have a homogeneous temperature across the detector volume
S5	To prevent gas bubbles	To prevent argon gas bubble formation in the detector volume
S7	To provide services to support main service functions	Fluids storage, distribution, purification, regeneration, gas analysis
C1	To guarantee cryostat pressure scale	To limit argon gas pressure; to avoid opening of magnetic safety devices; to avoid atmospheric under-pressure (ingress of air)
C7	To cool-down	To cool down the apparatus before the start of the filling in 5 days while maintaining the prescribed maximum pressure gradients on the wire chambers

isolation valves, one vent valve and one charge valve, whose function is to circulate the cryogenic liquid. Most of the time the lower level PCOs correspond to the individual PBS equipment fulfilling the individual technical functions identified in the functional breakdown structure.

6.2.2 Option modes

Some PCOs have associated option modes defined so that these units can be setup in different operational states, i.e. in different working modes of the process. For instance, the LN2_CRY_SHLD PCO, which ensures the circulation of liquid nitrogen to the cryostat shield, has 3 associated modes. “With Gravity” option mode corresponds to the liquid nitrogen being supplied by gravity from the liquid nitrogen storage tank during cool-down or whenever the nitrogen pump is stopped. “With pump” option mode corresponds to the liquid nitrogen being circulated by the main pump. “With spare” option mode corresponds to the liquid nitrogen being circulated by the spare pump in case the main pump is unavailable. The option modes consist in user commands activated from the HMI. They are used as a condition either to switch on a set of dependent PCOs fulfilling the required functions at a given stage of the cryogenic system operation or to set a collection of defined states of the controlled objects, e.g. open or closed for a pneumatic valve, fixed position or regulation mode for a control valve, initialization of set-point.

6.2.3 Sequential function charts

The programming is mostly object oriented, while using Sequential Function Charts (SFC) whenever the process requires a sequence of operations like for the start-up of the cryogenic pumps for instance (See figure 54). These SFCs/Steppers are used to automatize the sequence of steps / transitions of a given process, while the same actions can be alternatively achieved following a manual procedure limited by interlocks.

2026 JINST 21 P04012

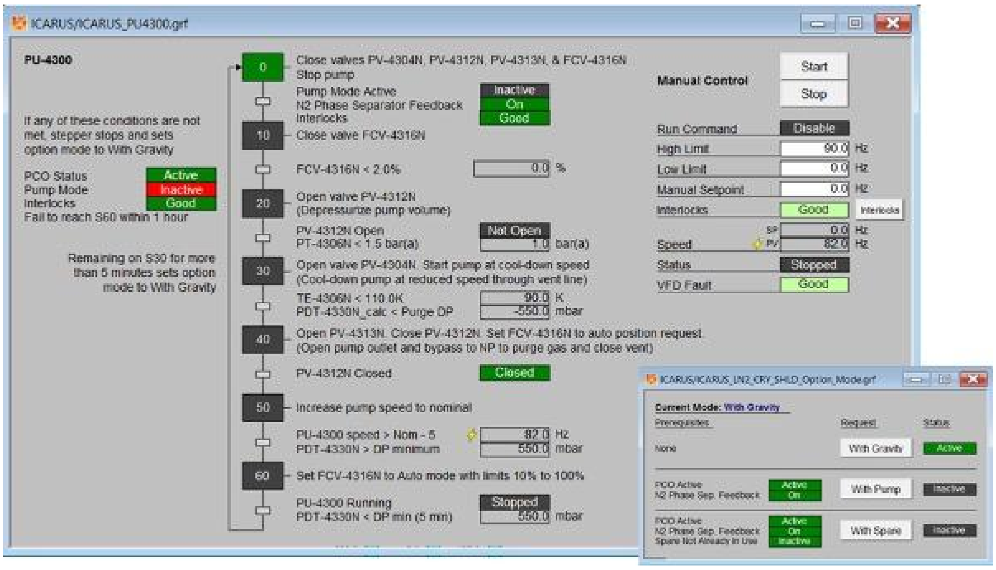

Figure 54. LN2 pump stepper.

6.2.4 Software interlocks

Software interlocks allow an actuator or a unit to go to its fail-safe position or they prevent it from starting in case of abnormal behavior and/or for security reasons. They override any automatic or manual request. Three types of software interlocks are used in the ICARUS cryogenics control system: full stops, temporary stops, and start interlocks:

- Full stops stop the unit/actuator and wait for manual acknowledgement before restarting. For instance, in case any ODH / bad vacuum condition is detected the side penetration valves and argon pumps are interlocked with a full stop.

- Temporary stops stop the unit/actuator and restart automatically when the interlock disappears.

- Start interlocks prevent the unit from starting (all dependent units/actuators stay in their fail-safe position).

As described earlier, the interlocks thresholds are set on the HH/LL limits of the corresponding process variable and can be enabled/disabled from the HMI by expert users.

6.2.5 Alarming

Full stops usually (but not systematically) trigger a critical alarm as defined in earlier sections. Temporary stops applied to the pressure vent valve are also triggering a critical alarm while the other temporary stops and the start interlocks usually trigger a non-critical alarm or no alarm at all.

Critical alarms are preferably set on low-low or high-high (LL/HH) limits of the corresponding process variable HMI panel while non-critical alarms are preferably set on low or high (L/H) limits of the corresponding process variable HMI panel.

2026 JINST 21 P04012

6.2.6 Selected software and programming principles

If CERN Unified Industrial Control System (UNICOS) partially inspired the HMI development and if its terminology was sometimes used for the logic specifications, the PLC programming itself does not make use of, nor reproduces, the UNICOS framework and tooling but uses the Siemens S7 embedded environment.

The logic specification and programming were achieved and implemented, sequentially, in batches of option modes and PCOs. This allowed to check-out the above described core functionalities on small size parts of the program and to spread the eventual adjustments to the other parts of the program.

Substantial programming development and testing efforts have been required to evolve from a control strategy commonly relying on sets of valve controllers and protection interlocks coupled to manual actions towards the chosen automated control strategy. Implementing and validating the core functionalities has been a long iterative process. This development required systematic testing which led to a smooth cryogenic commissioning phase.

6.3 Safe and continuous cryogenics operation

The cryogenic control system includes several features in order to ensure safe and continuous cryogenics operation, maintainability and flexibility for system evolution.

6.3.1 Redundancies

- All equipment essential to the functioning of the system, like PLCs, I/O modules, LN2 cryogenic pumps, controllers for vacuum sensors, Ethernet router for the SCADA, OPC Server and EWS are powered from redundant electrical power supplies including diesel generators and Uninterruptable Power Supplies (UPS). The cryo system is feed from a combination of building power/emergency power. Should the building power disappear, the UPS will handle it for a few seconds, when the generator will kick in. In case of generator failure, the control system may run on UPS (providing loads are reduced) for several hours.

- S7 Siemens PLC have 2 separate CPU's that are running the same program, which is synchronized as hot backup through a fiber link. Therefore, a failure of any CPU unit will not affect the controls, as a standby unit will take control within a few milliseconds. Furthermore, Interface modules (IM) are connected to different PLC CPU's, but might cross communicate with any of 2 CPUs, providing stable control over the connected modules. Signal modules are connected to the channels through MTA (Marshall Terminal Assemblies), that are powered by redundant power sources.

- All control cabinets have a redundant 24 V power. Some have just 2 redundant supplies tied to one redundancy module; some have 3 power supplies tied to 2 redundancy modules. All power supply statuses are monitored, and an alarm generated in case of failure. In any case, 24 V power is distributed to a bank of fuses, and a failure of any power supply will not affect 24 V distribution. MTA assemblies are powered from 2 independent fuses, so a single fuse trip will not disturb the operation.

2026 JINST 21 P04012

6.3.2 Safety aspects

- The vacuum levels of transfer-lines between the side penetrations and the argon pumps are monitored. Since a degraded vacuum could be a sign of argon potential leak and further ODH risk created by the accumulation of argon in the lowest locations, such a situation triggers a critical alarm, the evacuation of the area, as well as the increase of the air extraction speed. At the same time, interlocks to the cryogenics system are triggered stopping the pump and argon circulation.

- The cryostat modules over-pressure protection is implemented in controls in addition to over-pressure protection by magnetic valve reliefs. The controls are set for two vent valves per module to regulate at 150 mbarg and one larger vent valve at 175 mbarg. In the exceptional circumstances the ultimate high pressure threshold of 200 mbarg is reached, this vent valve is fast opened thanks to a dedicated electro valve placed on the vent valve actuator supply (hardware interlock based on redundant pressure switches).

6.4 Maintainability and flexibility for system evolution

It is possible to make change to PLC programming online, provided that current set points are backed up, with no disruptions to the experiment. In certain cases, though, interaction of process, controls and cryo engineers is needed. It's also possible to add hardware as needed.

7 Cryogenic and purification commissioning and operations

7.1 Cryogenic commissioning

Commissioning and operations of the ICARUS cryogenic system have been divided to 5 different modes (following the months-long evacuation of the modules to remove atmospheric contamination):

1. Preparation for cooldown, including activation of the different purifiers, lowering of the outgassing of the two cold vessels, purging of the different transfer lines and cold boxes, etc.

2. Cool-down of the two cold vessels and the detectors mounted in these vessels.

3. Filling of the two cold vessels by a total of about 400 ton of purified liquid argon per vessel.

4. Stabilization of the filled cold vessels, bringing the cold vessels pressure to stable values, while lowering the impurity level in the two argon baths.

5. Normal operation, purifying the argon in the two cold vessels in gaseous and liquid phase, guaranteeing a stable, low, impurity level of the argon in the two cold vessels.

In this sense, the commissioning of the Icarus cryogenic system had a staged approach as shown in appendix B. Each stage was preceded by verification of safety and receiving clearance for operations as per Fermilab safety requirements. The cryogenic commissioning was conducted as a common effort of the CERN and Fermilab cryogenic teams. The commissioning was started with the CERN team onsite and then continued with the CERN team supporting remotely the activity of the local Fermilab team. Meetings have been held almost daily, including weekends, since the beginning of March 2020.

2026 JINST 21 P04012

One of the most important requirements for a liquid argon based TPC detector is to allow the ionization tracks, created by interacting particles within the detector volume, to be transported in a uniform electric field up to a multi-wire anodic structure placed at the end of the drift path with reasonably low attenuation of charge A. The attenuation of charge A is defined based on the design drift time T and the achieved free electron lifetime τ per eq. (7.1):

$$A[\%] = 100\left(1 - e^{-T/\tau}\right) \tag{7.1}$$

The free electron lifetime in argon is directly related to the electronegative impurity concentration ρ, mostly oxygen, by an inverse linear relationship shown below in eq. (7.2):

$$\tau\,[\mathrm{ms}] \approx \frac{300\ \mathrm{ms} \cdot \mathrm{ppt}\ \mathrm{O_2}\ \mathrm{equivalent}}{\rho\ [\mathrm{ppt}\ \mathrm{O_2}\ \mathrm{equivalent}]} \tag{7.2}$$

Therefore, for the free electron lifetime to exceed design 3 ms with attenuation of 28.3% for the drift time of $T = 1$ ms, the impurity (ρ) measured in parts of oxygen should be below 100 ppt (10^{-10} parts).

Reaching the same 28.3% attenuation of charge for the DUNE cryostat to be hosted at the Long-Baseline Neutrino Facility (B. Abi et al., 2020) with 2.5 ms design drift time would already require the lifetime of 7.5 ms, more than twice better than the minimum design lifetime for the Icarus. The original Icarus installation in Gran Sasso achieved the electron lifetime in excess of 10 ms. With the same design drift time T between the cathode and the wire chamber being 1 ms, that resulted in attenuation of charge of 9.5%.

There are many factors that impact the purity and resulting lifetime for a TPC-based liquid argon detector, like Icarus. The initial purity depends on the purity of the liquid argon filled into the modules. As commercial argon has impurities far exceeding 100 ppt, and since the components inside the modules and piping outgas impurities, the Icarus cryogenic system was designed to remove H_2O and O_2 from LAr to achieve impurity concentrations below ppb level before TPC could be turned on. In Icarus, this was achieved by first pumping the empty modules to high vacuum for 9 months to remove a bulk of contamination from surfaces by desorption. In addition, an elaborate filtration system had to be installed and prepared [20] to remove the remaining impurities, mostly from the initial fill and continuing outgassing of impurities from the materials inside the modules and recapturing them into liquid argon bath during operations.

Initial activation of the copper in 14 removable cartridges (4 of 5-liter units for gas re-condensers and 10 of 25-liter units for liquid filters) was done in summer 2019. The process was done using the existing cryogenic system at MicroBooNE. The activation of Cu 0226 was done by initial heating to ~ 420 K with pure argon and then introducing mixture of 2.5%H_2–97.5%Ar to achieve removal of oxygen. The success of activation process is judged by heating of copper due to exothermic process forming of H_2O from O_2 and H_2. As the small quantities of copper in the cartridges did not produce significant heat of exothermic reaction and registered only poorly pronounced temperature spikes during activation, we measured the absorption of oxygen by activated copper to confirm the success, and then repeated the activation/regeneration procedure.

Then the activation of the fill purifier filters was done within 3 days starting January 27, 2020. The purifier contains three vessels, two containing 300 kg of Cu 0226, and one containing 80 kg of molecular sieve. The activation of copper was done again by using a hydrogen gas mixture to reduce the copper oxide of the media. Though such activation is typically done at Fermilab using mixture of

2.5%H_2 with 97.5%Ar, this activation was done with 1.0%H_2 with 99.0%Ar to replicate the process done at CERN for NP02/04 cryogenic systems. The procedure involved first heating the media with $\sim 140\,m^3$/hr of pure argon heated in 10 kW heater to reach ~ 440 K in the bulk of the copper. Then the standard 2.5%–97.5%Ar mix from the tube trailer was mixed with pure argon to dilute to 1%H_2 concentration and flown to individual filters Cu1 and Cu2 at the rate of $\sim 140\,m^3$/hr (see figure 55). Here Fermilab tried, again, to replicate successful activation of identical filters at CERN where they used $\sim 150\,m^3$/hr rate for 10 hrs at 1%H_2, thus requiring $\sim 15\,m^3$ H_2. The activation process took ~ 12 hrs per each 300 kg of copper with temperature peaks up to 547 K and dew point in the exhaust gas spoiled from −40°C to −2°C (~ 5200 ppm). The drying of molecular sieve was then done next (see figure 56). At the end of activation and drying process, the 600 kg of copper had an absorption capacity of ~ 388 g of O_2 while molecular sieve had a capacity of ~ 23 kg of H_2O.

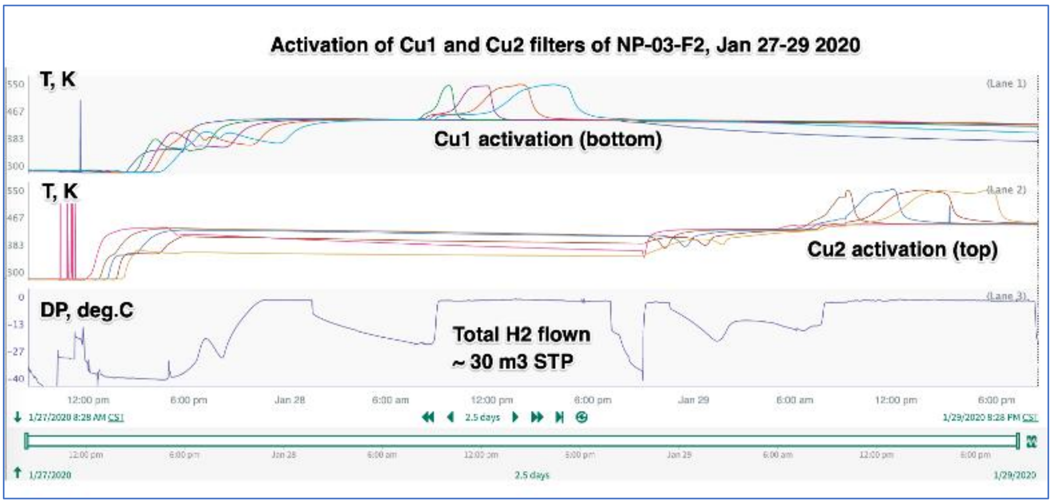

Figure 55. Initial activation of Cu in filter 1 and 2 of the fill purifier.

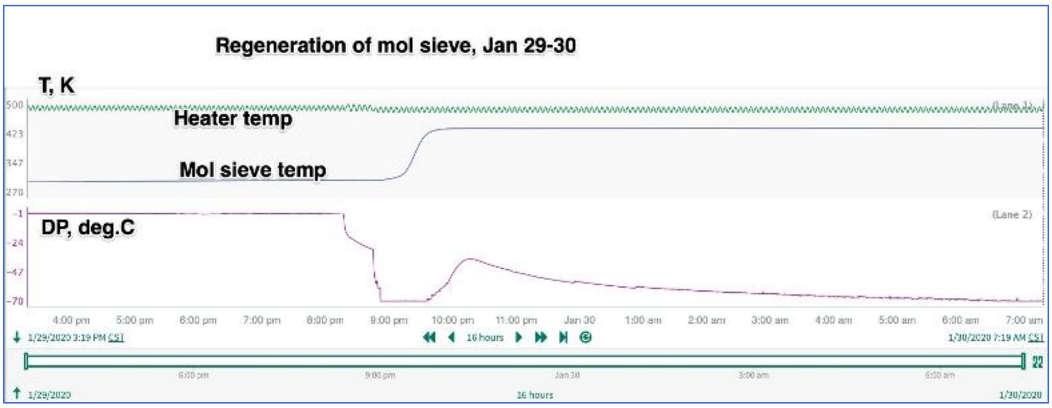

Figure 56. Initial drying of molecular sieve of fill purifier.

In summary, the cryogenic commissioning of the ICARUS detectors started on February 13, 2020 by breaking the vacuum in the two main cold vessels with ultra-purified argon gas. Cooldown started on February 14, 2020 by injecting liquid nitrogen in the cold shields by means of pressure and gravity transfer from LN_2 dewar via phase separator. It took about 4 days to bring the temperature on the wire

2026 JINST 21 P04012

chamber below 100 K. The cooling process was continuous and the maximum temperature gradient on the wire chambers was about 35 K (see figure 57). The LN_2 pumps were cooled down and started immediately after gravity transfer; it took several days to stabilize their operations due to failure of the bypass regulation valve for the LN_2 pump dedicated to the shields. The repairs proved to be unsuccessful, and the pump was left to operate with fixed 10% opening of the bypass valve.

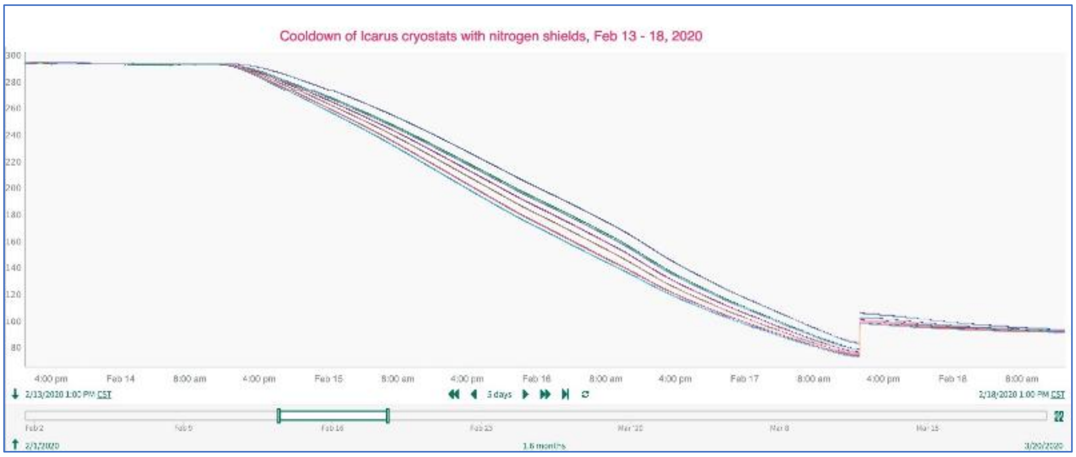

Figure 57. Cooldown of cryostat with LN_2 shields. The temperature jump towards the end of the curves is due to a change in one of the readout algorithm parameters.

On February 19, 2020, the gas recirculation condenser units were put into operation to purify the argon gas before the start of the liquid filling, but their operations were not stable without sufficient liquid level in the modules and therefore their operations were delayed until the end of the fill.

The filling with LAr started on February 19, 2020, by initiating a total of 46 daily deliveries by Air Products. Once the transfer lines and liquid purifier filters were cooled down, the transfer of ultra-purified liquid argon from LAr dewar via fill purifier to the modules ran 24/7 from February 24 until April 20 with interruption at midpoint on March 16–20 for the regeneration of fill purifier filters (see figure 58 and figure 59). The filling was stopped again when the liquid reached the -6 cm below the nominal level to perform the final pressurization qualification test of the two cold vessels. During the fill, the boiloff gas of $\sim$ 10% was vented to atmosphere to control the pressure in the modules. The impurities downstream of the fill filter were measured during the fill campaign to be in ppb range.

On April 21, 2020, the liquid recirculation was started. The recirculation path for the West module took LAr from the top side penetration, but the recirculation for the East module had to take LAr from the bottom side penetration in order to provide stable supply to the suction of the argon pump. That was due to the combination of length and gooseneck shape of the supply piping penetrating the insulation space from the East module. While both modules have identical top and bottom side penetrations, the piping for the East module is longer than the piping for the West module. The recirculation rates are 1.85 m^3/hr in the West module and 2.25 m^3/hr in the East module.

A general cryogenic stabilization phase was completed around the end of May 2020. That was mostly related to achieving desired level of ullage pressure in the modules at $\sim$ 1.070 bara by (a) adjusting the temperature of the nitrogen in the shields and (b) setting the gas purifier condenser units at their maximum capacity (adjusted for module pressure). The nitrogen shields pressures were

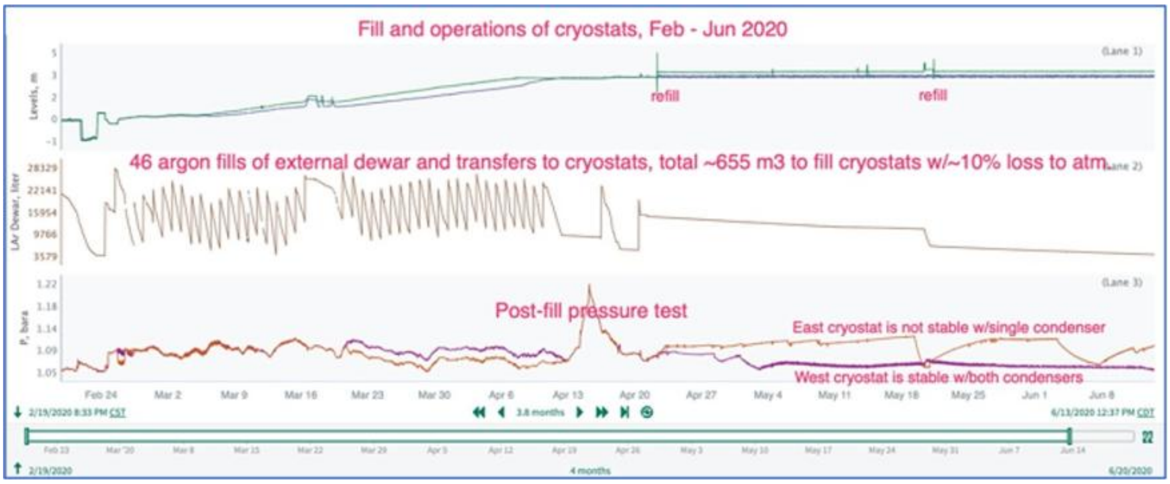

Figure 58. Regeneration of fill purifier filters during fill campaign.

Figure 59. LAr fill campaign — daily deliveries and purification periods.

varied between 2.85 and 2.95 bara with downstream control valves to adjust pressure of nitrogen from 4 bara supply from the pump to 2.2 bara in the phase separator.

After the initial fill and during the operations, most impurities are coming to the argon gas phase in the ullage from outgassing of materials (mostly cables) and from micro-leaks possibly developed in some of the 48 feedthrough flanges per module, each having 1152 wires, located at room temperature on top of the detector. To prevent these impurities from diffusing into the main LAr volumes of the modules, the Icarus filtration system is provided with gas recirculation condenser-filter units each containing an Ar/N_2 heat exchanger and a single 5-liter cartridge with activated Cu. To keep the modules above atmospheric pressure and prevent air back-streaming from leaks, these condenser-filter units, two per module, work by condensing gaseous argon with liquid nitrogen. The Cu filter media was activated prior to the start of Icarus commissioning.

Finally, during the operations, the Icarus cryogenic purification system provides circulation of liquid argon at ~ 0.8–1.0 kg/s per module with dedicated cryogenic pumps through the liquid argon filter. Each filter unit is dedicated to the module and contains five 25-liter cartridges filled with molecular sieve and Cu in 25%/75% fraction. The circulation rate is defined by the capacity of the largest liquid argon pumps (models BNCP-32C and BNCP-32E) available from Barber-Nichols at the time of the Icarus design. This flow rate defines the average time $T_r \approx 104$ hours to recirculate the full volume of each module.

One of the issues that resulted in lower-than-expected initial purity in both Icarus modules was due to the difficulties in commissioning the gas condenser-filter units responsible for filtering the impurities from the gaseous ullage space of the module. At least two of the units kept developing a gas vapor lock in their internal argon piping, thus preventing operation at full design 6.5 g/s per condenser-filter unit. The vapor locking was due to a so-called "gooseneck" in the cryogenic piping where the fluid was at conditions close to saturation. The internal piping for all four condenser-filter units was modified in Spring 2021 to remove the gooseneck, which improved the capacity up to 7 g/s (see figure 60).

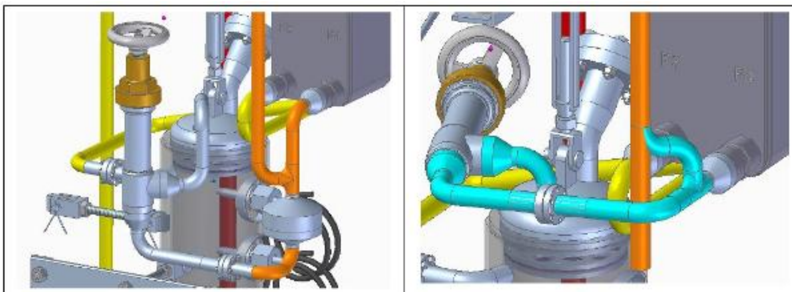

Orange piping represents the original (and built) piping routing from the Heat Exchanger F4 Interface to the Argon Filter Vessel.	*Cyan piping shows the modified design of the piping routing connecting the Heat Exchanger F4 Interface to the Argon Filter Vessel. This design will be implemented in the NP-01-50-CB Valve Box after validation.*

Figure 60. Modification of re-condensers.

At the start of the cryogenic commissioning, all activities in the detector building not related to cryogenics were suspended and the building was put in a higher safety condition, with strong limitations on the presence of people onsite. At the end of the liquid argon filling, after the final pressure test, the standard ODH safety conditions were restored and regular activities on top of the detector could be re-started.

The gas recirculation rate through the gas condenser-filter units must match the boiloff rate of argon in the modules in order to efficiently remove impurities and to properly control the pressure in the ullage and have enough flexibility to operate with wide margin. Unlike a passively insulated cryogenic vessel, the boiloff rate for the Icarus modules is defined by the temperature of the ten actively operated LN_2 cooling circuits inserted between the warm and cold vessels. The pressure in, and thus temperature of, each of the individual circuits is regulated by a valve placed in each of the ten circuits, with the liquid/gaseous mixture returning to the nitrogen phase separator. The nitrogen system includes two liquid nitrogen pumps ("filters" and "shields" pumps, BNCP-68 models) installed in vacuum-shielded valve boxes.

Unfortunately, one of the control valves maintaining the regime of the "shields" pump failed stuck in mid-position after the fill of the modules, preventing reliable shifting of the pump's operating point on its curve and reaching the desirable shields temperature and therefore maximum boiloff

2026 JINST 21 P04012

and removal of impurities from the ullage. While both nitrogen pump units could be replaced with a separate spare pump unit, the control valves of each pump were designed to be shared and in service at all times, preventing their maintenance or replacement without losing nitrogen circulation. With insufficient boiloff and gas recirculation, and in order to increase bulk purity of liquid argon, periodic venting of gaseous argon from ullage was started in late 2020. The automatic venting has been exercised up to four times a day, resulting in loss of ∼ 12 L/day or 1 cm of liquid level per module every two months. This required topping the modules in March 2021, August 2022 and December 2023. Though the refills were less than 2% of the total module volume and were transferred via regenerated fill purifier, they still introduced additional contamination and therefore additional loading of the gas and liquid filters with impurities.

The purity of the argon in East and West modules was the goal of investigations since completion of commissioning in 2020. As the purity depends on many contributing factors — initial purity after fill, ongoing outgassing from materials inside the modules, recirculation rate of liquid argon, recirculation and condensing rate of gaseous argon from the ullage, etc. — these investigations focused on optimizing conditions to achieve the design lifetime of 3 ms.

Starting in Sep–Oct 2020, the studies established how much the bulk purity depends on recirculation rates in the West module (see figures 61, 62, 63).

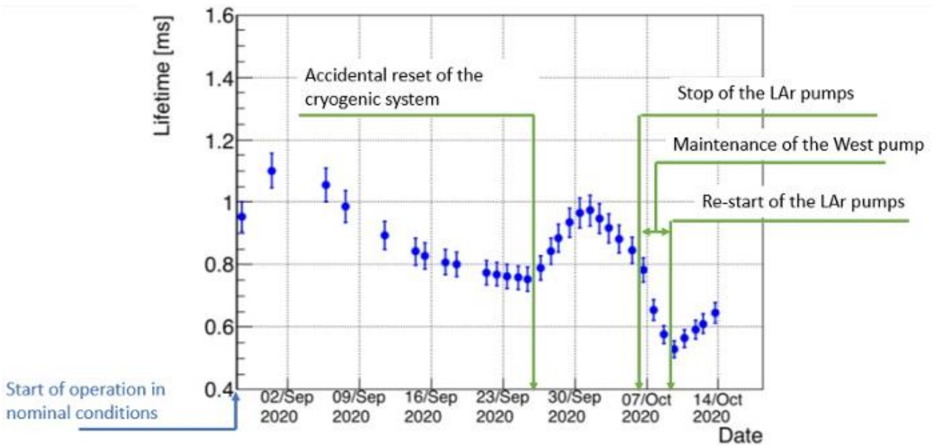

Figure 61. Investigation of purity dependence on operations.

Liquid recirculation studies show that the expected asymptotic impurities concentration C is given by the equilibrium condition:

$$0 = \frac{dN}{dt} = L - CS \;\Rightarrow\; C = \frac{L}{S}$$

where L is the rate of impurities entering the liquid (leak rate) and S is the nominal recirculation speed (≈ 2.35 m^3/hr for the East module and ≈ 2.09 m^3/hr for the West one). A 100% filtering capacity of the recirculated liquid is assumed. The leak rate L can be measured from the observed decrease of free-electron lifetime when the liquid recirculation pump is off. From this measurement, the calculated asymptotic values are ≈ 320 ppt for the East module and 236 ppt for the West one (corresponding lifetimes: 0.94 ms and 1.27 ms). The fact that the calculated values are very similar to those measured immediately before stopping the pumps (356 ppt and 300 ppt) tells us that purity is not limited by a lower-than-expected recirculation speed or purification capacity.

2026 JINST 21 P04012

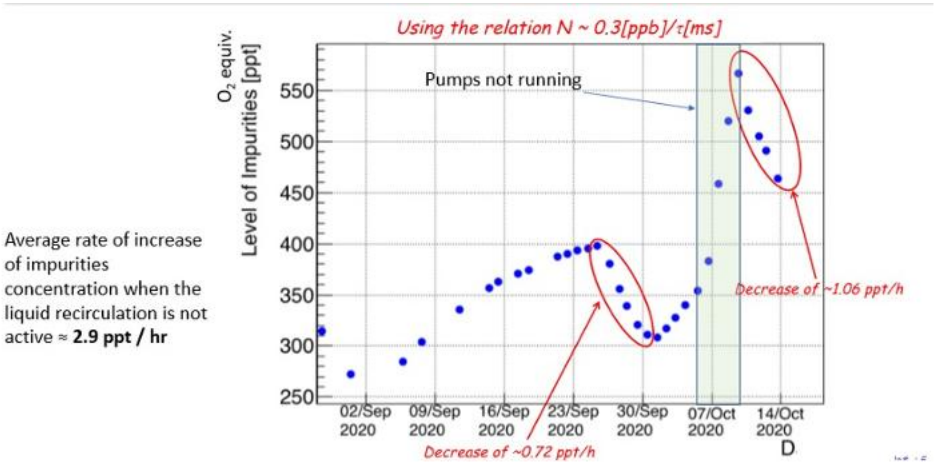

Figure 62. Investigation of purity dependence on operations.

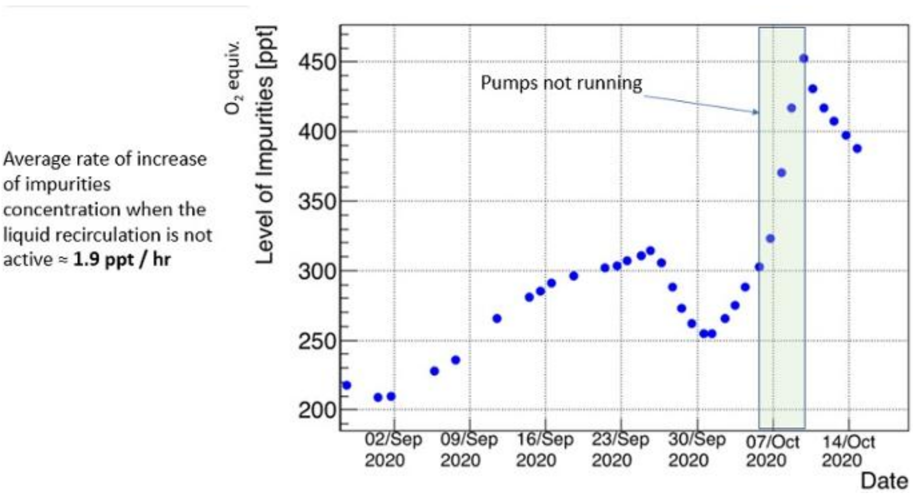

Figure 63. Investigation of purity dependence on operations.

The nominal adsorption capacity of each filter cartridge of the gas recirculation units is about 1.5 g of O_2. The influx of impurities from gas to liquid can be calculated by measuring the drop of lifetime in the argon bath when the circulation pump is off for a specific time period while impurities are still being removed from the ullage via gas recirculation. This influx was determined to be $\sigma \approx 0.40$ ppt/hr for the original Icarus at Gran Sasso. The value was measured to be $\sim$ 2–3 ppt/hr for Icarus at Fermilab at the start of commissioning and stabilized at $\sim$ 0.55 ppt/hr after one year of operations when the initial outgassing influx subsided and gas recirculation filtration improved.

The theoretical lifetime τ achieved in liquid argon at time t can be calculated using the following equation, based on σ (ppt/hr), the full-volume recirculation time T_r (hr), and initial concentration C_0 (ppb):

$$\tau(t)\ [\text{ms}] = \frac{0.3}{\sigma\, T_r \ + \ \left(10^9 C_0 - \sigma\, T_r\right)\ e^{-t/T_r}} \tag{7.3}$$

From this perspective, a slight increase of the West pump flow from 0.8 kg/s to 1.0 kg/s in Fall 2022, which decreased the recirculation time from 128 hr to 104 hr, resulted in an increase of the

2026 JINST 21 P04012

theoretical lifetime from 4 ms to 5 ms for the same influx $\sigma = 0.55$ ppt/hr and initial impurities concentration $C_0 = 2$ ppb.

Starting from November 2020, the argon gas from ullage in both modules was vented at variable frequency and duration (up to four times a day for 15 min at 50% opening of the vent valve). The conclusion is that the present gas recirculation rate is insufficient to efficiently prevent impurities to enter the liquid phase. The periodic venting is flushing the impurities that accumulate in the chimneys (figures 64, 65).

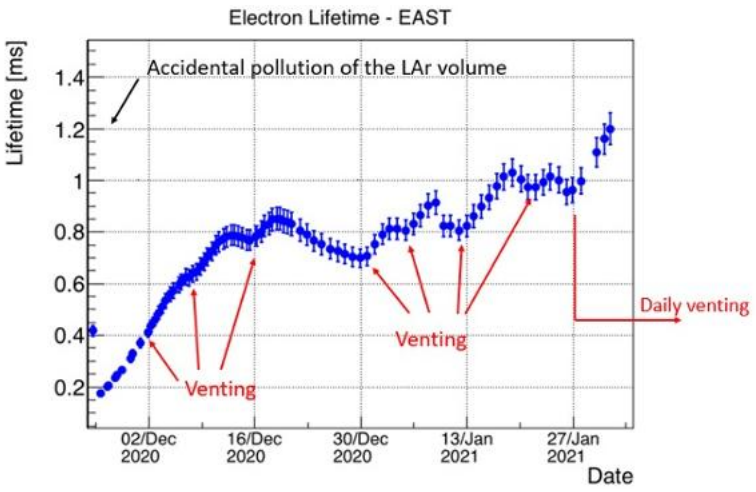

Figure 64. Investigation of purity dependence on venting (East module).

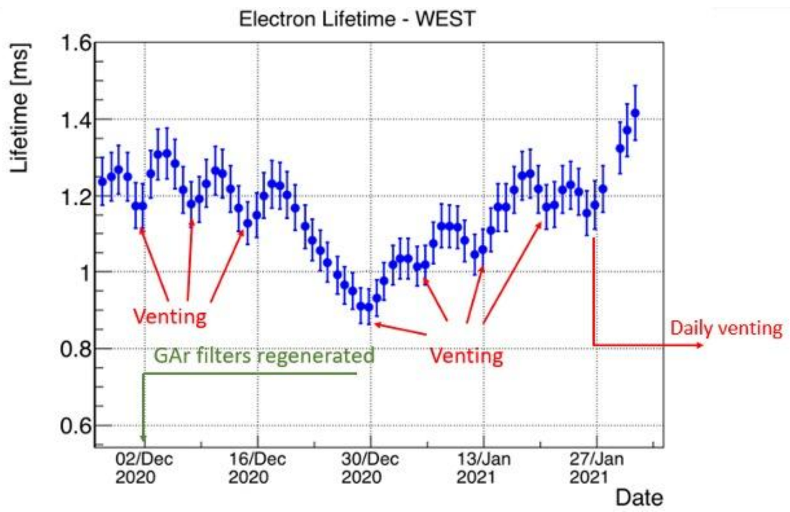

Figure 65. Investigation of purity dependence on venting (West module).

One of the issues that may have impacted purification was the design decision to replace Oxysorb media (Messers-Griesheim GmbH), previously used in Icarus at Gran Sasso and at CERN, with copper media Cu-0226 from BASF. Oxysorb is a chromium-based media that binds oxygen by chemical reaction, while Cu-0226 is a highly dispersed copper oxide impregnated on high-surface-area alumina which serves to remove O_2 and, to a lesser extent, H_2O. While Oxysorb and Cu have similar absorption

2026 JINST 21 P04012

capacities at room temperature, leading to re-use of the original volumetric sizing, the Cu media appeared to exhaust sooner than expected at liquid argon temperature.

Therefore, we first regenerated all four gas condenser-filter cartridges and then added a 10-liter filter with molecular sieve (30%) and Cu (70%) upstream of each condenser-filter unit. This increased the O_2 adsorption capacity by a factor ≈ 20 and added H_2O adsorption capacity but did not produce the desired improvement in lifetimes.

Specifically, the lower lifetime in the West module at the same liquid argon circulation rate pointed to a potential deficiency in adsorption capacity of the West liquid argon filter. Causes could include: ineffective activation of the media or unequal flow distribution among the five cartridges, causing one to load close to breakthrough.

Typically, molecular sieve requires heating above 250°C for full bake-out, and Cu media requires heating to at least 165°C before admitting Ar/H_2 mixture to remove O_2. Unfortunately, we could not reach those preheating levels with the original regeneration setup in 2020, so the media may have had less than 100% adsorption capacity.

Therefore, the West argon pump was turned off in Fall 2022 and the cartridges in the West argon filter were regenerated in the improved setup, allowing preheating above 200°C. After reinstallation of the filter cartridges and restarting LAr recirculation, the lifetime in the West module stabilized at a level above 6.5 ms, almost twice higher than before the regeneration and 1.3 times higher than the theoretical value for the measured influx of 0.55 ppt/hr

As the recirculation rate remained the same, it must be attributed to the drop in influx σ from 0.55 ppt/hr to 0.43 ppt/hr due to venting of the modules four times a day.

Final stages of stabilizations started in May 2021 after the 40CB condenser was modified and brought online with increased capacity of up to 7.9 g/s. By mid-2023, the following state of the system was achieved.

LN_2 circulation system.

- *LN_2 "filters" pump 60-CF PU-4100*, which supplies LN_2 to all shields of the liquid filter boxes, transfer lines and condensers, is set to run at 82 Hz, 4 bara discharge while maintaining a differential of 1.2 bara. The "filters" pump supplies LN_2 to 40FC and 50FC purifier boxes, intercepting heat from the filter cartridges (five per filter box) and from the long argon transfer lines from the filter boxes located on the north side to the module entries on the south side. Presently, inlets are opened 36–38%, while returns are regulated based on temperature between 2.75–2.95 bara. The "filters" pump also supplies LN_2 to 40CA, 40CB, 50CA and 50CB condenser boxes. Each condenser is regulated individually. LN_2 supply from the pump is common to each condenser pair (40 or 50), while the 2-phase nitrogen returns flow back to the phase separator (PS) through individual transfer lines. There are no isolation valves in the delivery transfer line upstream of each condenser; the only isolation is via the control valve located 750 mm deep in the condenser box, which results in accumulation of ice inside 40CA and 50CA during maintenance.

- *LN_2 "shields" pump 60-CT PU-4300*, supplying LN_2 to all shields of the liquid filter boxes, transfer lines and condensers, is set to run at 84 Hz, 4.2 bara discharge while maintaining a 1.6 bara differential. Ten individual LN_2 shield circuits are fed via inlet valves (60-TI) and returned via outlet valves (60-TO). While inlet valves are kept in manual position (adjusted to maintain pump flow in the desired range), outlet valves regulate pressure (and therefore temperature) of the shields. To maximize boil-off and cleaning of the argon ullage, the shields are operated at ~ 3.6 bara. Control-valves limits are set to allow for appropriate regulation range.

LAr circulation system.

- *West 40-CP PU-6000 pump (BNCP-32C)* Set to 42 Hz, 1.33 bara discharge, maintaining ~ 0.96 kg/s flow to the West module via 40FC filter box.
- *East 50-CP PU-6500 pump (BNCP-32E)* Set to 49.1 Hz, 2.0 bara discharge, maintaining ~ 0.96 kg/s flow to the East module via 50FC filter box.

Condensers.

Gaseous argon is collected from the modules' ullages via individual connections to each chimney. There are 10+10 chimneys on the north side feeding condensers 40CA/50CA, and 10+10 on the south side feeding 40CB/50CB. The goal is to collect and re-circulate gas to control pressure in the module while re-circulating (and therefore filtering) max amount of gas. Therefore, the objective is achieved by setting the LN2 shields at max pressure (temperature) to maintain max boiloff, while setting the condensers at max flow rates. In mid-2023, the following operating point produced a total condensing rate of 14.2–14.5 g/s per module:

- LN_2 shields at 3.53 bara (PS at 2.2 bara, pump at ~ 250 g/s), all inlet valves 100% open.
- Purifier boxes and Ar transfer lines tuned to 2.9 bara, with inlets at 42% and 40%.
- The condensers are tuned to their almost max capacity:
  - 40CA: ≥ 6.80 g/s at 100% Ar, 57% N_2 in, 2.285 bara N_2 out
  - 40CB: ≥ 7.35 g/s at 100% Ar, 70% N_2 in, 2.297 bara N_2 out
  - 50CA: ≥ 6.8 g/s at 100% Ar, 57% N_2 in, 2.260 bara N_2 out
  - 50CB: ≥ 7.5 g/s at 100% Ar, 55% N_2 in, 2.280 bara N_2 out

To improve purity, vent valves are opened 2–3 times per day for a predefined duration at 50% opening, venting ~ 10 L/day to atmosphere.

The most time consuming and disruptive operations for the Icarus cryogenic system are those related to the startup of the cryogenic pumps and maintaining stability of the liquid argon and nitrogen flows to the loads, e.g. filters and shields, via reasonably long transfer lines. The liquid argon and nitrogen pumps by Barber-Nichols require replacement of the bearings every 6000 to 9000 hours. While the service is typically done by Fermilab qualified technicians by using OEM parts, such service results in interruption of circulation for the argon pumps, which do not have an inline spare, for at least 72 hours with the deterioration of bulk LAr purity by ~ 40 ppt. As for the service for the nitrogen pumps, it involves cooldown and switchover to the spare inline pump, which typically requires restart of the entire nitrogen system. That is due to the design of the common suction manifold from the phase separator to all three pumps. It manifests in disruption of the nitrogen flow in one pump's suction and gas vapor locking when the other pump suddenly starts pumping liquid after being primed. It is also exacerbated by the loss of the control valve in the shields valve box. Loss of a nitrogen pump then

2026 JINST 21 P04012

leads to vapor locking in the long vacuum-jacketed transfer lines leading to the filters or shields. Use of intermediate phase separators and cooldown valves would improve startup operations.

As we learned valuable lessons in design and operations of the world's largest LAr-TPC detector, the Icarus-T600 demonstrated a remarkable success in taking scientific data in the Fermilab Booster Neutrino Beam. Already in August 2020, just a few months after the fill, the purity in the Icarus detectors reached 0.3 ppb, equivalent to 1 ms lifetime, and the detectors started taking scientific data with cosmic neutrino radiation. The plot in figure 66 shows the electron lifetime in the Icarus detectors as related to the technical improvements and scientific data taking.

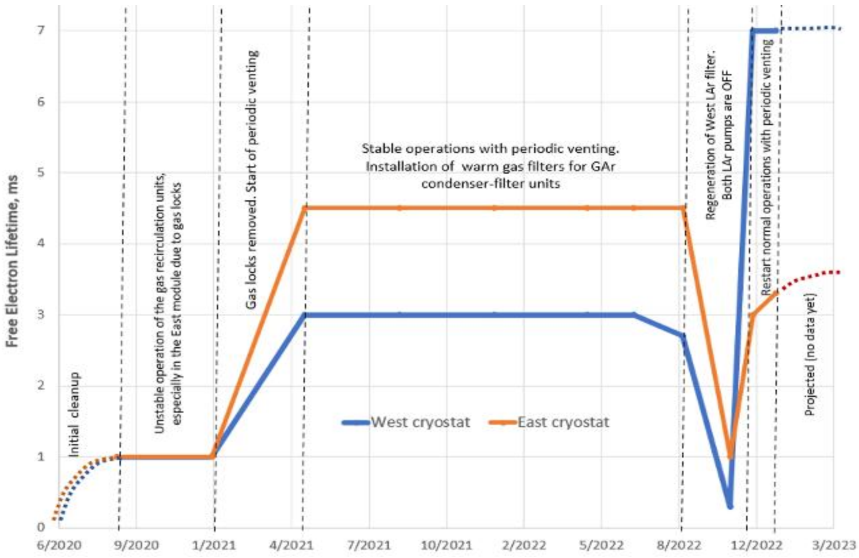

Figure 66. Electron lifetime achieved for the Icarus LAr-TPC detectors (2020–2022).

7.2 Detector operation

In May 2021, the free-electron lifetime was about 3 ms in both modules, and it later stabilized at about 3.2 ms in the West module and 4.5 ms in the East module (figure 67). The corresponding concentrations of impurities (O_2 equivalent) are 0.09 ppb and 0.067 ppb, respectively. This allowed the start of a first continuous neutrino run (RUN0) toward the end of 2021, coinciding with Fermilab's beam operation. Some neutrino events collected during this first run are shown in figure 68 to illustrate the quality of the recorded data.

During the summer of 2021, the capacity of the argon gas recirculation system was further increased by inserting filter cartridges before the inlet of the condensers (figure 69). The cartridges are filled one-quarter with molecular sieves 4A and three-quarters with copper medium, operate at room temperature, and have a total volume of about 11 L of filtering media. The additional filters enhanced H_2O removal from the gas recirculation system and increased filtering capacity by about a factor of 20, eliminating the need for periodic regeneration of the cold cartridges, with considerable advantages in terms of reduced maintenance effort, reduced operational risk, and improved continuity of operations. Insertion of the warm filters into the GAr recirculation circuit resulted in a pressure drop of about 10 mbar, with minimal effect on recirculation speed.

2026 JINST 21 P04012

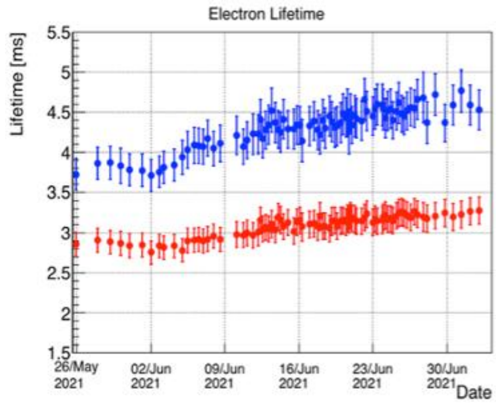

Figure 67. Free-electron lifetime during the first neutrino run (RUN0). Blue: East module; red: West module.

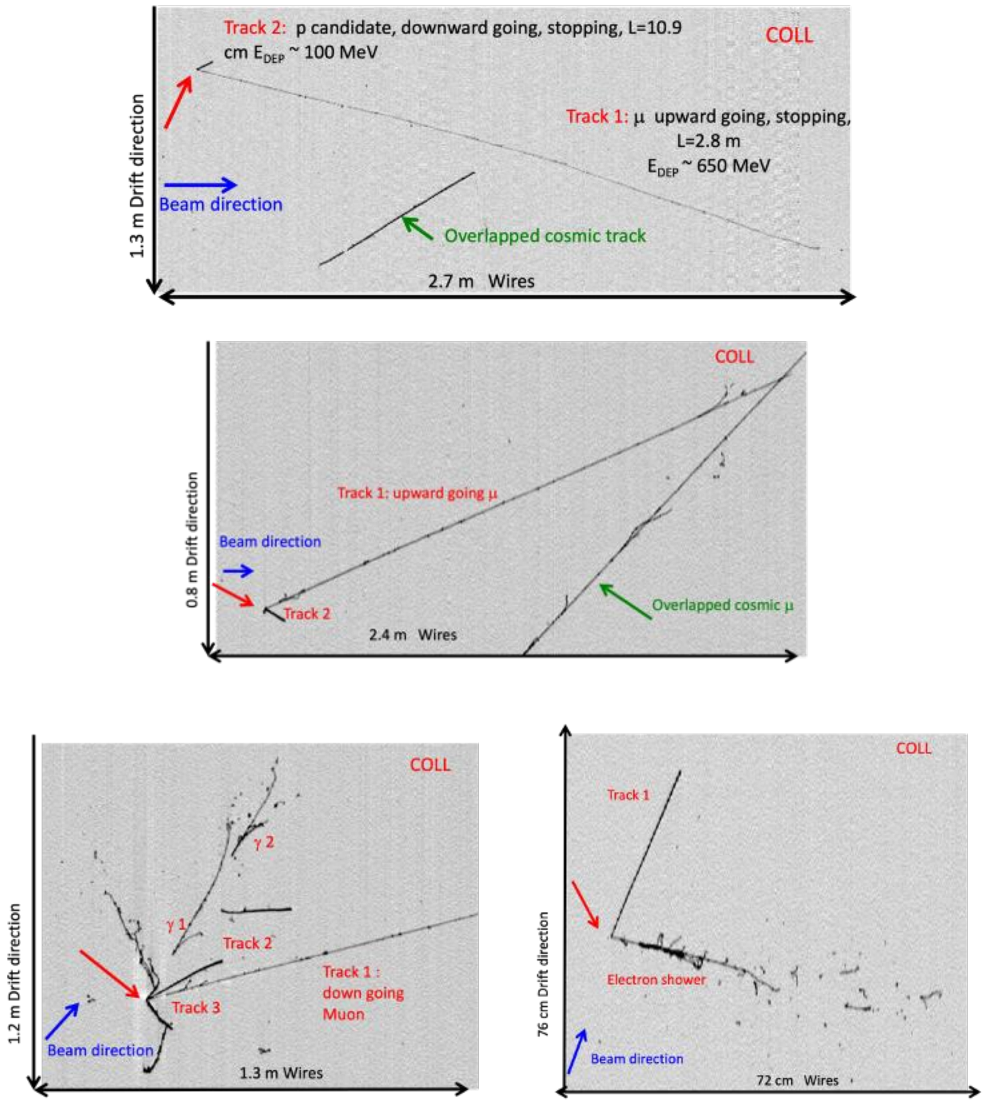

Figure 68. Small sample of neutrino events collected during the first neutrino run (RUN0). The red arrow indicates the neutrino interaction vertex. Only the collection view is shown.

2026 JINST 21 P04012

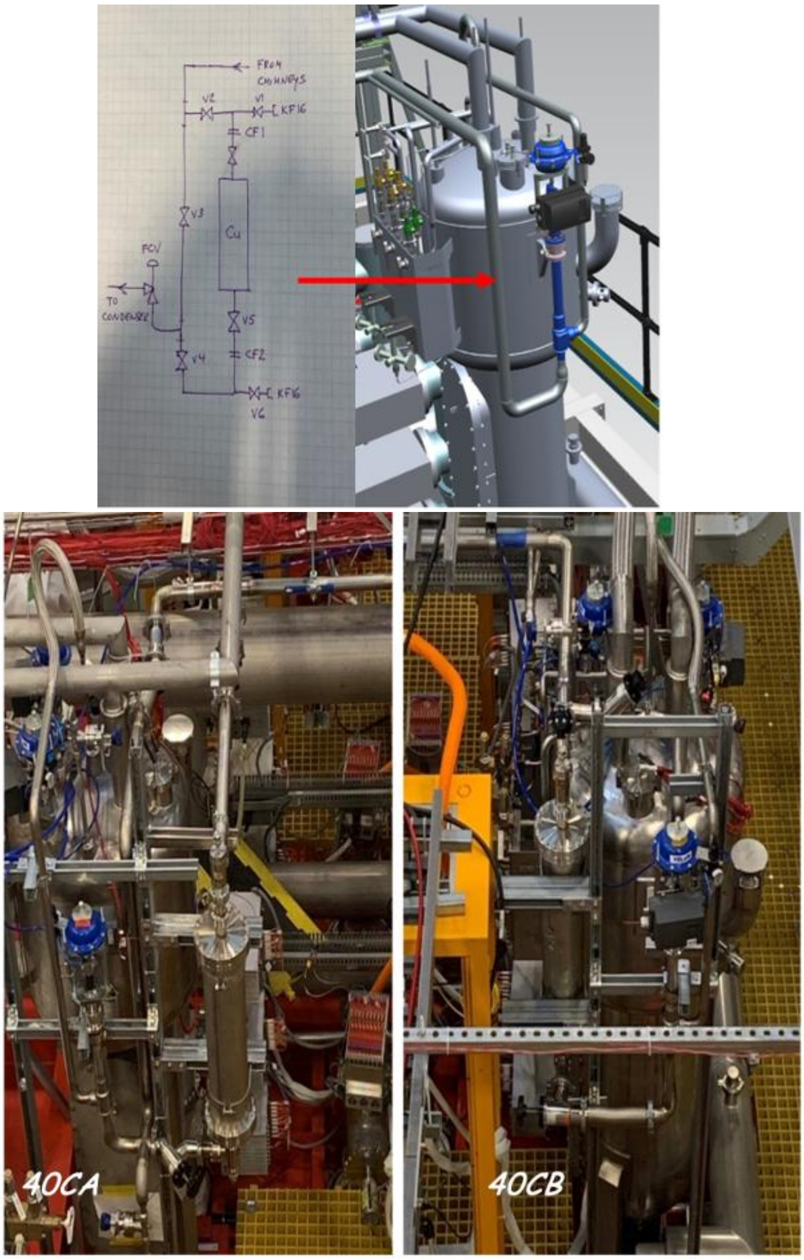

Figure 69. Top: schematics of warm filters added to gas recirculation circuits. Bottom: photos of the West-module GAr units after installation of warm filters.

During the summer of 2022, after the first long-duration neutrino run (RUN1) and following a slow but steady decrease of the free-electron lifetime in the West module, it was decided to regenerate the corresponding filters of the liquid-argon recirculation system. The regeneration — also affected by a small accident during this nontrivial operation — resulted in a stop of liquid recirculation in the West module for about two months and about three weeks in the East module, where the filters were not regenerated. Normal operation was restored at the beginning of October 2022 in the East module and about one month later in the West module, where the liquid-recirculation pump was also upgraded.

2026 JINST 21 P04012

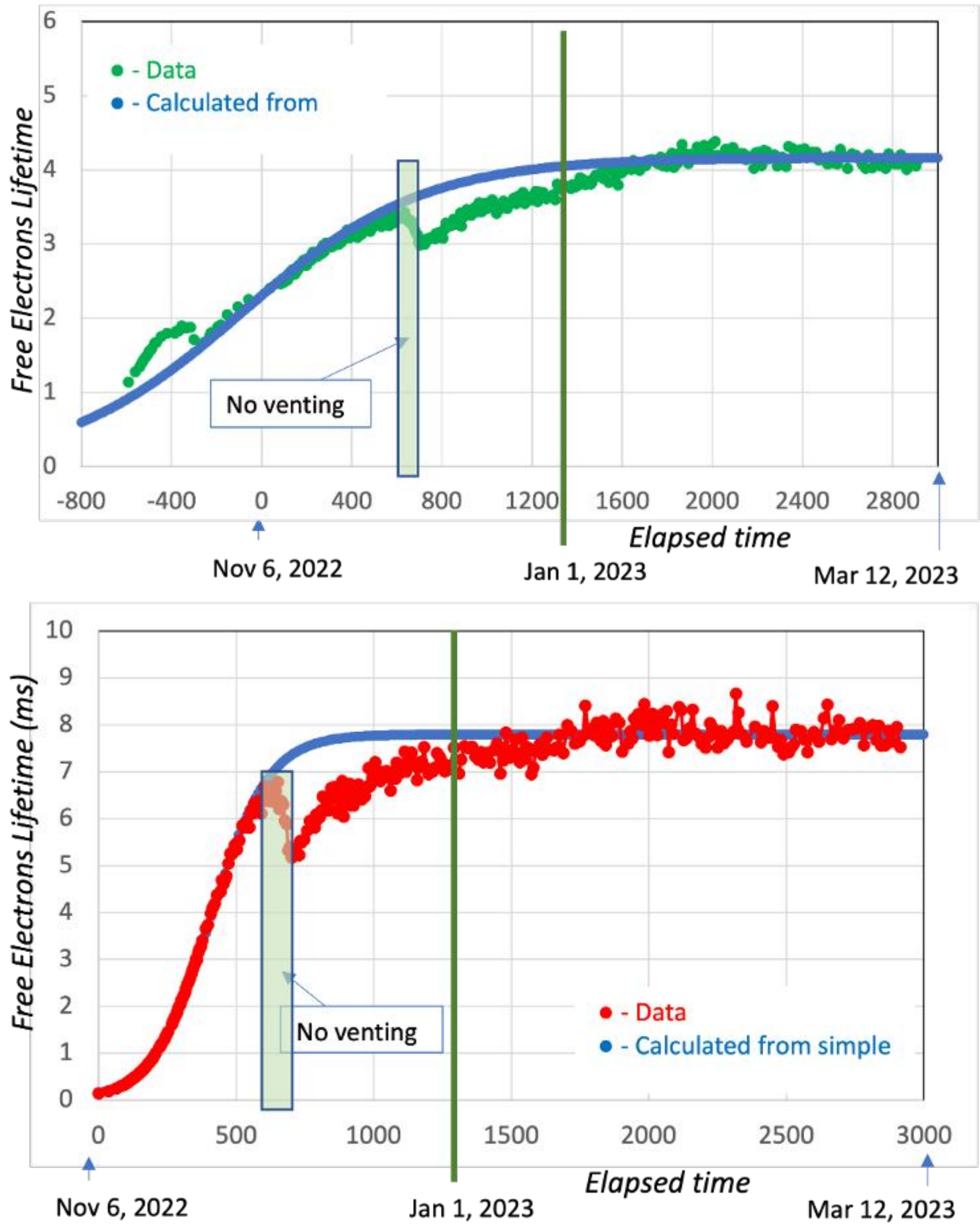

Figure 70. Free-electron lifetime evolution after restart of LAr recirculation at end of 2022. Top: East module; bottom: West module. A simple recirculation model prediction is superimposed.

After restart of liquid recirculation, the free-electron lifetime in the West module increased rapidly, whereas the improvement in the East module was significantly slower (figure 70). The free-electron lifetime stabilized at about 8 ms in the West module and 4 ms in the East module during January 2023, allowing a very successful second long-duration neutrino run (RUN2) (figure 71).

The liquid filters of the East module were also regenerated in late summer 2023. After restart of liquid recirculation, the purity in the East module increased rapidly, following a trend very similar to that of the West module. The free-electron lifetime exceeded 6 ms in less than one month and, at the time of this writing, is still increasing.

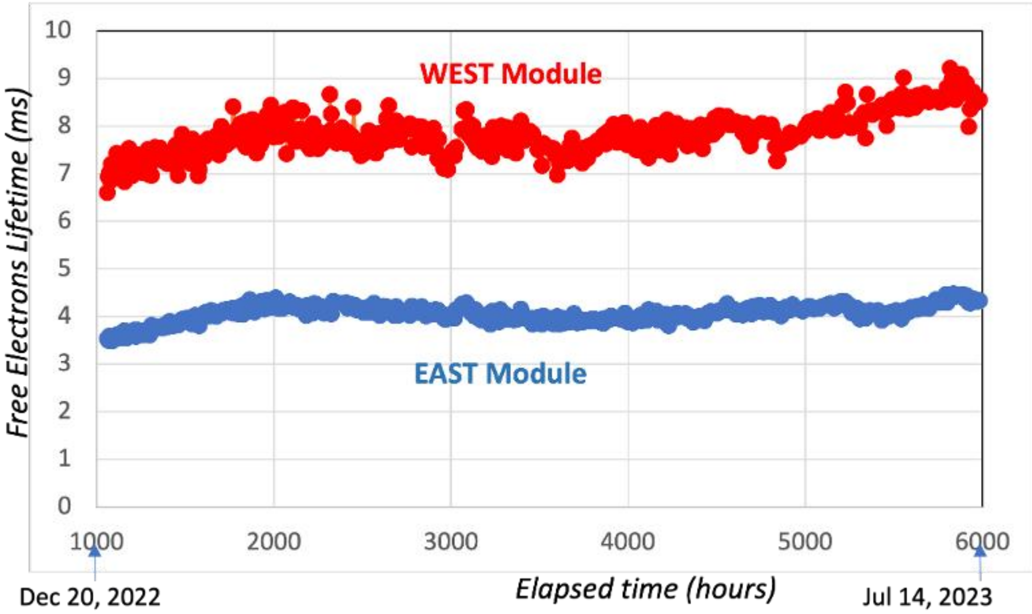

Figure 71. Free-electron lifetime evolution during neutrino RUN2.

8 Conclusions

The cryogenic and purification systems are now fully operational to support scientific mission of the ICARUS-T600 detector in the Booster and NuMI neutrino beams at Fermilab. Many useful lessons have been learned and improvements have been made to achieve this success. The plans include regeneration of the East liquid argon filter in 2023 and adding an additional external filter to support refills of argon needed due to vented argon.

It must be noted that, after the initial hiccups following the cold commissioning, concentrated on the stabilization of the gas recirculation systems, whose solution, mainly due to the rather severe limitations of operating during the hot phases of the COVID-19 pandemic, required several months, the ICARUS-T600 cryogenic and purification systems have shown a remarkable stability and performance.

Also considering that the initial cryogenic stabilization occurred during the detector commissioning, no significant data loss has occurred due to cryogenic interventions and the quality of the argon, both in terms of purity and thermal stability, has been well within the requirements for physics quality data since May 2021.

Acknowledgments

This manuscript has been authored by Fermi Forward Discovery Group under Contract No. 89243024CSC000002 with the U.S. Department of Energy, Office of Science, Office of High Energy Physics. L. Pasqualini supported by the research contract per Law 240/2010, Art. 24 (3)(a), and D.G.R. 693/2023 (REF. PA:2023-20090/RER — CUP: J19J23000730002) by FSE+ 2021–2027.

2026 JINST 21 P04012

A Process safety

Fermilab is managed by the Fermi Forward Discovery Group for the U.S. Department of Energy Office of Science under Contract No. 89243024CSC000002. As such, Fermilab must abide by the appendix I of DOE Orders and Notices, List B, which is so called Fermilab Work Smart Standards. The Work Smart Standards lists a large number of governing documents applicable to the management and operation of Fermilab, for example, specific Codes of Federal Regulations, ANSI/ASME standards and Fermilab ES&H Manual (FESHM) chapters.

As the components of the cryogenic systems were delivered by three different institutions and their contractors but installed at Fermilab, which is operated by U.S. Department of Energy, one of the main challenges was to demonstrate compliance to all governing codes and standards that are part of Fermilab Work Smart Set of Standards. As a result, Fermilab conducted extensive studies for equivalency between applicable U.S. National Consensus Codes and E.U. International Codes. That allowed Fermilab to approve use of cryogenic equipment designed and constructed per E.U. International Codes, such as pressure vessels, piping, reliefs, etc. See table 5.

In addition, it was demonstrated, but not officially approved, that minimum required pressure relieving capacities required for vacuum insulated cryogenic vessels per EN 21013-3 (previously 13648) equal or greater than the minimum required relieving capacities required for same (process or storage) vessels per U.S. standards API 521 and CGA S-1.3. It was also demonstrated, but not officially approved, that the requirements per EN 13458 are commensurate with requirements per CGA A-1.3 as applied to the cryogenic static vacuum insulated vessels.

The path to receive Operations Readiness Clearance for the Icarus cryogenic system and its pressurized equipment, such as cryostat modules, vessels and piping, was based on verification of conformity of the installed equipment to the governing standards (see table 5). The verification process, which is established at Fermilab through FESHM, involves describing each pressure or vacuum vessel, piping system, or structure and their safety in a so-called Engineering Note. The Engineering Notes are then reviewed by a group of experts and safety professionals before issuing permission for final validation tests and recommendation for operations. Such reviews were straight-forward for the equipment and systems that were either marked by the manufacturer with U stamp (ASME) or CE stamp (PED), e.g. cryogenic dewars, filter vessels, nitrogen phase separator, etc.

Validation of safety for the Icarus cryostats was the most challenging aspect of the safety validation. The cryostats are fully described in section 3. They are designed to be filled with $\sim$ 380 tons of liquid argon at maximum 320 mbarg gas pressure in the ullage (based on relief set pressure).

Due to ullage pressure being below 0.5 barg (though additional $\sim$ 0.5 bar of hydrostatic pressure at the bottom of the vessel), the vessels were reviewed per Fermilab FESHM 5031.5 “Low-Pressure Vessels and Fluid Containment”. The vessels are operated under internal pressure during “normal” operations, but they also were pumped down to full vacuum for leak checking and cleanup before commissioning. The vessels were successfully tested at full mechanical vacuum at CERN and then at Fermilab. Since the cryostat vessels were not ASME- or CE-marked and used material not listed in the EN 13445 design code/standard, Fermilab and CERN followed an elaborate path to ensure and validate the pressure safety of the cryostats. That included redundant protection from overpressure at 320 mbarg with three (per module) Velan magnetic safety devices and additional VELAN control valve (one per module) at 200 mbarg or below. Only two out of three magnetic devices are sufficient to handle all pressurization scenarios and are expected to be never opened. The control valve has a

Table 5. Established equivalency between U.S. National Consensus Codes and E.U. International Standards.

Study	Component Type	National Consensus Code	International Code
1	Pressure Vessels	ASME BPVC VIII	EN13445
2	Process Piping	ASME B31.3	EN13480
3	Pressure Relief Devices	ASME BPVC VIII and API521	EN4126
4	Structures	IBC/ASCE7, AISC360, ADM1	Eurocode EN1990, EN1991, EN1993, EN1998
5	Electrical Equipment for Measurement, Control and Laboratory use	UL 61010	IEC 61010

flow capacity verified to be more than enough to relieve all pressurization scenarios except fire and is also interlocked from a pressure switch set at 200 mbarg.

As CERN demonstrated that design and construction of the cryostat vessels followed Sound Engineering Practice (SEP) per appropriate design standard EN 13445, which is accepted as equivalent to ASME BPVC Section VIII per FESHM, and Fermilab demonstrated independent evaluation by FEA, the vessels were allowed to be validated by pressurization per approved Risk Assessment. The first phase of validation by pressurization was done in April 2019 by pneumatic pressurization of each module to 350 mbar (1.1 $\times$ design pressure) while measuring strains with strain gauges mounted in various locations on the cold vessels. The strains were shown to be about -20% to $+5\%$ than predicted (relative to predicted values) with the maximum strain $\sim$ 0.1% and demonstrated symmetric and linear structural behavior of the cold vessel. The second phase of validation was done in April 2020 by filling the modules with liquid argon and additional pressurization of ullage to 225 mbarg while reading the strain gauges and comparing them with the theoretical values from the FEA analyses. Again, the strains demonstrated very good correlation with the predicted values under the same loading conditions and allowed to finalize validation of structural integrity of the modules under combined hydrostatic and pneumatic loads at cold conditions.

Validation of safety for the Proximity cryogenic equipment presented lesser, but still a challenge. The Proximity cryogenic equipment, which was manufactured by Demaco, was only categorized where PED allowed such; most of the vessels and piping were not categorized due to small diameters and relatively low design pressure and therefore were executed per Sound Engineering Practice (SEP) per PED, article 4, par. 3. As CERN/Demaco delivered all equipment packaged in vacuum-jacketed valve boxes and transfer lines, Demaco guaranteed that QA/QC for the design and manufacturing processes are certified by a Notified Body, Lloyds Register, to conform to Modules H/H1. Demaco issued a statement that it had one universal quality system that has been determined to comply with Module H/H1 by the Notified Body (Lloyds Register) for the categorized products. All Demaco PED CE-marked products and those products that were not marked (SEP) were designed and manufactured to the same assessment procedures. As the two guiding standards, EN 13445 and EN 13480, per which Demaco designed, manufactured and tested the equipment, were already accepted in FESHM as being equivalent to ASME BPVC Section VIII and B31.3, the Proximity cryogenic equipment met the requirements of FESHM. The Proximity cryogenic equipment is protected with dual switchable Herose pressure reliefs sized for all pressurization scenarios, including the fire conditions and loss of vacuum.

Since the Icarus cryogenic system is mostly housed in the SBNFD detector building, the release of cryogens in building can cause depletion of oxygen and an Oxygen Deficiency Hazard (ODH) for personnel. The total anticipated fatality rate from spilling cryogens into building was assessed per FESHM 4240. This ODH assessment is a quantitative assessment of the increased risk of fatality from exposure to reduced atmospheric oxygen due to failure of components and release of inert gases into building. It is a methodology of calculating a total fatality rate and assigning an appropriate ODH class for each of the areas of the building. The analysis typically uses most conservative assumptions, for example release to $t \to \infty$, conservative assumption for failure rates, leak rates and escape paths.

The ODH assessment for SBNFD building resulted in calculating the total fatality rate (combined for all areas and operations) for mezzanine, pit and top of cryostat as 5.76×10^{-8} 1/hr, therefore requiring assigning ODH0 class. Still, while the area above the grade level is assigned classification of Engineered ODH Class 0, all areas below grade level (mezzanine, pit, top of cryostat) are administratively assigned a higher ODH Class 1. Therefore, the following ODH control measures were implemented for the SBNFD building before introducing any inert gases into building:

- Placing ODH equipment on emergency generator power, including ODH monitors, ventilation equipment and controls equipment, including PLC.
- Detection with six (6) ODH sensors installed at strategic locations where the spilled cryogens may propagate or settle.
- Installation of vacuum sensors in the insulating space of the cryogenic transfer lines connecting to the side penetrations. The side penetrations are closed on loss of vacuum or ODH alarming at 18%.
- Ventilation with two (2) ODH fans of total capacity of 15,000 scfm (7 m^3/s), plus additional fans for the access stairways. Minimum ventilation rate of ~ 20% is always sustained, while ramping up to full capacity activated on ODH alarming at 19.5% oxygen. The fans are automatically tested for full capacity once every 24 hours and set to alarm if failing to demonstrate full capacity.
- Alarming with 4 strobes and 4 horns placed at strategic locations throughout SBNFD building. Personnel is required to evacuate the building immediately when ODH alarms.
- Configuring all argon cryogenic supplies and pumps to be shut off at 18% oxygen.
- Providing crash buttons installed for each module on the pit level close to the argon pumps.
- Managing entry to SBNFD building via keycard readers, therefore allowing administrative control for access. Allowing only ODH-qualified and trained personnel to enter levels below ground while maintaining two-person rule.

A final Operations Readiness Clearance for the Icarus cryogenic system was obtained in February 2020. The timeline and details of cryogenic and purification commissioning are described in section 7.

2026 JINST 21 P04012

B Icarus cryogenic system commissioning stages

Table 6. Icarus cryogenic system commissioning stages.

Stage of commissioning	Objective	When
Fill of LN_2 and LAr dewars	Demonstrate reliable leak-tight operations, measure heat losses	Aug–Oct 2019
Initial pumping mode for modules	Pumping modules to high vacuum to remove contamination	May 2019–Feb 2020
Proximity cryo system purification	Purification of the valve boxes and transfer lines	Oct–Nov 2019
Insulation space purge for warm structure	Purge warm structure and insulation space with GN_2 to remove atmospheric moisture and prepare for cooldown of shields	Jan–Feb 2020
Starting gas analyzers	Calibrate and demonstrate reliable operations of gas analyzers	Jan 2020
Activation of cartridge purifiers	Removal of O_2 and H_2O from 14 removable cartridges (four 5-liter units for gas re-condensers and ten 25-liter units for liquid filters)	Jun–Jul 2019
Initial activation of fill purifier	Removal of O_2 and H_2O from 3 filters of the fill purifier (two vessels containing 300 kg of Cu 0226, and one vessel containing 80 kg of molecular sieves)	Jan 2020
Start of cryogenics control system	Verification of I/Os, loops, alarms, interlocks, algorithms	Sep 2019–Feb 2020
Fill of modules with GAr	Letting the vacuum up with GAr and stabilizing pressure control	Feb 2020
Cooldown of modules, transfer lines and valve boxes with LN_2	Cooldown of modules to $\sim$ 90 K by flowing LN_2 by pressure feed and gravity through shields	Feb 2020
Start of LN_2 circulation system	Starting of LN_2 pumps and stabilizing LN_2 flows	Feb 2020
Fill of modules with LAr	Receiving 46 loads, verifying for conformance to specification and 24/7 transfer to both modules while controlling pressure and temperature gradients	Feb–Apr 2020
Start of gas re-condensers and stabilization of modules' pressures	Starting to circulate, condense and purify GAr boiloff from ullage with gas re-condensers	May 2020
Start of LAr circulating pumps	Starting circulation of LAr pumps via LAr purifiers	Apr 2020
Verification of initial purity	Use HV drift chambers and TPC to verify initial purity of argon	Jul–Aug 2020
Improvements for argon purity and pressure control	Investigations for improvements for the non-functional gas re-condensers (SE and SW units) finally resulting in internal piping modification	Aug 2020–May 2021
Final tuning for pressure stability and design purity	Tuning shields for maximum temperature and maximum gas formation in ullage to match maximum capacity of condensers. Periodic venting of gas from ullage to increase bulk purity of argon in modules.	Jan 2021–May 2021

2026 JINST 21 P04012

References

[1] C. Rubbia, *The Liquid Argon Time Projection Chamber: A New Concept for Neutrino Detectors*, CERN-EP-INT-77-08 (1977).

[2] C. Rubbia et al., *Underground operation of the ICARUS T600 LAr-TPC: first results*, 2011 *JINST* **6** P07011 [arXiv:1106.0975].

[3] ICARUS collaboration, *The trigger system of the ICARUS experiment for the CNGS beam*, 2014 *JINST* **9** P08003 [arXiv:1405.7591].

[4] M. Antonello et al., *Experimental observation of an extremely high electron lifetime with the ICARUS-T600 LAr-TPC*, 2014 *JINST* **9** P12006 [arXiv:1409.5592].

[5] M. Antonello et al., *Precise 3D track reconstruction algorithm for the ICARUS T600 liquid argon time projection chamber detector*, *Adv. High Energy Phys.* **2013** (2013) 260820 [arXiv:1210.5089].

[6] ICARUS collaboration, *Muon momentum measurement in ICARUS-T600 LAr-TPC via multiple scattering in few-GeV range*, 2017 *JINST* **12** P04010 [arXiv:1612.07715].

[7] C. Farnese, *Atmospheric Neutrino Search in the ICARUS T600 Detector*, *Universe* **5** (2019) 17.

[8] LSND collaboration, *Evidence for neutrino oscillations from the observation of $\bar{\nu}_e$ appearance in a $\bar{\nu}_\mu$ beam*, *Phys. Rev. D* **64** (2001) 112007 [hep-ex/0104049].

[9] MiniBooNE collaboration, *Improved Search for $\bar{\nu}_\mu \to \bar{\nu}_e$ Oscillations in the MiniBooNE Experiment*, *Phys. Rev. Lett.* **110** (2013) 161801 [arXiv:1303.2588].

[10] ICARUS collaboration, *Search for anomalies in the ν_e appearance from a ν_μ beam*, *Eur. Phys. J. C* **73** (2013) 2599 [arXiv:1307.4699].

[11] MicroBooNE collaboration, *First Constraints on Light Sterile Neutrino Oscillations from Combined Appearance and Disappearance Searches with the MicroBooNE Detector*, *Phys. Rev. Lett.* **130** (2023) 011801 [arXiv:2210.10216].

[12] MicroBooNE et al. collaborations, *A Proposal for a Three Detector Short-Baseline Neutrino Oscillation Program in the Fermilab Booster Neutrino Beam*, arXiv:1503.01520.

[13] ICARUS/NP01 collaboration, *Test and characterization of 400 Hamamatsu R5912-MOD photomultiplier tubes for the ICARUS T600 detector*, 2018 *JINST* **13** P10030 [arXiv:1807.08577].

[14] ICARUS collaboration, *Design and implementation of the new scintillation light detection system of ICARUS T600*, 2020 *JINST* **15** T10007 [arXiv:2006.05261].

[15] ICARUS/NP01 collaboration, *New read-out electronics for ICARUS-T600 liquid Argon TPC. Description, simulation and tests of the new front-end and ADC system*, 2018 *JINST* **13** P12007 [arXiv:1805.03931].

[16] WArP collaboration, *Effects of Nitrogen contamination in liquid Argon*, 2010 *JINST* **5** P06003 [arXiv:0804.1217].

[17] ICARUS collaboration, *Design, construction and tests of the ICARUS T600 detector*, *Nucl. Instrum. Meth. A* **527** (2004) 329.

[18] M. Antonello et al., *Operation and performance of the ICARUS-T600 cryogenic plant at Gran Sasso underground Laboratory*, 2015 *JINST* **10** P12004 [arXiv:1504.01556].

[19] C. Vignoli, *The ICARUS T600 Liquid Argon Purification System*, *Phys. Procedia* **67** (2015) 796.

[20] M. Geynisman et al., *The cryogenic and purification systems of the ICARUS T600 detector installation at Fermilab*, in the proceedings of the *16th Cryogenics IIR Conference*, Online, October 5–7 (2021), Paper 0039.

[21] C. Fabre, *NP-01 Functional Analysis*, CERN EDMS 2360024, https://edms.cern.ch/document/2360024/1.

[22] M. Chalifour, *PBS of the Neutrino Platform Proximity Cryogenics (NPPC)*, CERN EDMS 1995372, https://edms.cern.ch/document/1995372/1.

[23] UNICOS: Unified Industrial Control System, https://unicos.web.cern.ch/.

[24] C. Fabre, *Logics specification of the NP-01 Proximity Cryogenics*, CERN EDMS 2360026, https://edms.cern.ch/document/2360026/7.2.

[25] *Process Control Description of the NP-01 External Cryogenics*, Fermilab SBN-doc-14205.

[26] C. Fabre, *NP-01 Pressures-scale Manufacturing*, https://edms.cern.ch/document/2155766/1.

[27] O. Beltramello, *WA104 Cold Vessel — Mechanical Design Compliance with European Standards — Methodology*, CERN EDMS 1692011, https://edms.cern.ch/document/1692011/2.

[28] O. Beltramello, *FEA Calculations Results — ICARUS NP01 Cold Vessel*, CERN EDMS 1725838, https://edms.cern.ch/document/1725838/4.

[29] M. Nessi, *WA104 Cold Vessel — Buckling Analysis Results*, CERN EDMS 1730040, https://edms.cern.ch/document/1730040/2.

[30] O. Beltramello, *ICARUS WA104 Cold Vessel Door Bolts Calculation*, CERN EDMS 1749106, https://edms.cern.ch/document/1749106/2.

[31] *ICARUS Cold Vessel Low Pressure Vessel and Design Documentation*, Fermilab Teamcenter EN02601.

[32] M. Nessi, *WA104 Warm Vessel Structural Analysis*, CERN EDMS 1693384, https://edms.cern.ch/document/1693384/1.

[33] M. Nessi, *WA104 Warm Vessel Construction*, CERN EDMS 1697517, https://edms.cern.ch/document/1697517/1.

[34] M. Nessi, *Tender technical specification*, CERN EDMS 1699908, https://edms.cern.ch/document/1699908/1.

[35] *Icarus Warm Vessel Low Pressure Vessel and Design Documentation*, Fermilab Teamcenter EN02602.

The ICARUS collaboration

F. Abd Alrahman[8], P. Abratenko[27], N. Abrego-Martinez[5], A. Aduszkiewicz[8], F. Akbar[23], L. Aliaga Soplin[26], M. Artero Pons[18], J. Asaadi[26], W. F. Badgett[7], B. Behera[6], V. Bellini[10], R. Benocci[16], J. Berger[6], S. Berkman[7], O. Beltramello[3], S. Bertolucci[9], M. Betancourt[7], A. Blanchet[3], F. Boffelli[19], M. Bonesini[16], T. Boone[6], B. Bottino[11], A. Braggiotti[18,a], J. Bremer[3], S. J. Brice[7], V. Brio[10], C. Brizzolari[16], H. S. Budd[23], A. Campani[11], A. Campos[28], D. Carber[6], M. Carneiro[1], I. Caro Terrazas[6], H. Carranza[26], F. Castillo Fernandez[26], A. Castro[5], S. Centro[18], G. Cerati[7], M. Chalifour[3], P. Chambouvet[3], A. Chatterjee[21], D. Cherdack[8], S. Cherubini[14], N. Chithirasreemadam[20], T. E. Coan[25], A. Cocco[17], M. R. Convery[24], L. Cooper-Troendle[22], S. Copello[19], H. Da Motta[2], M. Dallolio[26], A. A. Dange[26], A. de Roeck[3], S. Di Domizio[11], L. Di Noto[11], D. Di Ferdinando[9], M. Diwan[1], S. Dolan[3], L. Domine[24], S. Donati[20], R. Doubnik[7], F. Drielsma[24], J. Dyer[6], S. Dytman[22], C. Fabre[3], A. Falcone[16], C. Farnese[18], A. Fava[7], N. Gallice[1], F. G. Garcia[24], C. Gatto[17], M. Geynisman[7,*], D. Gibin[18], A. Gioiosa[20], W. Gu[1], A. Guglielmi[18], G. Gurung[26], K. Hassinin[8], H. Hausner[7], A. Heggestuen[6], B. Howard[29,b], R. Howell[23], Z. Hulcher[24], I. Ingratta[9], C. James[7], W. Jang[26], Y.-J. Jwa[24], L. Kashur[6], W. Ketchum[7], J. S. Kim[23], D.-H. Koh[24], J. Larkin[23], Y. Li[1], C. Mariani[28], C. M. Marshall[23], S. Martynenko[1], N. Mauri[9], K. S. McFarland[23], D. P. Méndez[1], A. Menegolli[19], G. Meng[18], O. G. Miranda[5], D. Mladenov[3], A. Mogan[6], N. Moggi[9], E. Montagna[9], C. Montanari[7,c,*], A. Montanari[9], M. Mooney[6], G. Moreno-Granados[28], J. Mueller[6], M. Murphy[28], D. Naples[22], M. Nessi[3], T. Nichols[7], S. Palestini[3], M. Pallavicini[11], V. Paolone[22], L. Pasqualini[9], L. Patrizii[9], L. Paudel[6], G. Petrillo[24], C. Petta[10], V. Pia[9], F. Pietropaolo[3,d], F. Poppi[9], M. Pozzato[9], M. L. Pumo[14], G. Putnam[4], X. Qian[1], A. Rappoldi[19], G. L. Raselli[19], S. Repetto[11], F. Resnati[3], A. M. Ricci[20], E. Richards[22], M. Rosenberg[27], M. Rossella[19], N. Rowe[4], P. Roy[28], C. Rubbia[12], M. Saad[22], S. Saha[22], G. Salmoria[2], S. Samanta[11], M. Satgia[11], A. Scaramelli[19], D. Schmitz[4], F. Schwartz[7], A. Schukraft[7], D. Senadheera[22], S.-H. Seo[7], F. Sergiampietri[3,e], G. Sirri[9], J. S. Smedley[23], J. Smith[1], L. Stanco[18], J. Stewart[1], H. A. Tanaka[24], F. Tapia[26], M. Tenti[9], K. Terao[24], F. Terranova[16], V. Togo[9], D. Torretta[7], M. Torti[16], F. Tortorici[10], R. Triozzi[18], Y.-T. Tsai[24], K. V. Tsang[24], S. Tufanli[3], T. Usher[24], F. Varanini[18], N. Vardy[6], S. Ventura[18], M. Vicenzi[1], C. Vignoli[13], B. Viren[1], F. A. Wieler[2], Z. Williams[26], R. J. Wilson[6], P. Wilson[7], J. Wolfs[23], T. Wongjirad[27], A. Wood[8], E. Worcester[1], M. Worcester[1], M. Wospakrik[7], S. Yadav[26], H. Yu[1], J. Yu[26], A. Zani[15], J. Zennamo[7], J. Zettlemoyer[7], C. Zhang[1], S. Zucchelli[9], M. Zuckerbrot[7]

[1] *Brookhaven National Laboratory, Upton, NY 11973, U.S.A.*
[2] *CBPF, Centro Brasileiro de Pesquisas Físicas, Rio de Janeiro, Brazil*
[3] *CERN, European Organization for Nuclear Research, 1211 Geneva 23, Switzerland*
[4] *University of Chicago, Chicago, IL 60637, U.S.A.*
[5] *Centro de Investigación y de Estudios Avanzados del IPN (Cinvestav), Mexico City, Mexico*
[6] *Colorado State University, Fort Collins, CO 80523, U.S.A.*
[7] *Fermi National Accelerator Laboratory, Batavia, IL 60510, U.S.A.*
[8] *University of Houston, Houston, TX 77204, U.S.A.*
[9] *INFN Sezione di Bologna and University of Bologna, Bologna, Italy*
[10] *INFN Sezione di Catania and University of Catania, Catania, Italy*
[11] *INFN Sezione di Genova and University of Genova, Genova, Italy*
[12] *INFN GSSI, L'Aquila, Italy*
[13] *INFN LNGS, Assergi, Italy*
[14] *INFN LNS, Catania, Italy*
[15] *INFN Sezione di Milano, Milano, Italy*
[16] *INFN Sezione di Milano Bicocca, Milano, Italy*
[17] *INFN Sezione di Napoli, Napoli, Italy*
[18] *INFN Sezione di Padova and University of Padova, Padova, Italy*
[19] *INFN Sezione di Pavia and University of Pavia, Pavia, Italy*

2026 JINST 21 P04012

[20] INFN Sezione di Pisa, Pisa, Italy
[21] Physical Research Laboratory, Ahmedabad, India
[22] University of Pittsburgh, Pittsburgh, PA 15260, U.S.A.
[23] University of Rochester, Rochester, NY 14627, U.S.A.
[24] SLAC National Accelerator Laboratory, Menlo Park, CA 94025, U.S.A.
[25] Southern Methodist University, Dallas, TX 75275, U.S.A.
[26] University of Texas at Arlington, Arlington, TX 76019, U.S.A.
[27] Tufts University, Medford, MA 02155, U.S.A.
[28] Virginia Tech, Blacksburg, VA 24060, U.S.A.
[29] York University, Toronto M3J 1P3, Canada

[*] Corresponding author
[a] Also at Istituto di Neuroscienze, CNR, Padova, Italy.
[b] Also at Fermi National Accelerator Laboratory.
[c] On leave of absence from INFN Pavia.
[d] On leave of absence from INFN Padova.
[e] Now at IPSI — INAF Torino, Italy.